Passive Viscoelastic Constrained Layer Damping Application for a Small Aircraft Landing Gear System

Craig Allen Gallimore

Thesis submitted to the faculty of the Virginia Polytechnic Institute and State University in partial fulfillment of the requirements for the degree of

Master of Science
In
Mechanical Engineering

Dr. Kevin B. Kochersberger, Committee Chair

Dr. Alfred L. Wicks

Dr. Raffaella De Vita

Dr. John B. Ferris

9/30/2008
Blacksburg, VA

Keywords:

Viscoelastic, Damping, Loss Factor, Landing Gear, Aircraft

Passive Viscoelastic Constrained Layer Damping Application for a Small Aircraft Landing Gear System

By

Craig A. Gallimore

Committee Chairman: Dr. Kevin B. Kochersberger

Mechanical Engineering Department

(ABSTRACT)

The main purpose of this report was to test several common viscoelastic polymers and identify key attributes of their applicability to a small aircraft landing gear system for improved damping performance. The applied viscoelastic damping treatment to the gear was of a constrained layer type, promoting increased shear deformation over free surface treatments, and therefore enhanced energy dissipation within the viscoelastic layer. A total of eight materials were tested and analyzed using cyclic loading equipment to establish approximate storage modulus and loss factor data at varying loading frequencies. The three viscoelastic polymers having the highest loss factor to shear modulus ratio were chosen and tested using a cantilever beam system. A Ross, Kerwin, and Ungar analysis was used to predict the loss factor of the cantilever beam system with applied treatment and the predictions were compared to experimental data.

Customer requirements often govern the scope and intensity of design in many engineering applications. Limitations and constraints, such as cost, weight, serviceability, landing gear geometry, environmental factors, and manufacturability in regards to the addition of a viscoelastic damping treatment to a landing gear system are discussed.

Based on results found from theoretical and experimental testing, application of a damping treatment to a small aircraft landing gear system is very promising. Relatively high loss factors were seen in a cantilever beam for simple single layer constrained treatments for very low strain amplitudes relative to strains seen during loading of the landing gear. With future design iterations, damping levels several times those seen in this document will be seen with a constrained treatment applied to a landing gear system.

ACKNOWLEDGEMENTS

First and foremost I would like to thank God for blessing me with the opportunity and ability to compete and succeed at such a challenging university. Please give me the strength to continue to conquer life and continue to walk in your will. You have pulled so many strings and put the right people in the right place at the right time to help me overcome some pretty impossible hurdles.

I want to extend special gratitude to my family and friends for their seemingly endless supply of encouragement and support. Mom and Dad, the success of our family is a result of your excellent parenting, rock solid foundation, creativity, and love for your children. Without you I would be lost. Jeff, Scott, and Laura, we are truly blessed to be so close. Thank you for all of your support and for always extending an emotional outlet when I feel like I am going to explode. My close friends, Dan, Carlyn, Shawn, James, Ginny, Adam, and Abbey, you are some of the most important people in my life, and I owe much of my development, both as an engineer and as a person, to you all.

To the occupants of the Unmanned Systems Lab, namely Jimmy, Praither, Chris, Johnathan, John (even though you left us you traitor), and Unmanned Systems guru's of old Adam Sharkasi, Andrew Culhane, and Shane Barnett, I want to thank you for forming such a great atmosphere at the Lab. I could always rely on you to create fun ways to procrastinate for a short while and take my mind off of the long list of uncompleted work. Well, the list is done now.

I want to thank my advisor, Dr. Kevin Kochersberger, and my committee members Dr. Al Wicks (you coached us to the championship), Dr. John Ferris, and Dr. Raffaella De Vita for agreeing to be on my committee. Dr. K, your attention to detail and ability to be so many places at once inspire success and hard work. With your help, I feel I have bettered myself as an engineer and look forward to future opportunities working with you. I want to thank you for bringing me on as a grad student. My education, something I am very proud of, would not have been the same without you. My committee, as well as the other faculty here at Tech, form a wealth of technical knowledge in all walks of science. You create passion and the desire to succeed in a world with too little of both. I only hope I have lived up to your expectations.

Additionally, I would like to thank Cathy Hill for being an awesome program coordinator. You have helped so many graduate students achieve their degrees by guiding us through the endless amounts of logistics and forms and also give us the information on exactly who we need to talk to get what we need to graduate. You do your job very well, and I want to thank you for that.

Lastly, but certainly not least, I want to thank AAI for fitting the bill for this research. You helped make my life easier as a graduate student.

"Out of overflow of the heart, the mouth speaks"

Table of Contents

List of Figures

Author's Note: Unless otherwise noted, all photographs, images, and tables are property of the author.

List of Tables

Chapter 1

Introduction

This report provides a final summary of the progress made over the past year on the study of passive viscoelastic constrained layer damping, specifically applied to high stiffness structural members. Viscoelastic materials are materials which dissipate system energy when deformed in shear. This research has a wide variety of engineering applications, including bridges, engine mounts, machine components such as rotating shafts, component vibration isolation, novel spring designs which incorporate damping without the use of traditional dashpots or shock absorbers, and structural supports. This research adds to significant published work in constrained layer damping treatments used to control vibration on thin, plate-like structures where pressure is the dominant forcing function. The main focus of this research has been to develop a successful design of small aircraft (400 lbs.) landing gear where such design considerations as weight, aerodynamics, and operational environment need to be taken into consideration.

1.1 Research Goals

The goals of this research program at Virginia Tech include the following:

- To develop a landing gear design for a small aircraft to which a viscoelastic damping treatment could be applied to improve dynamic response
- To experimentally gather data to determine damping properties of several viscoelastic polymeric materials
- To formulate a reliable prediction of damping performance based on accumulated data of damping materials

- To successfully extrapolate data from tested materials to formulate the best solution for a passive constrained layer viscoelastic treatment to the aforementioned landing gear

To successfully satisfy these goals, several common, inexpensive damping materials were chosen and tested and viscoelastic material theory used to find the damping properties of each material based on accumulated cyclic loading test data. Theoretical damping predictions based on calculated damping properties are formulated and compared against experimental results found from a cantilever beam with a viscoelastic damping treatment. Lastly, the application of a constrained layer viscoelastic damping treatment to an aircraft landing gear is discussed accounting for weight, cost, serviceability, manufacturability, aerodynamic efficiency, and operational environment design considerations.

Chapter 2

History, Development, Modeling, and Applications of Viscoelastic Treatments and Materials

The damping of structural components and materials is often a significantly overlooked criterion for good mechanical design. The lack of damping in structural components has led to numerous mechanical failures over a seemingly infinite multitude of structures. For instance, the problem of insufficient damping and unstable vibration was even recognized by the Roman Empire in the early centuries A.D. Roman officers would train their regiments to march out of cadence while going over bridges so as to not excite a resonance mode of the bridge, which could ultimately lead to catastrophic failure and the loss of hundreds of soldiers. However, some scientific work in the area of damping is known to have taken place as early as the 1930's. Few scientists, such as Foppl, Zener, and Davidenkoff, investigated the damping of metals (Jones, 2001). As World War II approached, there was undoubtedly development in the area of damping materials, but publications were sparse because of the mass mobilization and rapidity of the scientific community. The first major advancements in the application and use of materials which could applied as a treatment, surface or embedded, which enhance the damping characteristics of structures and components did not occur until the 1950's. During this time, many scientists were investigating the properties and mechanical behavior of polymeric materials (Jones, 2001). Ross and Kerwin were among the first to formulate an analytical method of layered damping treatments (Ross, 1959). Also during this period Mycklestad had the first publication investigating the complex modulus modeling of damping materials in 1952 (Jones, 2001). A significant spur in this direction

of research was from the aerospace industry. Aircraft manufacturers and designers were seeking a way to reduce vibration and noise transmission through aircraft fuselage panels, without a significant increase in weight. Additionally, as time neared the mid 1960's, NASA funded research for thin, lightweight films which could be used for the same purpose of damping in rocket housings.

From the early 1970's to present day, there has been a large, almost overwhelming, ongoing investigation into damping technology. Though there were few new developments into modeling of damping materials, much advancement in enhancing the damping properties of materials and extended applications have been found. Furthermore, a plethora of technical papers and textbooks have been published alongside the development of damping technology, making it fairly easy for an up-and-coming scientist or engineer to access technical data and theoretical information.

Since it was discovered that damping materials could be used as treatments to structures to improve damping performance, there has been a flurry of ongoing research over the last few decades to either alter existing materials, or develop entirely new materials to improve the structural dynamics of components to which a damping material could be applied. The most common damping materials available on the current market are viscoelastic materials. Viscoelastic materials are generally polymers, which allow a wide range of different compositions resulting in different material properties and behavior. Thus, viscoelastic damping materials can be developed and tailored fairly efficiently for a specific application.

2.1 Typical Applications and Viscoelastic Material Characteristics

Many polymers exhibit viscoelastic behavior. Viscoelasticity is a material behavior characteristic possessing a mixture of perfectly elastic and perfectly viscous behavior. An elastic material is one in which there is perfect energy conversion, that is, all the energy stored in a material during loading is recovered when the load is removed. Thus, elastic materials have an in phase stress-strain relationship. Figure 2.1a illustrates this concept. Contrary to an elastic material, there exists purely viscous behavior, illustrated in Figure 2.1b. A viscous material does not recover any of the energy stored during loading after the load is removed (the phase angle between stress and strain is exactly $\frac{\pi}{2}$ radians). All energy is lost as 'pure damping.' For a viscous material, the stress is related to the strain as well as the strain rate of the material. Viscoelastic materials have behavior which falls between elastic and viscous extremes. The rate at which the material dissipates energy in the form of heat through shear, the primary driving mechanism of damping materials, defines the effectiveness of the viscoelastic material. Because a viscoelastic material falls between elastic and viscous behavior, some of the energy is recovered upon removal of the load, and some is lost or dissipated in the form of thermal energy. The phase shift between the stress and strain maximums, which does not to exceed 90 degrees, is a measure of the materials damping performance. The larger the phase angle between the stress and strain during the same cycle (see Figure 2.1c), the more effective a material is at damping out unwanted vibration or acoustical waves.

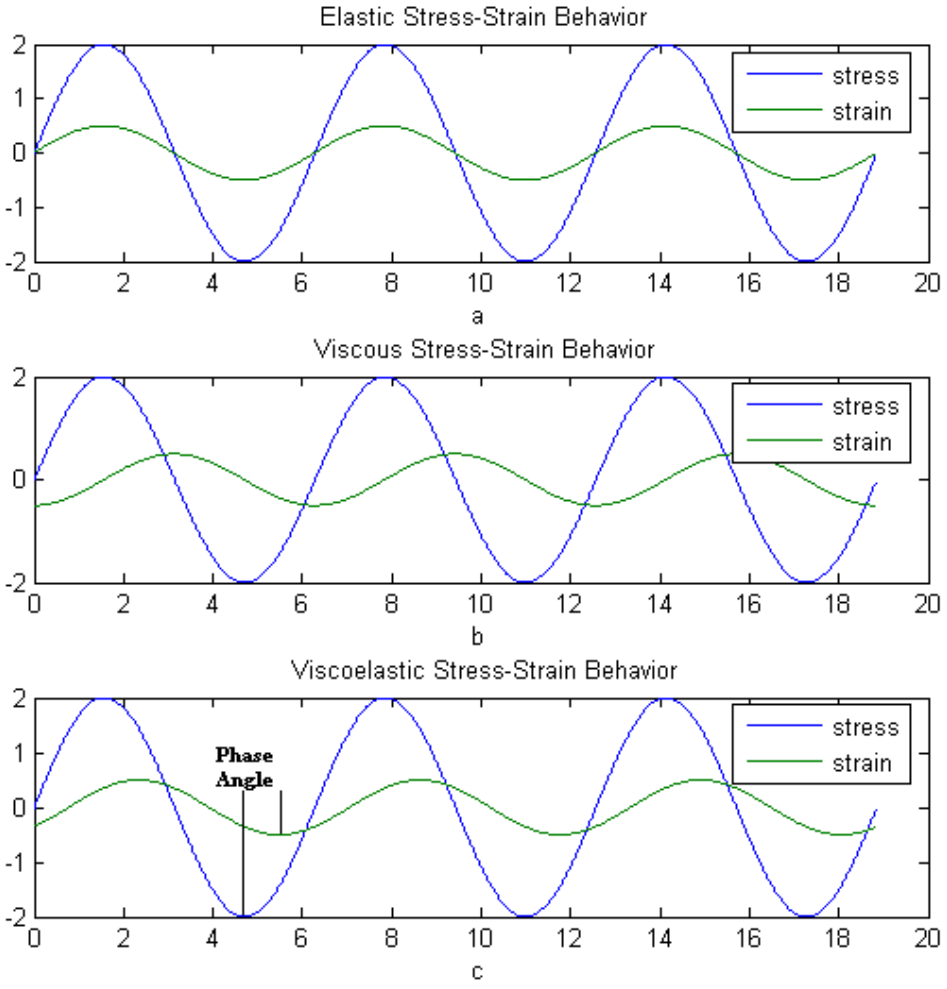

Figure 2.1. **a)** Elastic stress-strain behavior. **b)** Viscous stress-strain behavior. **c)** Viscoelastic stress-strain behavior.

Because viscoelastic materials are generally polymers, there is enormous variability in the composition of viscoelastic materials. This will be discussed in more detail in relation to properties of viscoelastic materials, namely complex moduli, in section 2.1.1, but some typical materials which are used for damping are presented in Table 2.1.

Table 2.1 List of common viscoelastic polymeric materials (Jones, "Handbook of Viscoelastic Damping," 2001).

1	Acrylic Rubber
2	Butadiene Rubber (BR)
3	Butyl Rubber
4	Chloroprene
5	Chlorinated Polyethylenes
6	Ethylene-Propylene-Diene
7	Fluorosilicone Rubber
8	Fluorocarbon Rubber
9	Nitrile Rubber
10	Natural Rubber
11	Polyethylene
12	Polystyrene
13	Polyvinyl Chloride (PVC)
14	Polymethyl Methacrylate (PMMA)
15	Polybutadiene
16	Polypropylene
17	Polyisobutylene (PIB)
18	Polyurethane
19	Polyvinyl Acetate (PVA)
20	Polyisoprene
21	Styrene-Butadiene (SBR)
22	Silicone Rubber
23	Urethane Rubber

Viscoelastic polymers are generally used for low amplitude vibration damping such as damping of sound transmission and acoustical waves through elastic media. Some typical applications of the polymers presented in Table 2.1 are shown in Table 2.2.

Table 2.2. Some common applications for viscoelastic materials

Common Viscoelastic Material Applications
Grommets or Bushings
Component Vibration Isolation
Acoustical Damping of Planar Surfaces
Aircraft Fuselage Panels
Submarine Hull Separators
Mass Storage (Disk Drive) Components
Automobile Tires
Stereo Speakers
Bridge Supports
Caulks and Sealants
Lubricants
Fiber Optic Compounds
Electrical and Plumbing

2.2 Modeling of Viscoelastic Materials

Unlike structural components which exhibit fairly strait-forward dynamic response, viscoelastic materials are somewhat more difficult to model mathematically. Because most high load bearing structures tend to implement high strength metal alloys, which usually have fairly straight-forward stress-strain and strain-displacement relationships, the dynamics of such structures are simple to formulate and visualize. An engineer or analyst need only take into account the varying geometries of these structures and the loads which are applied to them to accurately model the dynamics because the material properties of the structure and its components are generally well known. However, difficulty arises when viscoelastic materials are applied to such structures. This difficulty is mainly due to the strain rate (frequency), temperature, cyclic strain amplitude, and environmental dependencies between the viscoelastic material properties and their associated effect on a structure's dynamics (Jones, 2001, Sun, 1995).

Additionally, many viscoelastic materials and the systems to which they are applied exhibit nonlinear dynamics over some ranges of the aforementioned dependencies, further complicating the modeling process (Jones, 2001).

2.2.1 Properties of Viscoelastic Materials

Mycklestad was one of the pioneering scientists into the investigation of complex modulus behavior of viscoelastic materials (Jones, 2001, Sun, 1995). Viscoelastic material properties are generally modeled in the complex domain because of the nature of viscoelasticity. As previously discussed, viscoelastic materials possess both elastic and viscous properties. The moduli of a typical viscoelastic material are given in equation set (2.1)

$$\begin{aligned} E^* &= E' + iE'' = E'(1 + i\eta) \\ G^* &= G' + iG'' = G'(1 + i\eta) \end{aligned} \qquad (2.1)$$

where the '*' denotes a complex quantity. In equation set (2.1), as in the rest of this report, E and G are equivalent to the elastic modulus and shear modulus, respectively. Thus, the moduli of a viscoelastic material have an imaginary part, called the loss modulus, associated with the material's viscous behavior, and a real part, called the storage modulus, associated with the elastic behavior of the material. This imaginary part of the modulus is also sometimes called the loss factor of the material, and is equal to the ratio of the loss modulus to the storage modulus. The real part of the modulus also helps define the stiffness of the material. Furthermore, both the real and imaginary parts of the modulus are temperature, frequency (strain rate), cyclic strain amplitude, and environmentally dependent.

2.2.1.1 Temperature Effects on the Complex Modulus

The properties of polymeric materials which are used as damping treatments are generally much more sensitive to temperature than metals or composites. Thus, their properties, namely the complex moduli represented by E, G, and the loss factor η, can change fairly significantly over a relatively small temperature range. There are three main temperature regions in which a viscoelastic material can effectively operate, namely the glassy region, transition region, and rubbery region (Jones, 2001, Sun, 1995). Figure 2.2 shows how the loss factor can vary with temperature.

The glassy region is representative of low temperatures where the storage moduli are generally much higher than for the transition or rubbery regions. This region is typical for polymers operating below their brittle transition temperature. However, the range of temperatures which define the glassy region of a polymeric material is highly dependent on the composition and type of viscoelastic material. Thus, different materials can have much different temperature values defining their glassy region. Because the values of the storage moduli are high, this inherently correlates to very low loss factors. The low loss factors in this region are mainly due to the viscoelastic material being unable to deform (having high stiffness) to the same magnitude per load as if it were operating in the transition or rubbery regions where the material would be softer.

On the other material temperature extreme, the rubbery region is representative of high material temperatures and lower storage moduli. However, though typical values of storage moduli are smaller, like the glassy region the material loss factors are also typically very small. This is due to the increasing breakdown of material structure as the temperature is increased. In this region, the viscoelastic material is easily deformable,

but has lower interaction between the polymer chains in the structure of the material. Cross-linking between polymer chains also becomes a less significant property as temperature is increased. A lower interaction between the chains results in the material taking longer to reach equilibrium after a load is removed. Eventually, as the temperature hits an upper bound critical value (also known as the flow region temperature), the material will begin to disintegrate and have zero effective loss factor and zero storage modulus.

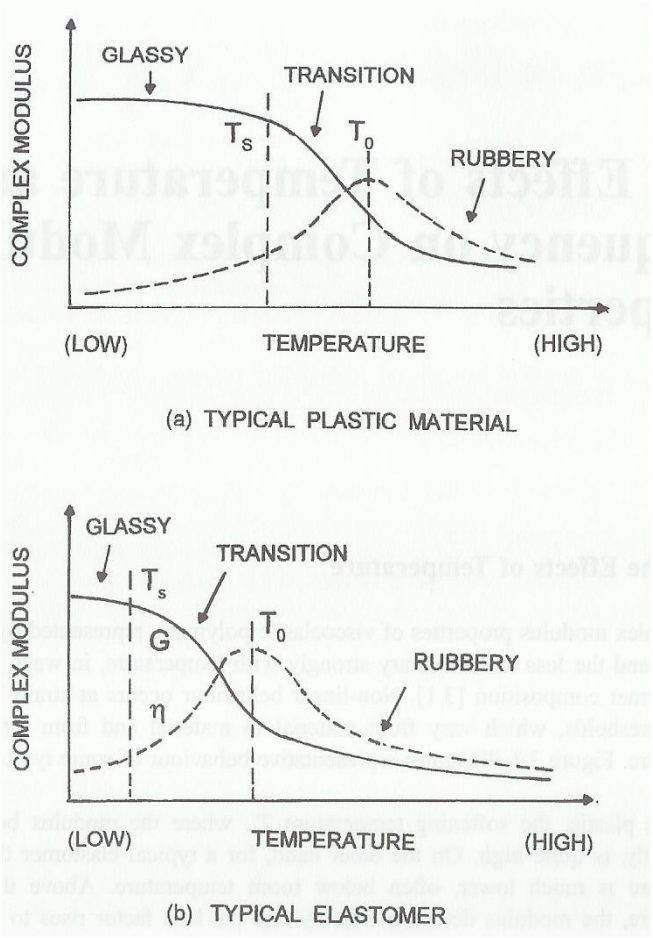

Figure 2.2. Temperature effects on complex modulus and loss factor material properties (Jones, "Handbook of Viscoelastic Damping," 2001).

The region falling between the glassy and rubbery regions is known as the transition region. Materials which are used for practical damping purposes generally should be used within this region because loss factors rise to a maximum. In more detail, if a material is within the glassy region and the temperature of the material is increased, the loss factor will rise to a maximum and the storage modulus will fall to an intermediate value within the transition region. As the material temperature is further increased into the rubbery region, the loss factor will begin to fall with the storage modulus. This behavior is illustrated in Figure 2.2. Therefore, it is extremely important to know the operating temperature range during the design phase of a host structure to which a viscoelastic damping treatment will be applied so that the viscoelastic treatment will be maximally effective.

2.2.1.2 Frequency Effects on the Complex Modulus

Like temperature, frequency also has a profound effect on the complex modulus properties of a viscoelastic polymer, though to a much higher degree with an inverse relationship. The three regions of temperature dependence (glassy, transition, rubbery) can sometimes be a few hundred degrees, more than covering a typical operational temperature range of an engineered structure. But the range of frequency within a structure can often be several orders of magnitude. The frequency dependence on complex moduli can be significant from as low as 10^{-8} Hz to 10^{8} Hz, a range much too wide to be measured by any single method (Jones, 2001). Furthermore, relaxation times after deformation of a viscoelastic material can be anywhere from nanoseconds to years and will greatly effect one's measurement methods, especially at low temperatures (Jones, 2001, Sun, 1995).

Frequency has an inverse relationship to complex moduli with respect to temperature. At low frequency, the storage moduli are low and the loss factors are low. This region is synonymous with the rubbery region (high temperatures). This is due to the low cyclic strain rates within the viscoelastic layer. As the frequency is increased, the material hits the transition region where the loss factor hits a maximum value. As the frequency is increased further, the storage moduli increase as the loss factor decreases. Thus, the transition region is again the range of frequency for which a material should be chosen to correspond to a host structure's typical operating range. Figure 2.3 illustrates this behavior.

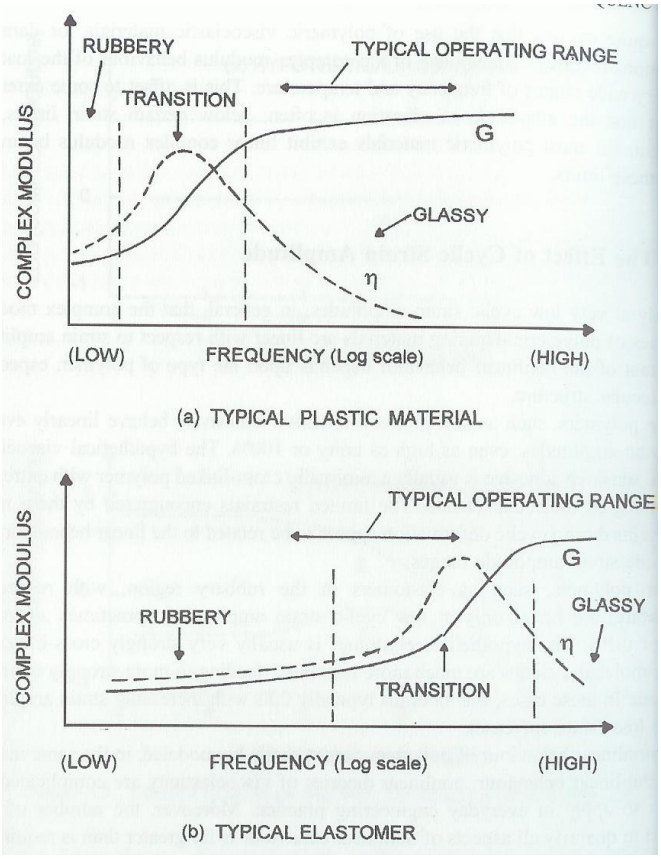

Figure 2.3. Frequency effects on complex modulus and loss factor material properties (Jones, "Handbook of Viscoelastic Damping," 2001).

2.2.1.3 Cyclic Strain Amplitude Effects on Complex Modulus

The effect of cyclic strain amplitude on polymeric complex moduli is highly dependent on the composition and type of the polymer, particularly the molecular structure (Jones, 2001, Sun, 1995). Experiments have shown that the complex moduli of polymers generally behave linearly only at low cyclic strain amplitudes (Jones, 2001). There are, however, polymers such as pressure sensitive adhesives, which exhibit linearity even at high cyclic strain amplitudes. These polymers usually have very few cross links between long, entangled polymer chains. Therefore, the low interaction between these chains seems to have an effect on the linear behavior over wide strain amplitude ranges (Jones, 2001). However, most viscoelastic polymers used in typical damping applications behave nonlinearly at high strain amplitudes. This nonlinearity is very difficult to model accurately and involves very complicated theories and a significant number of tests, many more than for linear complex modulus behavior, to gather data sufficient to establish trends for a specific material (Jones, 2001, Sun, 1995).

2.2.1.4 Environmental Effects on Complex Modulus

The environment plays a significant role in all outdoor engineering applications. Temperature ranges, climate, amount of rainfall or direct exposure to sunlight, as well as foreign substance exposure (such as petroleum products, alkalis, harmful chemicals, etc.) are necessary design factors to take into consideration for any outdoor engineering project. The same holds true when considering applying a viscoelastic treatment to an engineered structure. Temperature dependence on the behavior of viscoelastic complex moduli has already been discussed. But depending on the application, polymer type, and composition of the material, exposure to foreign substances must also be addressed. Oils

and other petrols can penetrate into some materials and alter the behavior as well as jeopardize the bond between a material and the host structure, something which will be shown to be very important. Therefore, it is important to study the effects of these foreign elements on the behavior of the material which will be used in a particular application. Some elements may be more important than others depending on the operating environment, so these elements should hold the highest interest of the designer.

Chapter 3

Analytical Mathematical Models and Viscoelastic Theory

There have been several analytical methods developed since the late 1950's to predict response of damped systems. Some of the more popular methods include those developed by Ross, Kerwin, and Ungar (Ross, 1959), Mead and Markus (Mead, 1969), DiTaranto (DiTaranto, 1965), Yan and Dowell (Yan, 1972), and Rao and Nakra (Rao, 1974). However, the development of finite element software has increased the accuracy and precision of estimations of the dynamic responses of damped structures. For fairly simple structures, analytical methods can be used as a substitution for finite element predictions. Furthermore, finite element packages are often computationally expensive, something that might not be needed for damping predictions of simpler systems. In this case, a simple code or program can be written implementing an analytical method to derive a simple, sufficiently accurate damping model. As the complexity of the system increases, however, finite element formulations should be strongly considered as the boundary conditions and system parameters may prove too difficult to define using a simple analytical based formulation.

3.1 Ross, Kerwin, and Ungar Damping Model

Ross, Kerwin, and Ungar developed one of the earliest damping models for three-layered sandwich beams based on damping of flexural waves by a constrained viscoelastic layer. They employed several major assumptions, including (Sun, 1995):

- For the entire composite structure cross section, there is a neutral axis whose location varies with frequency

- There is no slipping between the elastic and viscoelastic layers at their interfaces
- The major part of the damping is due to the shearing of the viscoelastic material, whose shear modulus is represented by complex quantities in terms of real shear moduli and loss factors
- The elastic layers displaced laterally the same amount
- The beam is simply supported and vibrating at a natural frequency, or the beam is infinitely long so that the end effects may be neglected

These assumptions apply to any constrained layer damping treatment applied to a rectangular beam. Figure 3.1 shows an example system which the Ross, Kerwin, and Ungar (RKU) equations could be applied to. This laminate beam system is also the lay-up for the cantilever beam used for materials testing later in this report.

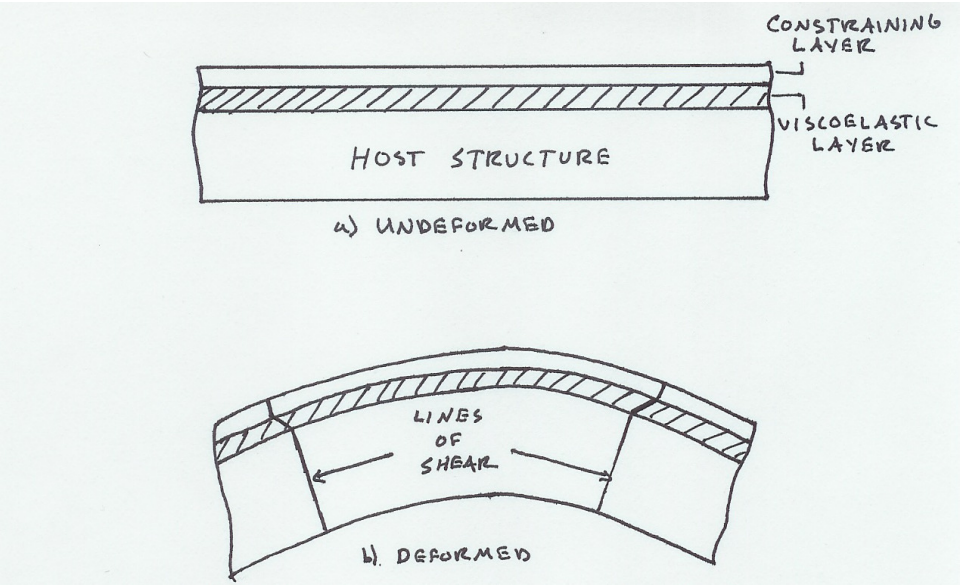

Figure 3.1. Three layer cantilever beam with host beam, viscoelastic layer, and constraining layer clearly defined.

Comparison between experimental data and this theory have shown that results from theory correlate well to experiment (Ross, 1959). The model is represented by a complex flexural rigidity, (EI)*, where the '*' denotes a complex quantity, given by

$$\begin{aligned}(EI)^* &= \frac{E_s h_s^3}{12} + \frac{E_v^* h_v^3}{12} + \frac{E_c h_c^3}{12} - \frac{\frac{E_v h_c^2}{12}(d-D)}{(1+g_v^*)} + E_s h_s D^2 \\ &+ E_v^* h_v (h_{vs} - D)^2 + E_c h_c (d-D)^2 \\ &- \left[\frac{E_v^* h_v (h_{vs} - D)}{2} + E_c h_c (d-D)\right]\left[\frac{(d-D)}{(1+g_v^*)}\right]\end{aligned} \tag{3.1}$$

where D is the distance from the neutral axis of the three layer system to the neutral axis of the host beam,

$$\begin{aligned}D &= \frac{E_v^* h_v (h_{vs} - \frac{d}{2}) + g_v^* (E_v^* h_v h_{vs} + E_c h_c d)}{E_s h_s + \frac{E_v^* h_v}{2} + g_v^* (E_s h_s + E_v^* h_s + E_c h_c)} \\ h_{vs} &= \frac{h_s + h_v}{2} \\ g_v^* &= \frac{G_v^*}{E_c h_c h_v p_1^2} \\ d &= h_v + \frac{h_s + h_c}{2}\end{aligned} \tag{3.2}$$

In these equations E_s, E_v^*, E_c and h_s, h_v, h_c are the elastic moduli and thicknesses of the host structure, viscoelastic layer, and constraining layer, respectively. The term g_v^* is known as the 'shear parameter' which varies from very low when G_v^* is small to a large number when G_v^* is large. The term 'p' within the shear parameter is the wave number, namely the n^{th} eigenvalue divided by the beam length. The shear parameter can also be expressed in terms of modal frequencies by

$$g_v^* = \frac{G_v^* L^2}{E_c h_v h_c \xi_n^2 \sqrt{C_n}}$$
$$\xi_n^4 = \frac{\rho_s b h_s \omega_n^2 L^4}{E_s I_s} \qquad (3.3)$$

where ω_n is the n^{th} modal frequency and C_n are correction factors determined by Rao (Rao, 1974) and are given in Table 3.1.

Table 3.1. Rao correction factors for shear parameter in RKU equations (Jones, "Handbook of Viscoelastic Damping," 2001).

Boundary Conditions	Correction Factor	
	Mode 1	Mode 2+
Pinned-Pinned	1	1
Clamped-Clamped	1.4	1
Clamped-Pinned	1	1
Clamped-Free	0.9	1
Free-Free	1	1

Additionally, a more detailed analysis using the Ross, Kerwin, Ungar (RKU) equations will be presented in the analysis portion of this document allowing for correction factors. This system of equations will be the main method of analysis used in the remainder of this report.

3.2 Beam Theory Methods of Analysis

Several other methods of analysis have been developed by authors like Mead and Markus, DiTaranto, Yan and Dowell, and Rao and Nakra, all of which rely on either Euler-Bernoulli beam theory or principles such as virtual work, often resulting in sixth-order linear homogenous differential equations. Though these analyses are useful in many applications, they are often specific or most easily applied to a special type of boundary condition or loading function. Kalyanasundaram (Kalyanasundaram, 1987)

and Buhariwala (Buhariwala, 1988) also developed and used beam theory models of viscoelastic structures. Kalyanasundaram analyzed and predicted dynamics of viscoelastic structures using the Timoshenko beam method. Buhariwala used d'Alembert's principle and the principle of virtual work to predict dynamics of viscoelastically damped structures. It will be shown that the RKU equations, when used with other vibration analysis tools, are easier to manipulate and provide very simple, sufficiently accurate predictions of structural damping.

3.3 Rayleigh Quotient Analysis

In undamped vibration theory, the Rayleigh Quotient is a useful method for estimation of modal frequencies of a system. The Rayleigh Quotient for an undamped system is given by

$$R[Y_r(x)] = \omega_r^2 = \frac{\int_0^L Y_r(x)\frac{d^2}{dx^2}\left[EI\frac{d^2Y(x)}{dx^2}\right]dx}{\int_0^L m(x)Y_r^2(x)dx} = \frac{V_{MAX}}{T_{REF}} \qquad (3.4)$$

where $Y_r(x)$ is an approximated mode shape, ω is a modal frequency, V_{MAX} is the maximum potential (strain) energy, and T_{REF} is a reference kinetic energy. A complex version of the Rayleigh Quotient was developed by Torvik (Torvik, 1996), where he used complex approximations of the mode shapes. The resulting Complex Rayleigh Quotient is derived from the equations of motion and given by

$$\Omega^2\mathbf{M}\{u\} = \mathbf{L}\{u\}$$

$$\Omega^2 = \frac{\int_0^L \{\bar{u}\}^T\mathbf{L}\{u\}dx}{\int_0^L \{\bar{u}\}^T\mathbf{M}\{u\}dx} \qquad (3.5)$$

where **M** and **L** are complex matrix symmetric linear operators which include spatial derivatives. The terms in these matrices depend on the derivation of the equations of motion of the system. The second equation in (3.5) is the complex Raleigh Quotient. The {u} terms are vectors containing complex mode shapes. If real quantities are used in the Complex Rayleigh Quotient (CRQ), the equation reduces to modal strain energy, or the real form of the Rayleigh Quotient.

3.4 Fractional Calculus Analysis

Fractional calculus and the fractional derivative were developed by Liouville in a paper from 1832. Fractional calculus is a branch of mathematics which studies the possibility of taking real number powers of differential operators. This concept can also be applied to viscoelastic analysis as used by Bagley and Torvik (Bagley, 1985). It is also the primary method of analysis used by Jones, and Nashif and Henderson (Nashif, 1985). The foundation of the fractional calculus model is found in accepted molecular theories governing mechanical behavior of viscoelastic media (Bagley, 1985). The analysis of structural responses can be calculated for any loading having a Laplace transform. Thus, the responses are always real, continuous, and causal functions of time (Bagley, 1985, Jones, 2001). When compared to other current methods, the fractional calculus model has two significant advantages. First, there are not a large number of derivative terms as with the method of trying to relate time dependent stresses and strains through time derivatives acting on stress and strain fields. Second, a complex frequency dependent modulus, as in the Rayleigh quotient method, often does not satisfy specific mathematical relationships between the real and imaginary parts of the modulus.

3.5 Partial Viscoelastic Treatments

Damping treatments can also be applied in a partial manner, namely, to specific points in a structure rather than the entire structure. An analysis of partially damped structures was developed by Moreira et al. (Moreira, 2006). Partial constrained layer damping treatments have two significant advantages, they lower additional mass and stiffness, and more importantly can be just as effective at damping as a complete treatment if the correct application areas are targeted. Moreira found that if the viscoelastic layer is located near a neutral plane of the structure (i.e. sandwich type structures) the layer must be placed on nodal areas where shear deformation reaches a maximum on the neutral axis. Alternatively, if the viscoelastic layer is located far from the neutral plane (i.e surface treatments), more deformation is expected on anti-nodal areas since flexural deformation of the host structure reaches a maximum (Moreira, 2006). Intuitively, this makes sense because the primary mechanism of viscoelastic damping is shear. Thus, if damping material is applied to host structure areas having the highest surface strains, the partial treatment will utilize the areas of the structure having the majority of the strain energy within the structure, resulting in maximized damping for a partial treatment. Moreira's method utilizes an energy balance between the strain energy of the entire structure and the strain energy of the treated area. This ratio is deemed the Modal Strain Energy Ratio, given by

$$MSER = \frac{\{\phi\}_r^T [K_c] \{\phi\}_r}{\{\phi\}_r^T [K] \{\phi\}_r} \qquad (3.6)$$

Where $\{\phi\}_r$ is the r^{th} modal shape vector, [K] is the finite element stiffness matrix for the host structure, and $[K_c]$ is the stiffness matrix of the structure with applied viscoelastic

treatment. This ratio should, in general, be maximized so that the modal strain energy of the covered area is as close to the modal strain energy of the entire structure. However, this is somewhat difficult because the coverage areas depend on the mode of vibration. Therefore, it is difficult to design an effective partial viscoelastic treatment for a broadband application. Though this analysis seems fairly straight-forward, deriving the stiffness matrices in the Modal Strain Energy Ratio is complex for more complicated structures and is best solved using finite element software.

Chapter 4

Damping Considerations for Landing Gear Applications

The design of landing gear with respect to structural damping using viscoelastic materials poses a unique kind of problem. Traditional landing gear often implement shock absorbers and dashpots. However, these components can be bulky and heavy, affecting the aerodynamic efficiency and flight time of aircraft. Additionally, there are usually a host of customer requirements specific to the project and application which generally govern the scope and intensity of the design phase of the landing gear. With these factors in mind, the role of a damping treatment can be discussed in more detail.

4.1 Impact of Aerodynamics and Weight on Damping Treatment

Aerodynamics and weight are two significant concerns when designing landing gear. The gear of any aircraft should be streamlined and optimized so that the gear is not only as lightweight as possible, but also has a minimal frontal profile to minimize drag during flight. Lightweight materials should be chosen when possible so that the weight addition of the gear to the aircraft is at a minimum, effectively increasing the maximum flight time of the aircraft.

In this particular application, the damping treatment should be as thin and lightweight as possible, while still contributing a large amount of damping to the gear. This significantly narrows the field of damping materials which should be used, effectively eliminating high density polymers, though their damping may be quite significant over the small range of effective vibration modes a landing gear will experience during landing. Additionally, this implies that a viscoelastic polymer should

be chosen which has the highest loss factors and lowest shear modulus available at lower vibration modes, further narrowing the available selection of materials. Additionally, viscoelastic materials generally have better damping at higher modes because the strain rates, which depend on modal frequencies, are higher. The configuration of the viscoelastic material will be dependent on the geometry of the host structure. The host structure needs to be properly designed so that it not only has a minimal frontal profile, but that its profile is minimally affected by the addition of a damping treatment.

4.2 Landing Environment on Damping Considerations

The damping treatment for the landing gear discussed in this report is to be applied to a 400 pound fixed wing unmanned aerial vehicle which operates in all forms of weather conditions, including rain, sleet, snow, sand, foreign chemicals, direct heat or sunlight. Additionally, because the vehicle is unmanned, there are no pilot corrections for terrain or surface variability. The aircraft could land on grass, concrete, asphalt, packed dirt, or even snow or ice, each having different friction and coefficients of restitution.

Many different viscoelastic polymers have various resistances to the elements. As previously mentioned in section 2.1, viscoelastic polymers and their properties can be engineered and manufactured for a multitude of specific applications. Fortunately, the same is true for environmental resistance. Many viscoelastic polymers are designed specifically for outdoor environments and are resistant to harsh chemicals like alkalis or mild acids, moisture, oils and solvents, and some are even flame retardant.

An unmanned aerial vehicle is often subject to vehicle dynamics on the extreme boundaries of its design envelope. The UAV must calculate and act on flight speed,

approach angle, wind conditions, and flap adjustments in some of the most adverse environmental conditions. This often results in the aircraft having a 'heavy' landing causing a higher than normal impact load on the landing gear and fuselage. Thus, a viscoelastic treatment should be designed in such a way as to account for factors of safety and extreme landings. The treatment should be sparse enough as to not significantly increase the weight and aerodynamic drag of the aircraft, but also robust enough to handle the most extreme vibration a landing gear will see in the most extreme operating conditions.

Chapter 5

Instrumentation and Data Acquisition

There are two testing and data acquisition systems used in this research project. The first is a cantilever beam system for characterization of various damping materials used as prospective solutions for damping a cantilever type spring design for aircraft landing gear. The second is a cyclic loading machine used to extract the viscoelastic properties, namely the complex moduli, of various materials.

The data acquisition system for the damping characterization rig is presented in figures 5.1a and 5.1b. Figure 5.1a shows the general flow of information through the data acquisition system (DAQ) while Figure 5.1b shows the actual components of the DAQ.

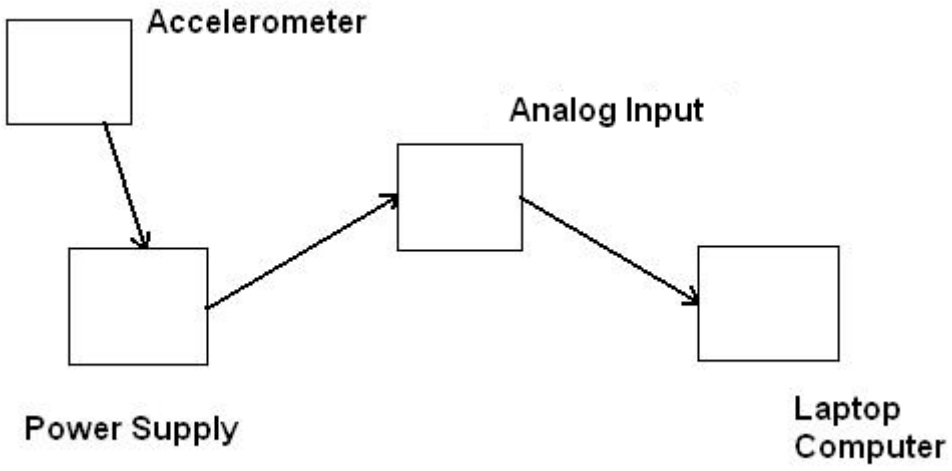

Figure5.1a. Shows the flow of information from the transducers the signal express software.

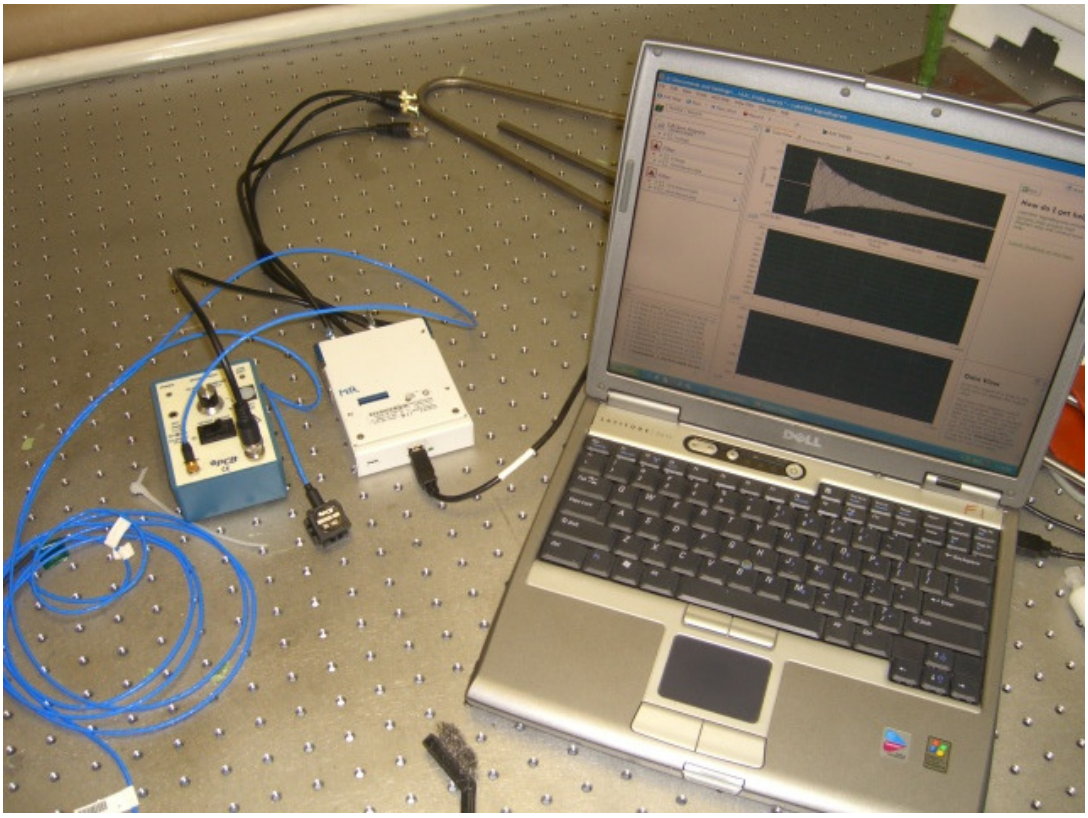

b)

Figure 5.1b. Shows the DAQ in its entirety with all components.

The transducers used were PCB (Piezoelectronics) model 3801D1FB206/M001 single axis accelerometers shown in Figure 5.2.

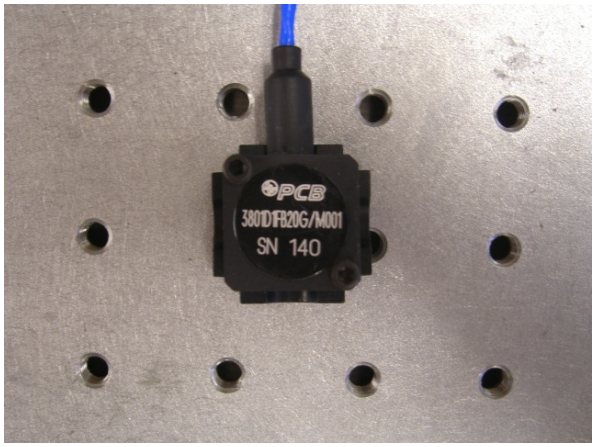

Figure 5.2. Photograph of accelerometers used in cantilever beam testing.

The accelerometers were powered by PCB model 478A01 tunable power supplies. The power supplies are tunable in that they can be adjusted to offset the analog voltage seen by the acquisition program. A photograph of the power supplies is shown in Figure 5.3.

Figure 5.3. Photograph of power supplies used to power accelerometers.

The power supplies fed analog signals through a 4-channel National Instruments (NI) 9239 analog input connected to a Hi-Speed NI USB carrier, shown in Figure 5.4.

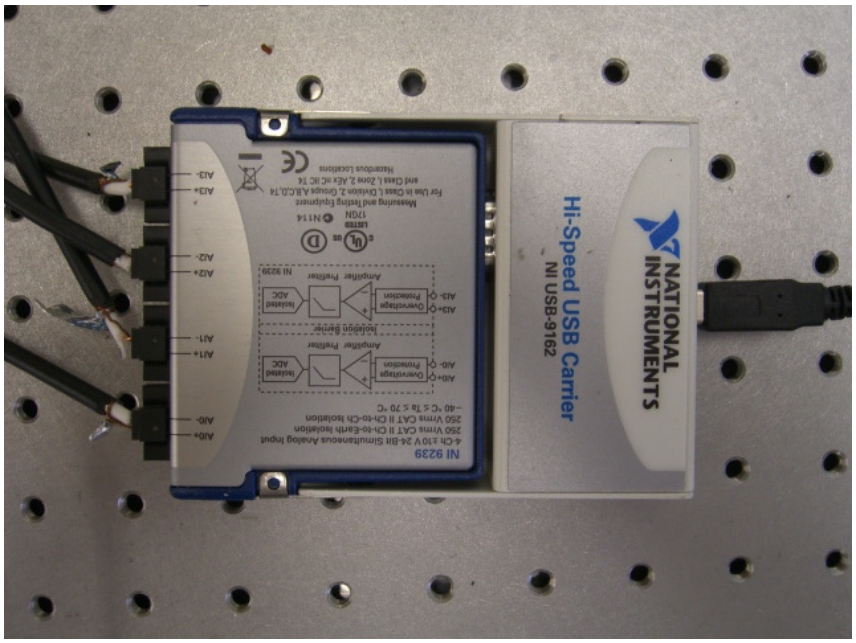

Figure 5.4. Four channel analog input and NI USB carrier.

Finally, LabVIEW's Signal Express 8.0 was used to collect and analyze data from the accelerometers. Signal Express was configured to collect 6000 samples at 1000 Hz for data analysis.

Viscoelastic material samples were tested using an ElectroPuls E1000 cyclic loading machine shown in figure 5.5a and 5.5b. Each specimen was loaded into the grips of the machine (Figure 5.5b) and cyclically loaded in tension and/or compression to generate stress-strain plots of the loading history of each viscoelastic material. The ElectroPuls machine is capable of controlling the strain rate and strain amplitude of each test, with an upper frequency limit of 300 Hz. Stress-strain behavior and the extraction of viscoelastic material properties from tests conducted with the ElectroPuls machine are explained in Chapter 6.

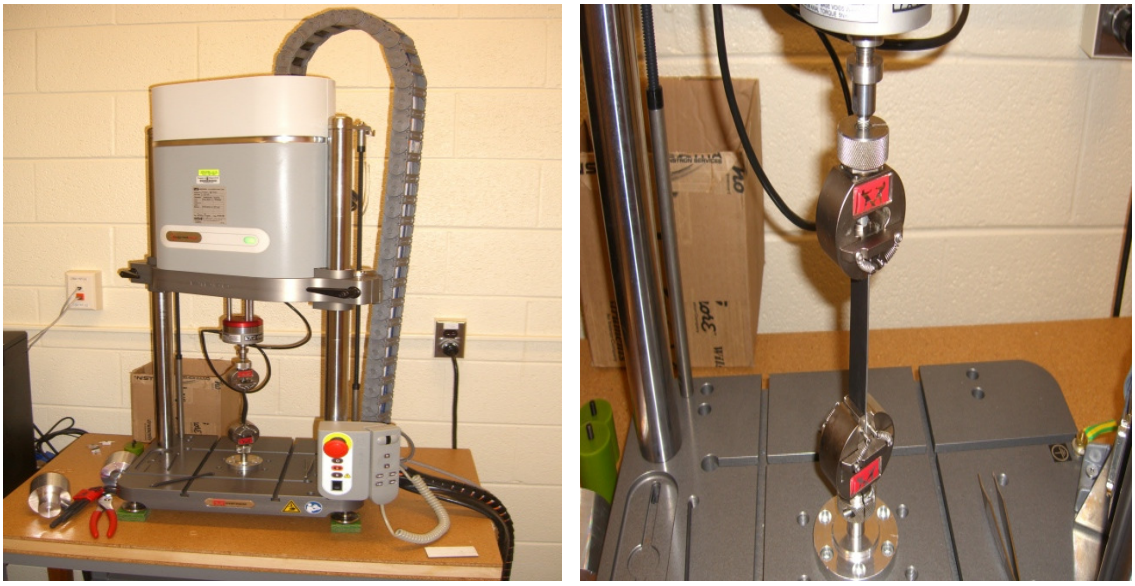

a) **b)**

Figure 5.5. a) Photograph of ElectroPuls E1000 cyclic loading machine. **b)** Photograph of ElectroPuls E1000 grips with sample viscoelastic specimen loaded for testing.

Chapter 6

Experimental Determination of Viscoelastic Material Properties

The stress-strain relationship for a viscoelastic material under cyclic loading takes on the form of an ellipse shown in Figure 6.1.

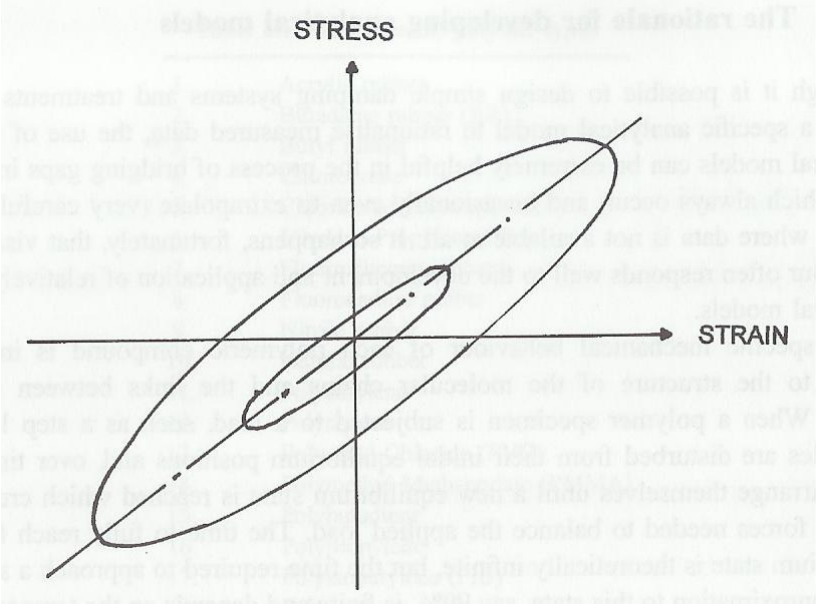

Figure 6.1. Stress-Strain hysteresis loop for linear viscoelastic material (Jones, "Handbook of Viscoelastic Damping," 2001).

The stress-strain relationship for a linear viscoelastic material is given by

$$\sigma = (E'+iE'')\varepsilon = E'\varepsilon + \frac{E''}{|\omega|}\frac{d\varepsilon}{dt} \qquad (6.1)$$

since $i|\omega|\varepsilon = \frac{d\varepsilon}{dt}$ for harmonic motion (Sun, 1995). Again, note the strain rate, or frequency, dependence on the stress within the viscoelastic material not found in stress-strain relationships for metals in the elastic region. As mentioned in section 2.1.1, the loss factor is the ratio of loss modulus (imaginary part of the complex modulus) to the storage modulus (real part of complex modulus). In the above equation, E' represents the

storage modulus, synonymous with the elastic modulus for metals. Sun and Lu explain that the area enclosed by the ellipse in Figure 6.1 is equal to the energy dissipated by the viscoelastic material per loading cycle. Additionally, the slope of the major axis of the ellipse in Figure 6.1 is representative of the storage modulus of the viscoelastic material. Thus, E' is easily found from the hysteresis plot of stress and strain.

From Figure 6.1, it should be noted that the general shape of the ellipse does not change for small variations of the maximum strain amplitude, ε_0. However, the shape does change as the loss factor changes (i.e. the inner ellipse and outer ellipse in Figure 6.1 are tests at the same frequency but different strain amplitudes). Thus, the ratio of the minor axis to major axis of the ellipse can be used as a measure of damping (Jones, 2001). However, this ratio is not the loss factor of the material. To find the loss factor of the material, the data generated using the ElectroPuls E1000 can be used to find the energy dissipated per cycle of loading for each viscoelastic material. The energy dissipated is given by the path integral

$$W_d = \oint \sigma d\varepsilon = \int_0^{2\pi/\omega} \sigma \frac{d\varepsilon}{dt} dt = \pi E'' \varepsilon_0^2 \qquad (6.2)$$

It is also important to find the peak potential energy within the material during a loading cycle. Peak potential energy is given by

$$U = \frac{1}{2} E' \varepsilon_0^2 \qquad (6.3)$$

From the energy dissipated per cycle and the peak potential energy the loss factor can be found to be

$$\eta = \frac{W_d}{2\pi U} = \frac{E''}{E'} \qquad (6.4)$$

Another method of measuring the properties of viscoelastic materials was formulated by Lemerle (Lemerle, 2002), but the analysis used by Sun and Lu is accurate and relatively simple by comparison.

6.1 Viscoelastic Materials Testing

The design of this landing gear system, as in many other engineering projects, is heavily dependent on customer requirements. Weight, aerodynamics, cost, and most significantly reliability and operability are all serious concerns which must be accounted for during the design phase. Cost, reliability, and predictability, in particular, are the main foci of this section. Eight different damping materials where chosen and tested, each having different material properties and durometers. Seven of these materials were chosen because they are common rubbers, available at almost any polymer distributer. Additionally, because they are common, they are often the cheapest because they are manufactured in the highest quantities. These common rubbers have little to no damping property documentation and are generally used for simple vibration isolation applications. After testing, all materials were found to be sufficiently predictable in their dynamics, and all are very reliable because of their high durability.

The materials chosen for testing were various grades of butyl, nitrile, vinyl, silicon, and SBR rubbers. Table 6.1 lists all materials tested as well as a summary of their known preliminary properties before testing.

Table 6.1. Materials tested and analyzed for landing gear applicability.

Materials Tested	Durometer	Density [g/cc]
Butyl Rubber	60A	1.25
Silicone Rubber	30A/50A	1.54
SBR Rubber	70A	1.61
Buna-N/Nitrile Rubber	40A/60A	
Vinyl Rubber	70A	
Dyad 601	44A	1.12

6.1.1 Modal Analysis of Undamped Cantilever Beam

Prior to each material being tested, the modal frequencies of the undamped cantilever beam, shown in Figure 6.2, must be determined so that a modal analysis prediction of damping can be executed. The following modal analysis was conducted for a beam having a .375 inch square cross section composed of 4140 "Chrome-Moly" steel ($\rho = 7860\frac{kg}{m^3}$). The beam was 14 inches in length and had a mass per unit length of $.7135\ \frac{kg}{m}$.

Figure 6.2. Undamped cantilever beam used for damping material characterization.

In this order, once the modal frequencies are known, the materials can be tested at these frequencies, their properties (Moduli and loss factors) determined, and thicknesses of damping layers found using a MATLAB program (see appendix A) to predict effective damping at each mode. Lastly, actual tests can be carried out using the thicknesses predicted from MATLAB to find a correlation between theoretical and experimental results.

To find the modal frequencies of an undamped cantilever beam with a tip mass, simple modal analysis can be used. By using a cantilever beam mode shape (Meirovitch, 2001),

$$Y_r(x) = A_r \sin \beta_r x + B_r \cos \beta_r x + C_r \sinh \beta_r x + D_r \cosh \beta_r x \qquad (6.5)$$

where A, B, C, and D are modal constants of each mode shape Y(x), approximated modal frequencies can be found. The parameter β is related to the modal frequency by

$$\beta_r^{\,4} = \frac{\omega_r^2 m}{EI} \qquad (6.6)$$

By using the boundary conditions of a cantilever beam with a tip mass, namely

$$\begin{aligned} &Y(0) = 0 \\ &Y'(0) = 0 \\ &Y''(L) = 0 \\ &Y'''(L) = -\frac{M}{mL}\beta^4 Y(L) \end{aligned} \qquad (6.7)$$

with each of these boundary conditions synonymous to the displacement, rotation, moment, and shear within the beam, respectively, a set of four equations can be formulated to solve for the constants A, B, C, and D for each mode. Additionally, these boundary conditions assume that the tip mass has very small rotary inertia compared to the beam. This set of equations is found by differentiating equation (6.5) three times and applying the appropriate boundary condition. The resulting set of equations is

$$\begin{bmatrix} 0 & 1 & 0 & 1 \\ 1 & 0 & 1 & 0 \\ -\sin\beta L & -\cos\beta L & \sinh\beta L & \cosh\beta L \\ -\cos\beta L + \bar{M}\,\beta L\sin\beta L & \sin\beta L + \bar{M}\,\beta L\cos\beta L & \cosh\beta L + \bar{M}\,\beta L\sinh\beta L & \sinh\beta L + \bar{M}\,\beta L\cosh\beta L \end{bmatrix} \begin{Bmatrix} A \\ B \\ C \\ D \end{Bmatrix} = 0$$

In this set of equations $\bar{M} = \frac{M}{mL}$ where M is the mass of the tip mass, m is the mass per unit length of the cantilever beam, and L is the length of the beam. By taking the determinant of the leading matrix in the above equation set and setting that determinant equal to zero, the roots of the resulting sinusoidal equation will yield the βL values for which the equation set is satisfied. These roots are the non-trivial solutions which can be

used to find the modal frequencies of the cantilever beam shown in Figure 6.2. If $\bar{M}$ =1, that is the mass at the tip is equal to the mass of the beam, the resulting modal frequencies are presented in Table 6.2 for the first five modes.

Table 6.2. Modal frequencies of first five modes for cantilever beam with tip mass M=mL.

Mode	Beta_L	Modal Frequency (rad/s)	Modal Frequency (Hz)
1	1.248	177.128	28.19082057
2	4.0312	1848.111	294.1362495
3	7.1341	5783.74	920.5115881
4	10.2566	11883.378	1891.299947
5	13.3878	20383.47	3244.132748

Chapter 7

Testing of Materials Using ElectroPuls E1000 Cyclic Loading Machine

A total of seven materials were tested in the ElectroPuls E1000 cyclic loading machine at frequencies of 1, 5, 10, 15 and 28.19 Hz. The first four frequencies, namely 1, 5, 10, and 15 Hz, where selected for testing to establish trends and ensure that the data for the first modal frequency was accurate. From the modal frequencies listed in Table 6.2, 28.19 Hz corresponds to the first modal frequency of the cantilever beam analyzed in section 6.1.1. However, the ElectroPuls has a maximum loading frequency of 100 Hz where sufficient strains within the sample can be measured accurately. Thus, only the data for the first modal frequency of each material sample will be analyzed in the following sections. This is sufficient, because when applied to the aircraft landing gear, the most obvious, and therefore more prominent, dynamics will occur at lower frequency, much lower than 294 Hz at the second mode. It is also reasonable to say that so long as the material is not operating within the glassy region of frequency and temperature, damping of vibrations at the second mode and above will be much greater than damping at the first mode. Thus, the damping values presented for the first modes of vibration in the materials will generally be lower than the subsequent modes, making the damping of first mode vibrations the driving factor in the design of the gear.

The storage modulus, shear modulus, and loss factor were determined for each material at each frequency. The method of analysis was generalized in section 6.0, and will be extended to the method of parameter determination for each material in the following sections. One of the seven materials exhibited nonlinear viscoelastic behavior,

so variations or approximations in the method in section 6.0 were made to approximate material properties. Additionally, for the cyclic loading tests at 28.19 Hz, the primary frequency of interest, the materials were assumed to behave as linearly viscoelastic materials, so the analysis used in section 6.0 sufficiently describes the relationship between the stress and strain of the viscoelastic material.

7.1 Analysis Methodology and Testing Assumptions

Each test sample was loaded into the ElectroPuls machine with a configuration shown in Figure 5.6b. Upon testing the sample at different frequencies, Microsoft Excel was used to analyze the data taken by the transducers within the ElectroPuls. The generated data consisted of time, load, and position. The position is in reference to the position of the grips used to secure the test article during data sampling. The load and position measured by the ElectroPuls were then converted to engineering stress and strain within Microsoft Excel. For this conversion, several major assumptions had to be made:

1. The stress is uniform throughout the cross section of the material and the approximation that stress is equal to the load divided by the original cross sectional area hold
2. The strain is uniform throughout the length of the specimen and is equal to the change in position of the grips divided by the original length of the specimen.

Neither of these approximations is entirely accurate for reasons which will be discussed. However, for the purposes of this report, they are sufficient to provide accurate *relative* results. The purpose of this testing is not to produce and publish exact material data for each material. This would have been possible if strain gauges or extensometers were available to accurately measure the strain within the sample. However, it is the purpose

of this testing to provide a relative comparison of several damping materials. Though the material data may not be exactly accurate due to the assumptions made above, each material was tested and analyzed using the same methods and assumptions. It inherently follows that each material can be compared with all other materials because they all fall under the same assumptions and experimental error. Thus, the best damping materials within the set of those tested can be established, though the data may not be as accurate if more precise testing methods could have been used.

The assumptions stated above are not entirely accurate for several reasons. The first is that the material is being held in place by grips which produce a lateral stress at locations near the grips. Thus, the material can no longer be assumed to be in a perfect state of uniaxial stress. However, at locations far from the grips (center of the test specimen), the assumptions are reasonably accurate. The second reason is that no material is completely homogeneous or isotropic, particularly polymers. There are always variations in the structure of a material sample no matter how precise the manufacturing methods. Unlike metals, polymers do not have predictable patterns of microstructure. Rather, they are a mixture of long entangled chains of random order and length. For the purposes of this report, it is assumed that each material is homogeneous and isotropic, so only two material properties are needed to describe a state of stress and strain. These material properties are the elastic or storage modulus, and Poisson's ratio, which for most of the test materials is assumed to be very close to .5. Because the materials are assumed homogeneous and isotropic, once the elastic modulus, or storage modulus, is known from the tests, the shear modulus can be found from

$$G' = \frac{E'}{2(1+\upsilon)} \qquad (7.1)$$

This equation should be found in any undergraduate mechanics of materials textbook.

As a further disclaimer, it should be noted that in no way does the data presented in the following sections exactly match the material properties of each material. Rather, the data presented in the following sections is to establish relative trends and approximate numbers so that the best damping material to apply to an aircraft landing gear, the ultimate goal of this report, can be identified.

7.1.1 Extracting Data using Microsoft Excel

As mentioned in section 7.1, during each test, data was recorded to Microsoft Excel for analysis. After the conversion of load and position to stress and strain, respectively, analyses had to be carried out to find the work done per cycle, the storage modulus, maximum strain amplitude, and loss factor using the theory presented in section 6.0. However, direct integration to find the work done by the viscoelastic material, or energy dissipated as heat, per cycle is impossible because of the nature of the data taken. In order to find the energy dissipated per cycle, equation (6.2) in section 6.0 is equivalent to

$$W_d = \oint \sigma d\varepsilon = \sum_{i=1}^{N} (\sigma_{i+1} - \sigma_i)\Delta\varepsilon_i = \sum_{i=1}^{N} (\sigma_{i+1} - \sigma_i)(\varepsilon_{i+1} - \varepsilon_i) \qquad (7.2)$$

where N is the number of samples taken and σ_1 is a static pre-stress on the material.

The storage modulus of the material at a given frequency (independent of strain amplitude) is found by examining an engineering stress vs. strain plot. The storage modulus is the linear trend of the data, shown in Figure 7.1, given by a trend line. The

storage modulus is equivalent to the slope of the major axis of the ellipse generated by the loading of the material.

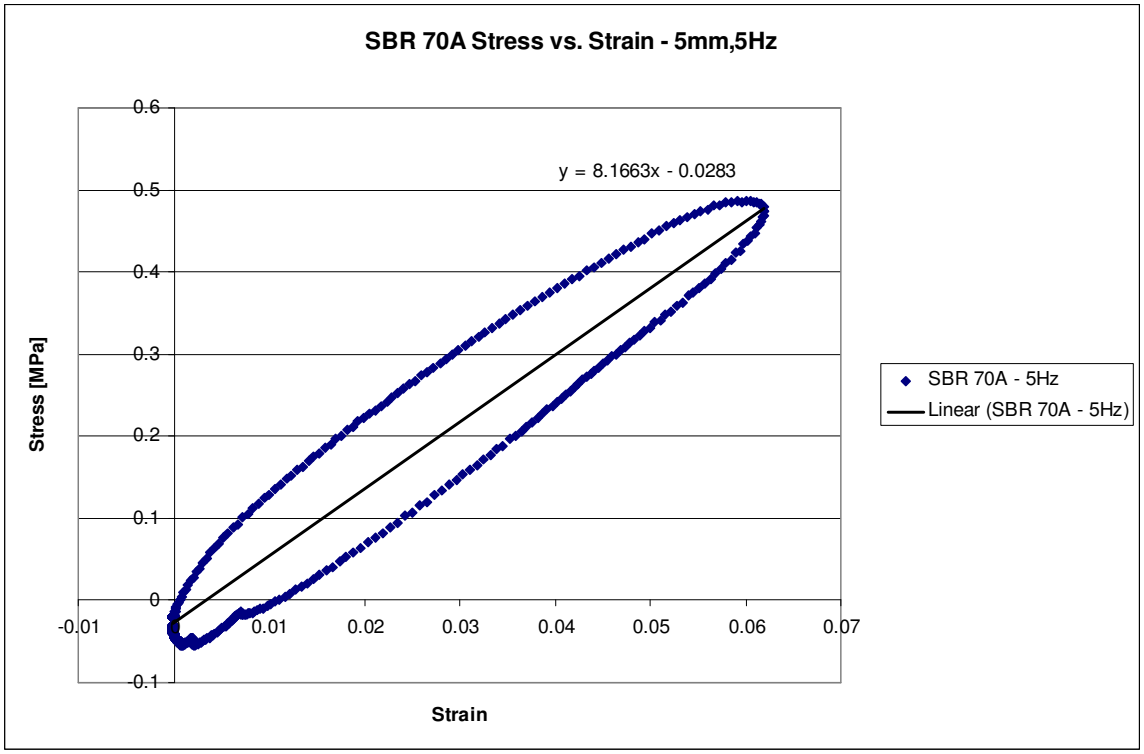

Figure 7.1. Example plot of stress and strain for SBR 70A Rubber. Trend line slope gives storage modulus.

Sample loading curves for a material at two different frequencies are shown in Figures 7.2a and 7.2b. Additionally, the corresponding stress vs. strain curves for Figures 7.2a and 7.2b are shown in Figures 7.3a and 7.3b, respectively. This illustrates how the shape, and inherently area, of the ellipses change with varying frequency. As the ratio of the minor to major axes of the ellipse changes with frequency, so does the loss factor. However, a change in strain amplitude does not have an impact on the damping factor of a material so long as the frequency is held constant.

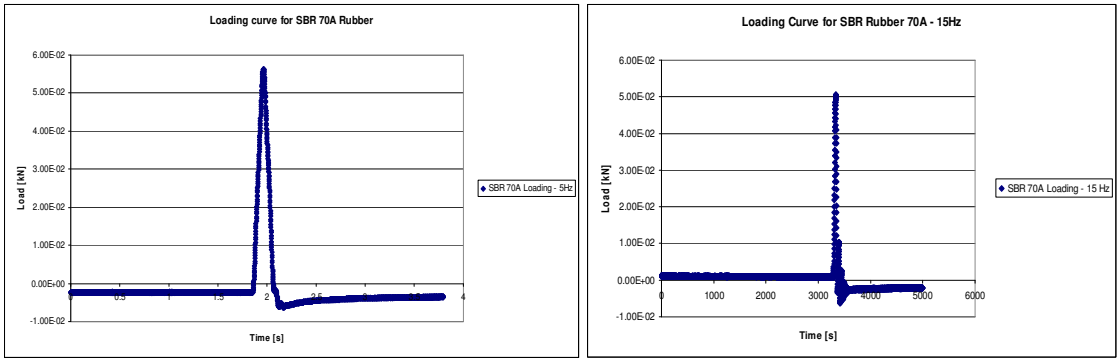

a) **b)**

Figure 7.2. **a)** Load versus time plot at low frequency. **b)** Load versus time plot at high frequency

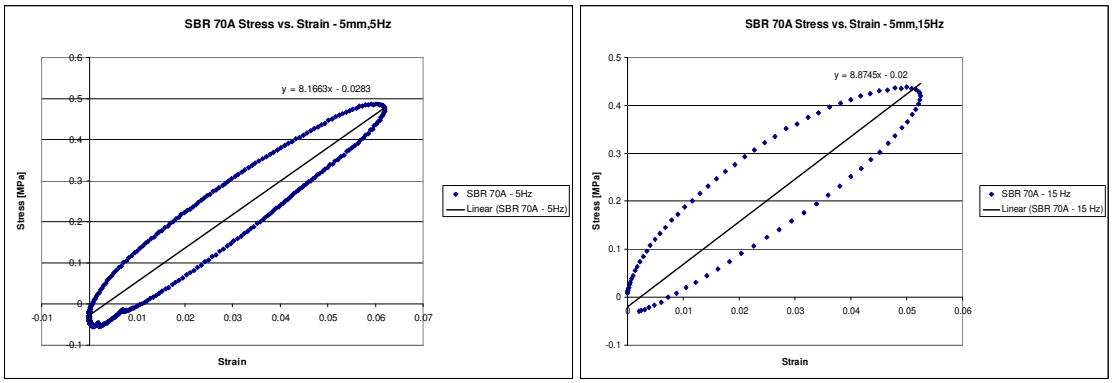

a) **b)**

Figure 7.3. **a)** Stress versus strain plot for Figure 7.2a. **b)** Stress versus strain plot for Figure 7.2b.

7.2 Butyl 60A Rubber Testing

Butyl rubber is a synthetic rubber produced by polymerization of about 98% isobutylene with about 2% of isoprene. Butyl rubber is also known as polyisobutylene or PIB. It has excellent impermeability and its long polymer chains give it excellent flex properties. Butyl is often used in making adhesives, agricultural chemicals, fiber optic compounds, caulks and sealants, cling films, electrical fluids, lubricants such as 2 cycle engine oil, as a gasoline/diesel fuel additive, and even chewing gum. The first major application of butyl was tire inner tubes because of its excellent impermeability to air. It was chosen for testing because it is very common and extremely cheap, while still providing excellent flexural and damping properties.

A sample of butyl rubber having a rectangular cross section was loaded into the ElectroPuls E1000 and loaded at 1, 5, 10, 15, and 28.19 Hz. As discussed in section 7.1, storage modulus and loss factor data were found from the data generated by the ElectroPuls machine. Table 7.1 shows the stiffness and loss factor data at the frequency listed above.

Table 7.1. Butyl material properties as a function a frequency.

Frequency [Hz]	Storage Modulus [MPa]	Shear Modulus [MPa]	Loss Factor
1	5.5556	1.889659864	0.1121
5	6.2841	2.13744898	0.14299
10	6.6737	2.269965986	0.1841
15	7.6246	2.593401361	0.2415
28.19	8.5503	2.908265306	0.4332

Furthermore, Figure 7.4 shows the trends of loss factor and storage modulus with frequency.

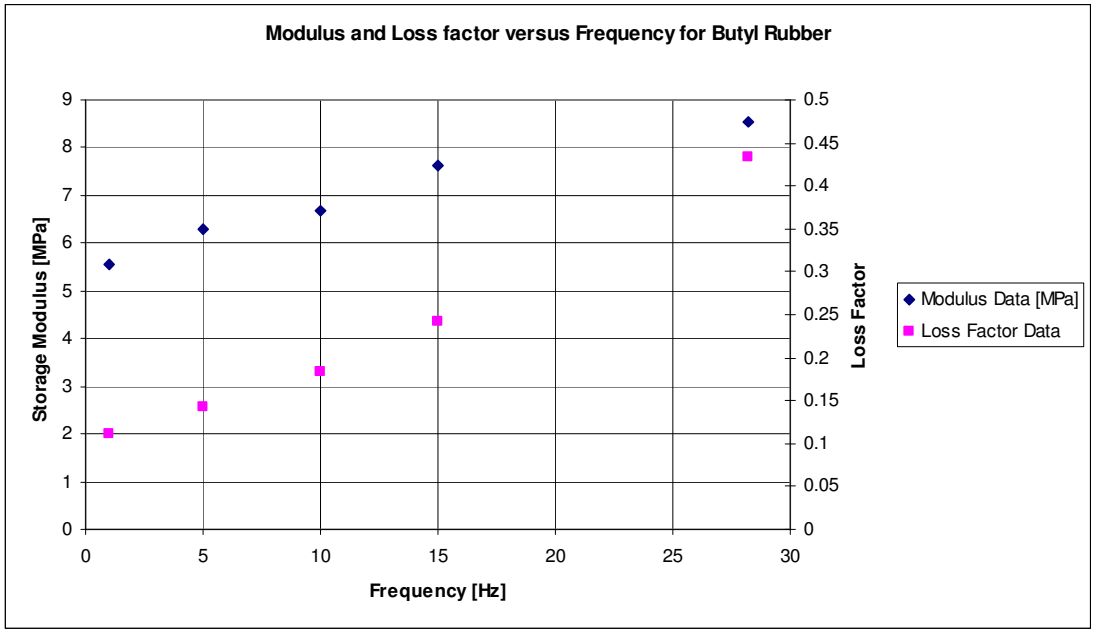

Figure 7.4. Storage Modulus and Loss Factor data for butyl rubber. Plot shows data in Table 7.1.

It is seen from Figure 7.4 that both the storage modulus and loss factor increase with increasing frequency. Over this relatively small frequency range, the loss factor almost quadruples its value as the frequency is increased from 1 Hz to 28.19 Hz. The storage modulus of the sample also sees fairly significant increases from 5.55 MPa to 8.55 MPa, about 1.5 times the original value at 1 Hz. Based on the low frequency and moderate temperature (the materials were tested at room temperature of about 70 degrees), the material is most likely operating in its rubbery region. Butyl rubber typically has a service temperature range of about -13 – 248 degrees Fahrenheit. At higher frequency it should be expected that the loss factor will continue to rise along with the storage modulus into the transition region, where the loss factor will reach a maximum value and begin to fall towards the glassy region. The storage modulus will continue to rise through the glassy region and taper to a maximum value within the transition region as the frequency is increased.

At the first modal frequency of the undamped cantilever beam, butyl was found to produce significant damping. The stress-strain data for a one second time interval with tensile loading at 28.19 Hz is shown in Figure 7.5. The hysteresis loop is shifted upwards along the stress axis because of a small static preload within the sample.

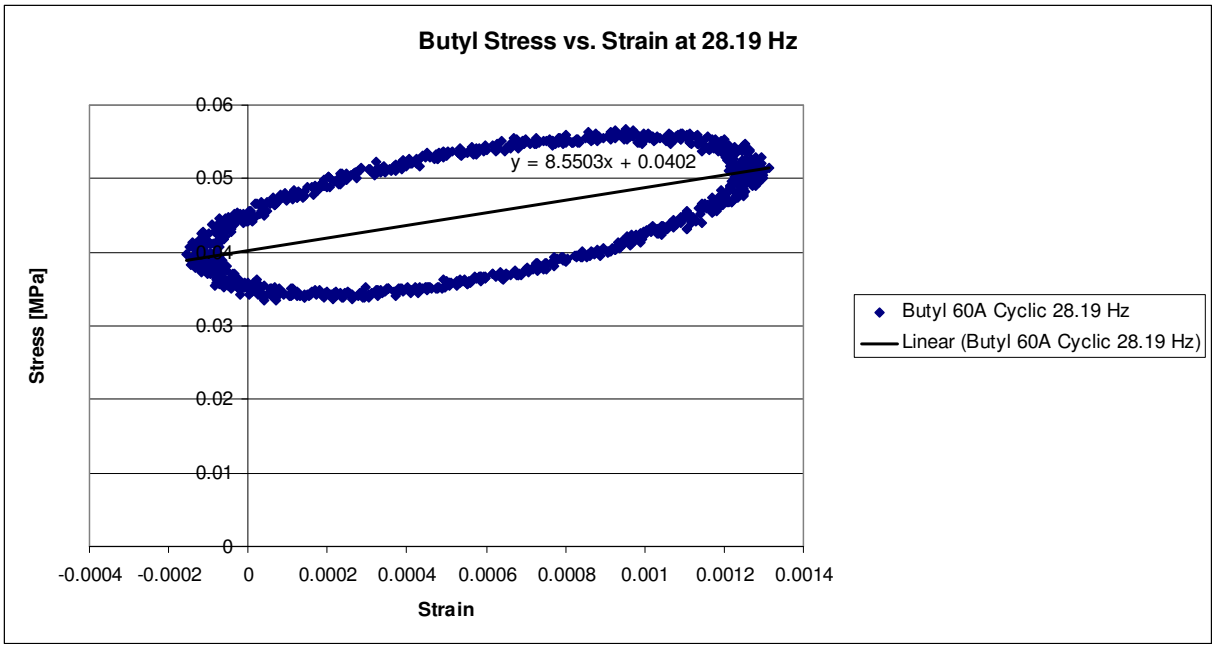

Figure 7.5. Hysteresis plot for Butyl 60A rubber at 28.19 Hz.

The slope of the trend line shown in Figure 7.5 is representative of the storage modulus of the butyl sample at the first modal frequency. Additionally, in order to formulate a value for the loss factor using the theoretical analysis presented in sections 6.0 and 7.1.1, one loading cycle of the material had to be isolated, namely an additional parameter in equation (6.4) where the energy dissipated over the entire time interval (1 second) is over 28.19 cycles. Thus, the average total energy dissipated over one cycle is equal to the total energy dissipated over one second divided by the frequency. That is

$$\eta = \frac{W_d}{2f\pi U} = \frac{E''}{E'} \qquad (7.3)$$

where now W_d is the energy dissipated over a full one second interval or 28.19 loading cycles. W_d is still calculated using equation (7.2) in section 7.1.1.

7.3 SBR 70A Rubber Testing

SBR rubber, short for styrene-butadiene rubber, is a synthetic copolymer rubber developed in the 1930's. It is produced in a similar polymerization process as butyl rubbers, but of a slightly different molecular make-up. It is one of the more cost effect rubbers to manufacture and was first produced to account for the dwindling natural rubber resources. SBR rubber is used in automotive tires, belts and hoses, for machinery and engines, gaskets, and break and clutch pads for vehicles. It is also often found in some children's toys, caulking compounds, sponges, and floor tiles. It is one of the more widely produced rubbers in the world and, like butyl, was chosen for testing because of its low cost and relatively high flexural and damping properties. From a manufacturing standpoint, SBR is as easy to produce as butyl rubber, but often for a much cheaper price because of the materials used and the fact that it is a copolymer, needing very little of the more expensive rubber materials to make it an effective rubber.

As with the other six damping materials, a sample of SBR having rectangular cross section was loaded into the ElectroPuls machine and loaded at 1, 5, 10, 15, and 28.19 Hz. Table 7.2 gives the storage moduli and loss factors at these frequencies.

Table 7.2. SBR stiffness and loss factor data for cyclic loading tests.

Frequency [Hz]	Storage Modulus [MPa]	Shear Modulus [MPa]	Loss Factor
1	7.2807	2.476428571	0.0647
5	8.1663	2.777653061	0.0826
10	8.5415	2.905272109	0.09335
15	8.8745	3.018537415	0.1163
28.19	12.331	4.194217687	0.2374

Figure 7.6 gives a graphical representation of the data presented in Table 7.2.

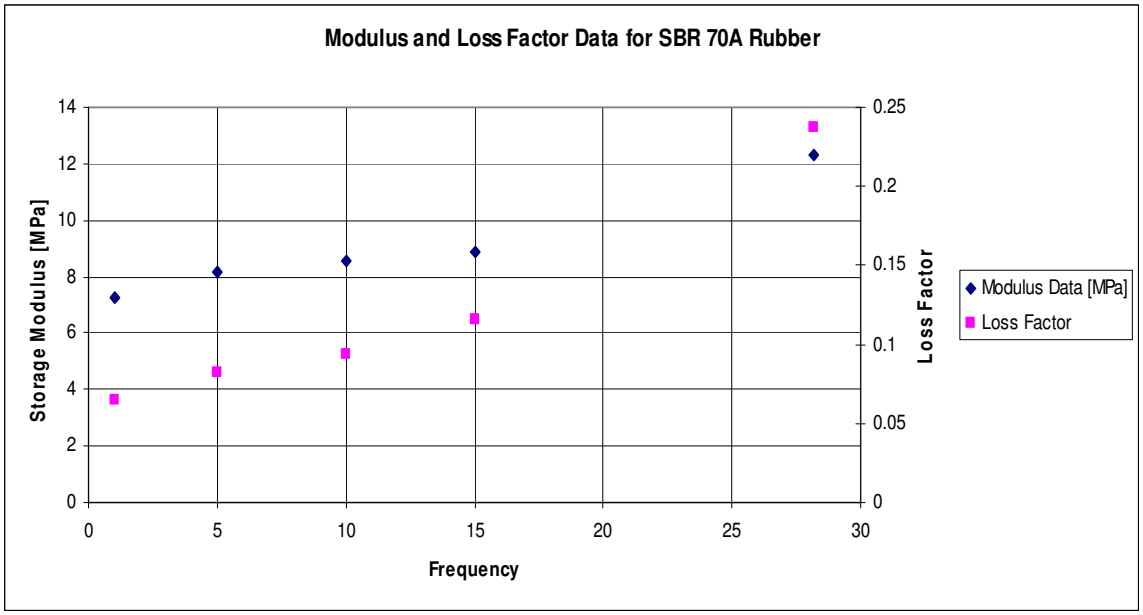

Figure 7.6. Storage Modulus and Loss Factor plot for SBR rubber as a function of frequency.

From Table 7.2 and Figure 7.6 it can be seen that, like butyl, there is a significant increase in both the storage modulus and loss factor as the frequency is increased. However, the maximum damping factor, the parameter of most significant interest, hits a peak value of only .2374 within the testing frequency range. This value is about half that of butyl, making it a relatively poor choice for a landing gear application when compared to other materials tested. Notice, however, that the measured storage modulus values for SBR are significantly higher than that for butyl. This is expected because the SBR has a durometer rating of 70 shore A, while the butyl is rated at 60 on the A scale. It will also be shown that SBR rubber has one of the largest values of storage modulus among the other test materials at all frequencies tested. It follows that there is a trade-off between stiffness and damping. If the stiffness of a structure is high, the natural damping of that structure will inherently be low because the structure is prone to recover energy upon unloading, making it more difficult to damp out unwanted vibrations. Fixed landing gear

structures, like the one of interest, are generally very stiff. Metals are a perfect example of high stiffness materials which have very low damping. Composites, however, are also very stiff, often much stiffer than metals, yet they generally have higher damping because of a multitude of different damping mechanisms such as interfacial damping and frictional damping (Birman, 2002, Markley, 1988, Saravanos, 1991), which are outside the scope of this report.

At the highest testing frequency of 28.19 Hz, the stress-strain plot for SBR 70A rubber is shown in Figure 7.7.

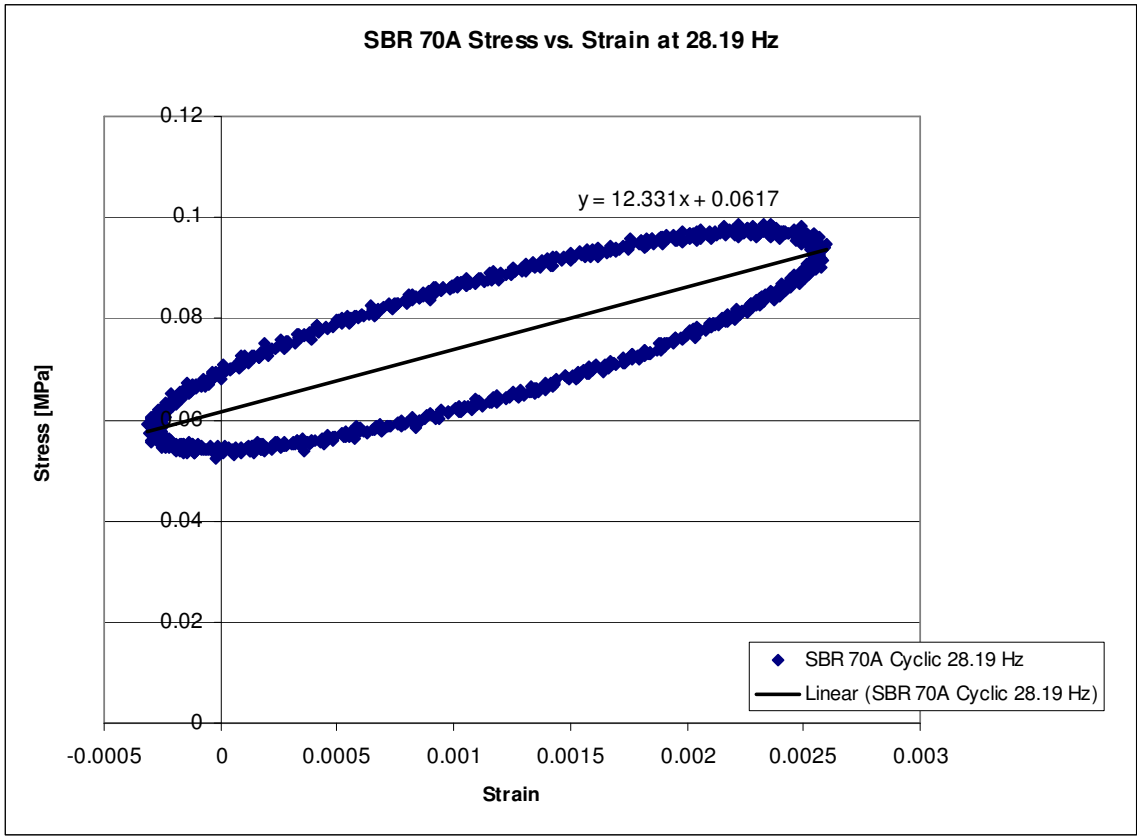

Figure 7.7. Hysteresis plot of stress and strain for SBR 70A rubber at 28.19 Hz.

This figure was analyzed in the same manner as that of butyl rubber in the preceding section, where the total energy dissipated over the one second test interval is divided by

the number of cycles (28.19) and applied to the theory outlined in section 6.0. Again, the elliptical shape of the plot, characteristic of viscoelastic materials, is shifted upwards due to a small static preload of the test material prior to load cycling. Additionally, it can be seen from Figure 7.7 that the SBR 70A rubber sample was cyclically loaded in tension due to the positive strain values. There is a small portion of the data showing negative strain, indicating a small portion of the loading history as compressive in nature.

7.4 Buna-N/Nitrile 40A Rubber Testing

Nitrile rubber, or Buna-N, is a synthetic copolymer rubber of acrylonitrile (ACN) and butadiene. This type of rubber falls into the nitrile-butadiene family of rubbers which consist of unsaturated copolymers of 2-propenenitrile and various butadiene monomers including 1,2-butadiene and 1,3-butadiene. The varying compositions of nitrile rubbers allow it to be very resistant to oils, fuels, and other chemicals. This makes it an excellent material to manufacture rubber gloves. Additionally, nitrile rubbers are used in the automotive industry to make oil handling hoses, seals, and grommets. Nitrile rubber also has a wide temperature range (about -40 to +120 degrees Centigrade) making it an excellent material choice for both high and low temperature applications. By varying the composition of nitrile rubber, it can be made more resistant to oils and acids, but will have inferior strength and flexibility. This aspect of nitrile rubbers makes it particularly appealing for an aircraft landing gear application. During operation, the material will undoubtedly come in contact with foreign substances such as oils, petrols and fuels, and perhaps strong acids. Thus, a resistance to these foreign substances will increase the longevity of such a damping material during operation, effectively increasing the service life of the landing gear.

Two samples of nitrile rubber, each having different durometers, were tested in the ElectroPuls machine. This section presents storage moduli and loss factor data of a nitrile rubber having a 40 durometer rating on the A scale. The sample was loaded at 1, 5, 10, 15, and 28.19 Hz. Table 7.3 gives the data taken from the experiments at the frequency mentioned.

Table 7.3. Storage Modulus and Loss Factor data for Buna-N/Nitrile rubber 40A.

Frequency [Hz]	Storage Modulus [MPa]	Shear Modulus [MPa]	Loss Factor
1	2.2917	0.779489796	0.047551
5	2.2487	0.764863946	0.06903
10	1.9368	0.65877551	0.0928
15	1.8604	0.632789116	0.15608
28.19	4.5533	1.548741497	1.0346

Figure 7.8 gives a graphical representation of the data in Table 7.3.

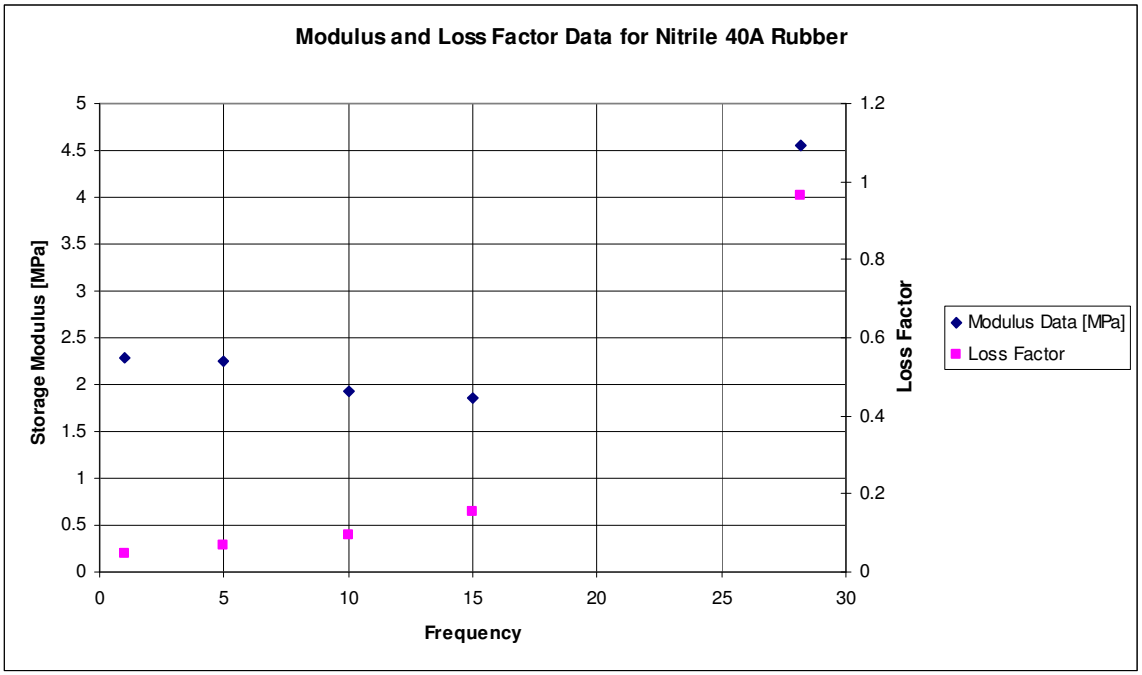

Figure 7.8. Storage Modulus and loss factor data for Buna-N/Nitrile rubber 40A.

This plot shows some interesting trends not seen in either SBR or Butyl rubber data. At lower frequency, the loss factor slowly rises while the storage modulus slowly falls. But at the first modal frequency (28.19 Hz) of the undamped cantilever beam, there is a sharp spike in both the storage modulus and loss factor of the material. This could indicate that the material is entering its transition region where both the storage modulus and loss factor rise until the loss factor hits a maximum value. Also, notice the large loss factor and lower storage modulus of nitrile 40A when compared to either SBR 70A or Butyl 60A. The loss factor of nitrile 40A is over double that of butyl 60A and quadruple that of SBR 70A at the first modal frequency. This makes the nitrile rubber the best material so far for the damping of a landing gear system. Also, the high loss factors combined with the environmental resistances of nitrile rubbers gives this family of rubbers excellent applicability to a landing gear.

At the first modal frequency of the cantilever beam, the stress-strain plot for nitrile 40A rubber is shown in Figure 7.9.

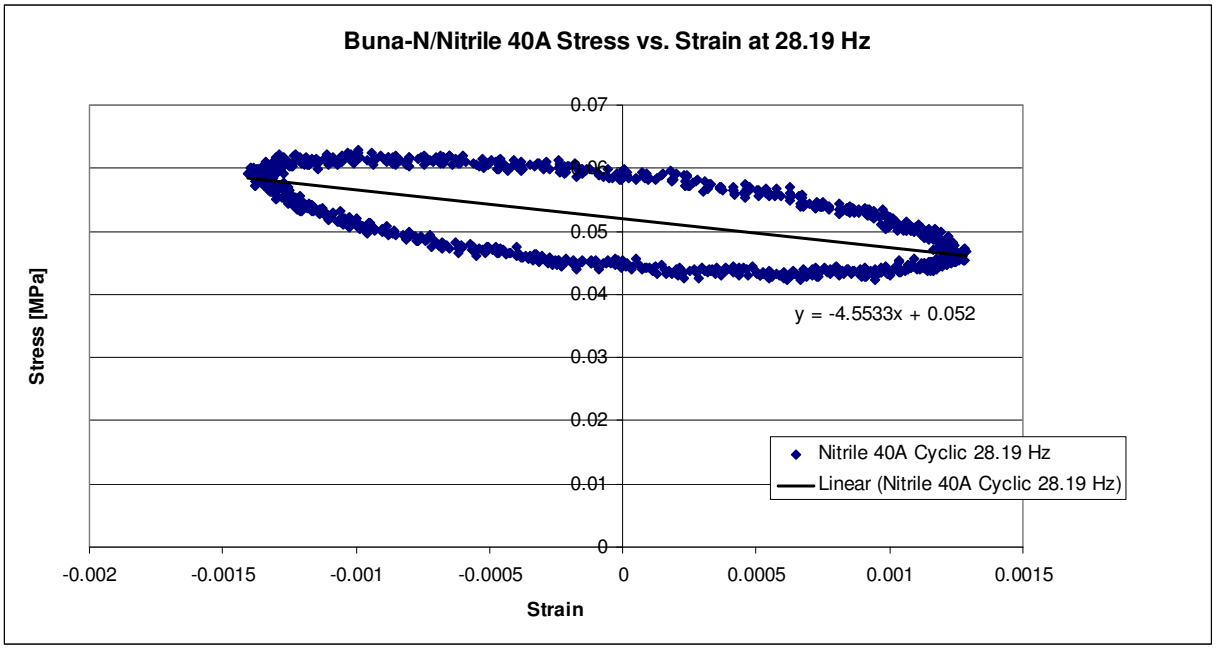

Figure 7.9. Hysteresis loop of stress and strain for nitrile 40A rubber.

This plot shows that the material was loaded in both tension and compression. It should be noted that though the slope of the ellipse is negative from the trend line in Figure 7.9, the absolute value of the trend line slope is the equivalent storage modulus of the material at a given frequency. The data is mirrored because of a necessary change in reference point in the ElectroPuls because of material sample dimensions. This data was analyzed in the same fashion as the butyl rubber in section 7.2 where the data for a complete one second time interval was used to find the total energy dissipated over that interval divided by the number of cycles. This allows an average energy dissipation per cycle to be used rather than isolating the data for any one cycle during the one second interval.

7.5 Buna-N/Nitrile 60A Rubber Testing

A second sample of nitrile rubber have a durometer of 60 on the A scale was also tested. This sample of nitrile rubber offers the same environmental resistance properties

as the 40A sample, but is slightly "harder" in durometer. Table 7.4 gives the properties of the materials at the frequencies of interest.

Table 7.4. Storage Modulus and loss factor data for Buna-N/Nitrile 60A rubber.

Frequency [Hz]	Storage Modulus [MPa]	Shear Modulus [MPa]	Loss Factor
1	9.8999	3.367312925	0.10893
5	11.357	3.86292517	0.13383
10	11.498	3.910884354	0.1774
15	10.557	3.590816327	0.206423
28.19	11.842	4.027891156	0.6490

The data in Table 7.4 shows that the sample of 60A Nitrile rubber is much stiffer over the entire testing frequency range, often tripling or even quadrupling the storage modulus of nitrile 40A at the lower frequencies. Figure 7.10 illustrates a graphical representation of the data in Table 7.4.

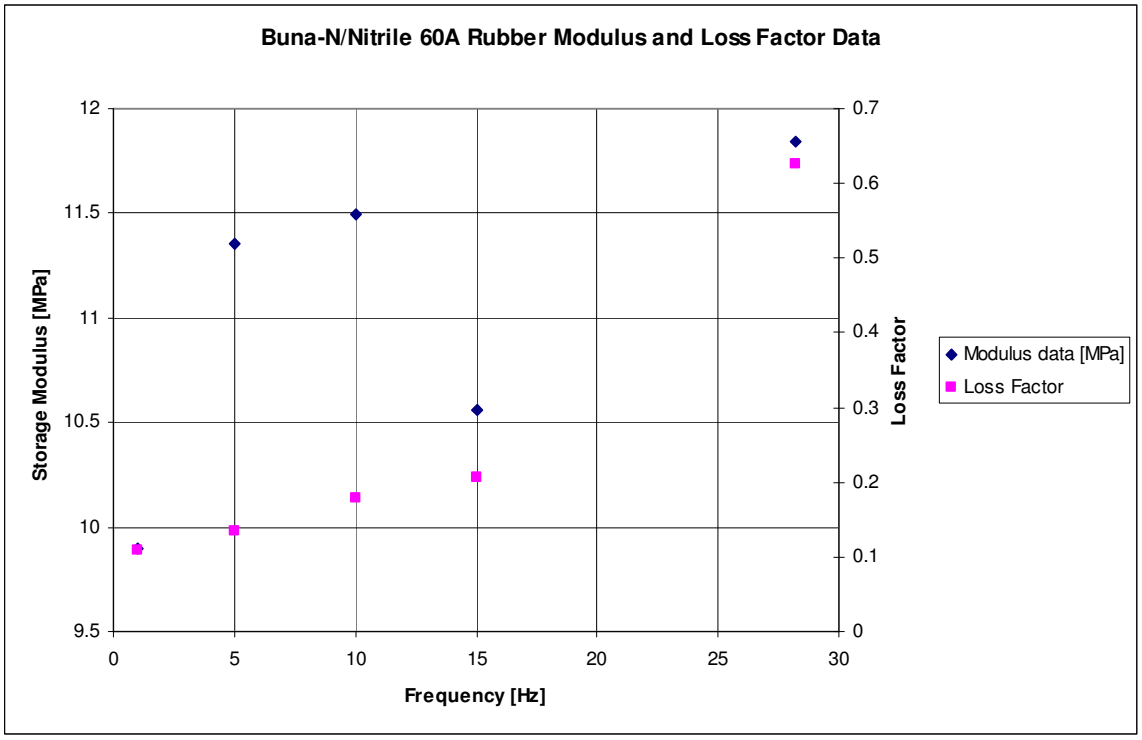

Figure 7.10. Storage Modulus and loss factor plot versus frequency for nitrile 60A rubber.

From Figure 7.10, there is no obvious trend between storage modulus and frequency. The data seems to oscillate slightly. However, a trend line would show that there is generally a small increase in storage modulus with increasing frequency, as is apparent with many other materials analyzed in the previous sections. The loss factor data however, shows a steady increase in value with increasing frequency. Furthermore, after comparing the loss factor data between nitrile 40A and nitrile 60A rubbers, nitrile 60A shows higher loss factors at the lower frequencies, but a lower loss factor at the first modal frequency of 28.19 Hz. This suggests that the nitrile 60A rubber has not yet hit a transition frequency where the loss factor would begin to significantly rise. Figure 7.11 shows the stress-strain plot for nitrile 60A at 28.19 Hz.

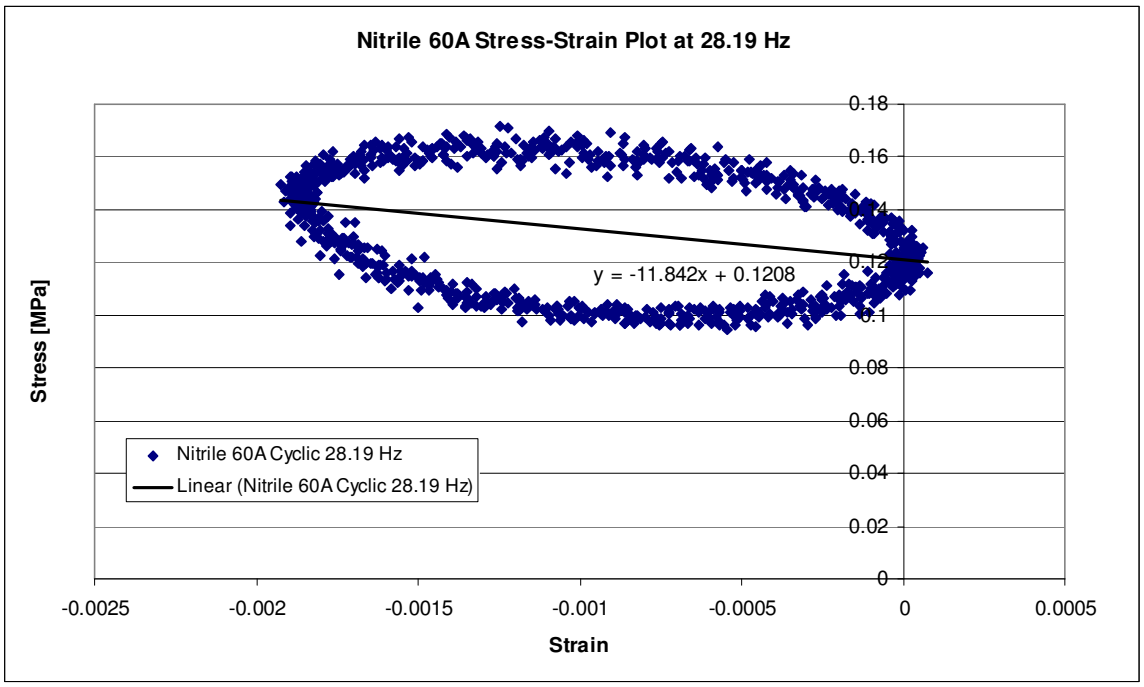

Figure 7.11. Hysteresis plot of stress and strain for nitrile 60A rubber at 28.19 Hz.

Figure 7.11 also shows that the material sample was loaded in tension after a static tensile preload was applied. The data shows a negative trend because the data is mirrored about

the stress axis due to a change in reference point caused by the dimensions of the sample. From this plot, a storage modulus of 11.842 MPa and a loss factor of .6490 were found by using the theory presented in section 6.0. Between the nitrile, butyl, and SBR rubbers which have been analyzed, both of the nitrile rubber samples hold the highest loss factor values at the first modal frequency.

7.6 Silicone 30A Rubber Testing

Silicone rubber is a polymer that has a backbone of silicone-oxygen bonds, the same bond found in quartz, glass, and sand. Silicone rubbers offer good temperature resistance, often having operational temperatures from -55 to +300 degrees centigrade. Silicone rubber is also resistant to ozone, and ultraviolet radiation, making it an elastomer of choice for extreme environments. However, silicone rubbers often have very low tensile strength, making it less desirable for applications involving high loads.

A sample of silicone 30A rubber was loaded into the ElectroPuls machine and tested at 1, 5, 10, 15, and 28.19 Hz. By physical inspection, silicone 30A rubber is very "sponge-like" and easily manipulated by applying small hand loads. This is contrary to many of the other rubbers, all of which have much higher durometers. Upon loading of silicone 30A in the ElectroPuls, load and position data was gathered and was used to generate the storage modulus and loss factor data summarized in Table 7.5.

Table 7.5. Storage Modulus and loss factor data for silicone 30A rubber.

Frequency [Hz]	Storage Modulus [MPa]	Shear Modulus [MPa]	Loss Factor
1	4.8319	1.643503401	0.0916
5	4.1329	1.405748299	0.056277
10	4.1077	1.397176871	0.06234
15	3.9549	1.345204082	0.07847
28.19	0.9363	0.318469388	1.4316

Additionally, Figure 7.12 shows the storage modulus and loss factor data for silicone 30A plotted against frequency.

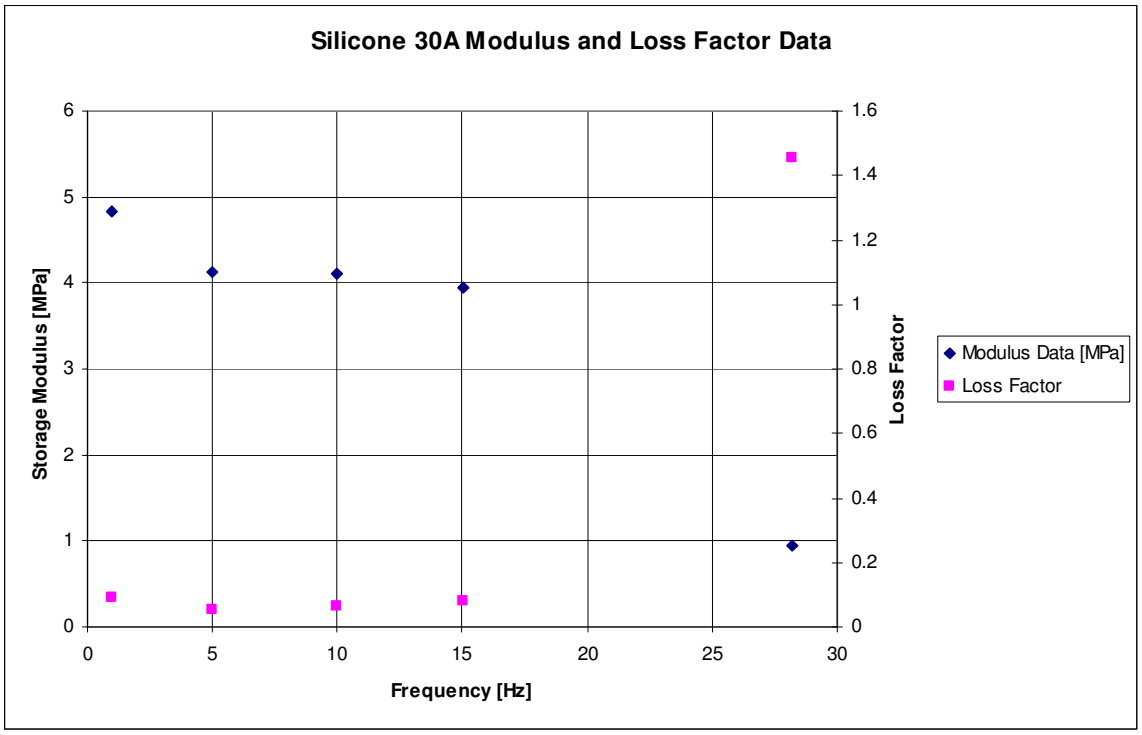

Figure 7.12. Storage Modulus and loss factor data for silicone 30A rubber.

This plot shows a relationship between storage modulus, loss factor, and frequency unlike any of the materials analyzed in the previous sections. As the frequency increases, the storage modulus shows a significant decrease, where the modulus values are the lowest of any material tested. The loss factor slowly increases with frequency and then spikes sharply at or around 28.19 Hz. The loss factor data for silicone 30A is among the lowest of any material tested at lower frequency, and then spikes to a value at 28.19 Hz more than 14 times the initial loss factor value at 1 Hz. This indicates that silicone rubber is perhaps the best damping material analyzed, having high loss factors and very low

moduli, giving a large ratio of imaginary to real parts of the complex modulus. Figure 7.13 shows the cyclic loading behavior of silicone 30A at 28.19 Hz.

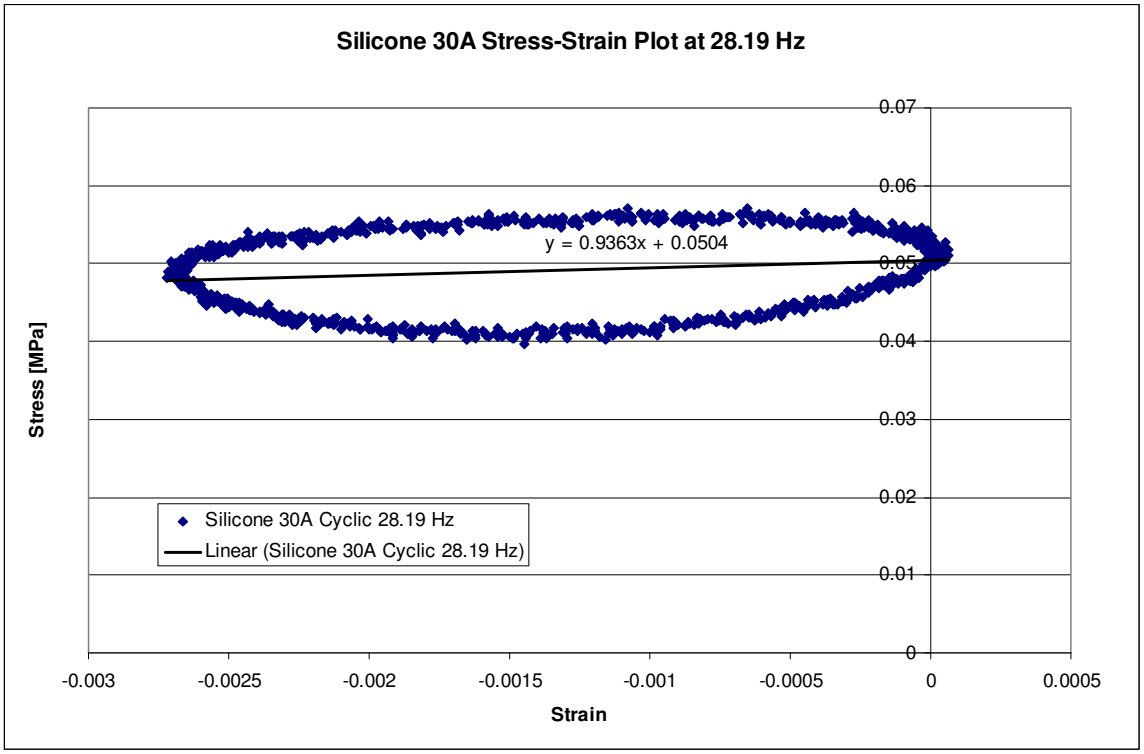

Figure 7.13. Silicone 30A cyclic stress versus strain relationship at 28.19 Hz.

Due to the negative strain values, the silicone 30A material sample was loaded in compression after a tensile static preload was applied. Rather, the material was preloaded in tension and then allowed to relax slightly to generate the plot in Figure 7.13. The loss factor at 28.19 Hz was higher than any other material tested, more than double the loss factor of nitrile 60A rubber and about 1.4 times the loss factor of nitrile 40A rubber.

As a final note on silicone 30A, during testing for one cycle at 1, 5, 10, and 15 Hz, the material showed a fairly significant nonlinear loading behavior, shown in Figure 7.14.

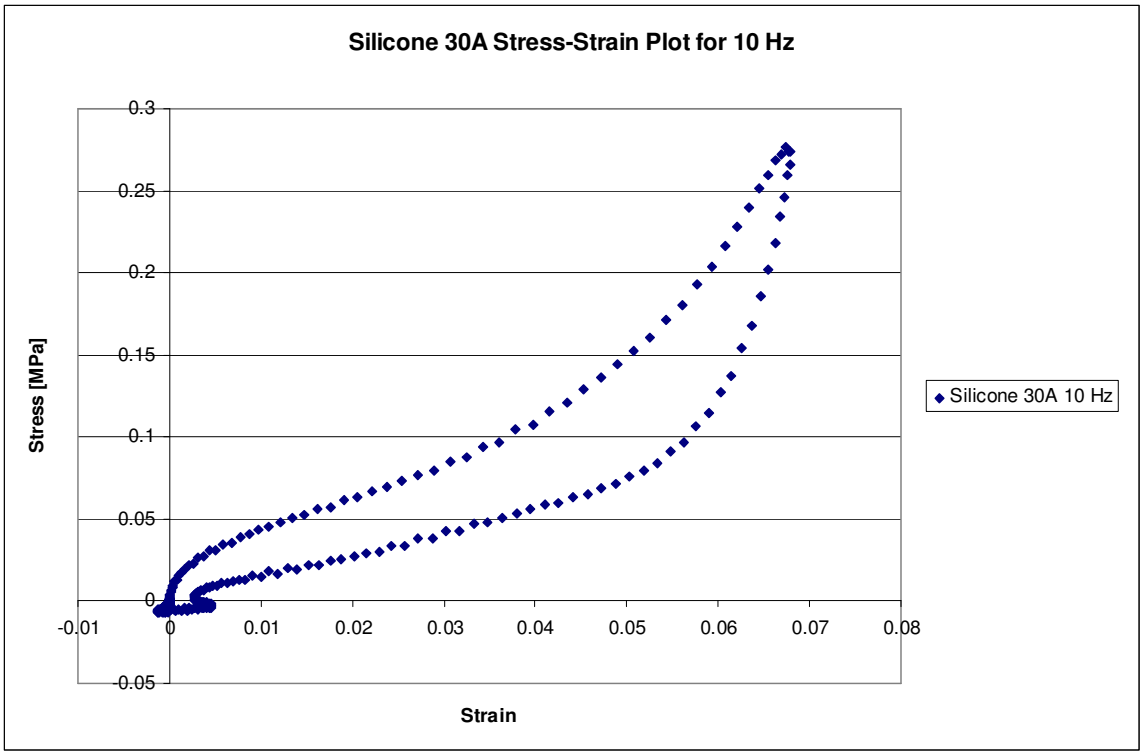

Figure 7.14. Example of loading nonlinearity of silicone 30A rubber.

This figure shows a loading behavior which has both loading (top curve) and unloading (bottom curve) as concave upwards. For most viscoelastic materials tested in this report, the loading behavior was that of Figure 7.1, where the loading curve was concave down and the unloading curve was concave up, forming an ellipse. Because of this unusual behavior relative to the other materials in the report, an average storage modulus was calculated. This average storage modulus was the slope from the preload origin to the maximum load point in the loading curve (point of maximum strain). This average modulus value was then used in equation (6.4) to calculate the loss factor. The energy dissipated during the cycle, however, was calculated in the same fashion as all other materials.

The nonlinear behavior in Figure 7.14 is most likely caused by the relatively large strain amplitudes. Most viscoelastic materials exhibit nonlinearity at large cyclic strain amplitudes, as discussed in section 2.2.1.3. The maximum elongations seen in the silicone 30A test sample for loading at 1, 5, 10, and 15 Hz were on the order of 5-8%, resulting in all plots showing varying degrees of nonlinearity. However, for 28.19 Hz, the cyclic strain amplitudes were very low, having a maximum elongation between .2-.3%, about 25 times lower than tests at lower frequencies. The low strains seen in the 28.19 Hz test result in linear behavior.

7.7 Silicone 50A Rubber Testing

A sample of silicone 50A rubber was also tested using the ElectroPuls machine. This sample of silicone rubber had a slightly higher durometer of 50A and exhibited greatly decreased damping when compared to the silicone 30A sample. Table 7.6 gives the storage modulus and damping value for silicone 50A at 1, 5, 10, 15, and 28.19 Hz.

Table 7.6. Silicone 50A modulus and loss factor data.

Frequency [Hz]	Storage Modulus [MPa]	Shear Modulus [MPa]	Loss Factor
1	2.8811	0.979965986	0.0263
5	2.7351	0.930306122	0.03476
10	2.468	0.839455782	0.043799
15	1.6567	0.563503401	0.10541
28.19	2.8274	0.96170068	0.37729

These results are further illustrated in Figure 7.15.

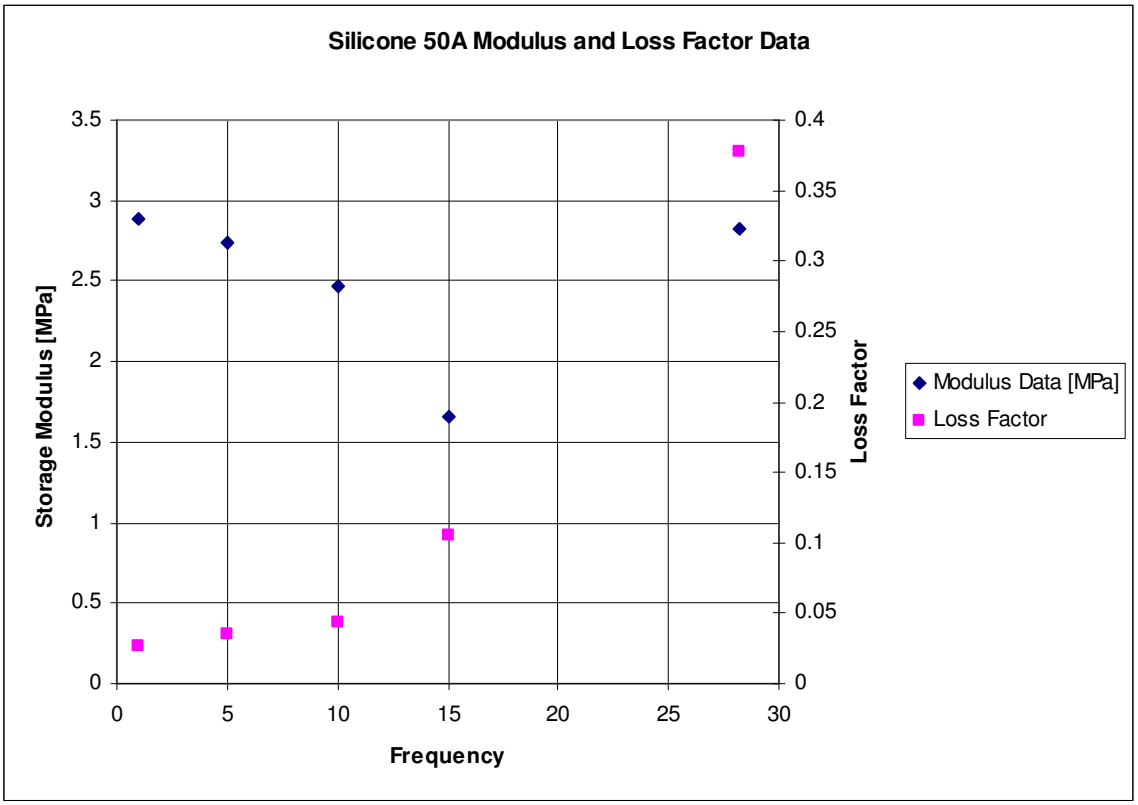

Figure 7.15. Storage Modulus and loss factor data for silicone 50A rubber.

Figure 7.15 shows a steady decrease in storage modulus with increasing frequency from 1 to 15 Hz. However, the storage modulus spikes at or around 28.19 Hz. The loss factor shows a steady increase with increasing frequency. This suggests that the material has not yet entered the transition region. The maximum loss factor found was .37729 at 28.19 Hz. This loss factor is lower than that of its silicone 30A counterpart, butyl, and both nitrile rubbers. The shear modulus, however, is still much lower than butyl and both nitrile rubbers. The predicted effectiveness of silicone 50A will be compared to the other damping materials in Chapter 8.

Like all other materials analyzed in the preceding sections, the maximum loss factor was found at the highest frequency corresponding to the first modal frequency of

the undamped cantilever beam, which will be the subject of discussion in subsequent sections. The stress-strain plot for silicone 50A rubber is shown in Figure 7.16.

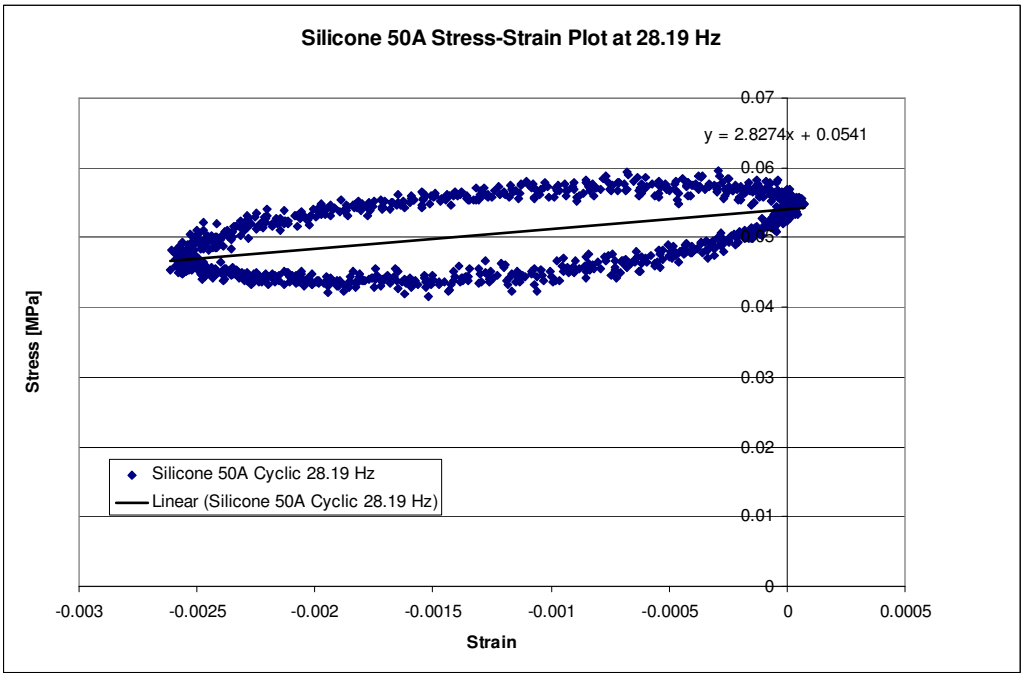

Figure 7.16. Cyclic loading history of silicone 50A at 28.19 Hz.

The material was loaded in compression for the cyclic loading test, which is evident by the negative strain values. Furthermore, the moduli for silicone 50A are greater than the moduli of silicone 30A at all test frequencies. This was expected because of the higher durometer. Silicone 50A also shows smaller loss factors than silicone 30A at all frequency except 15 Hz. This could be caused by the amount of scatter difference in the data, evident in Figure 7.16 for silicone 50A and Figure 7.13 for silicone 30A, as well as the trade-off between stiffness and damping. This scatter affects the average value for the energy dissipated per cycle, which is used to calculate the loss factor of the material. The larger the scatter in the data, the larger the deviation of the average energy dissipation per cycle from the actual energy dissipation for an exact cycle.

7.8 Vinyl 70A Rubber Testing

Vinyl polymers are a group of polymers derived from vinyl monomers. The backbone of a vinyl polymer is made by extending a carbon-carbon double bond to a chain where each carbon has a single bond with each of its adjacent neighbors in the chain. Vinyl polymers are most commonly used in PVC (polyvinyl chloride) tubing, popular in plumbing and ventilation systems. They were also used to make vinyl records, the predecessor to compact discs. Vinyl polymers are most commonly used to make plastics which are also a stiffer damping material than its rubber counterpart.

A sample of vinyl rubber having a 70A durometer was loaded using the ElectroPuls machine at 1, 5, 10, 15, and 28.19 Hz. As shown in Table 7.7 and Figure 7.17, vinyl rubber does produce excellent loss factors, higher than SBR 70A and even other materials which have lower durometer. This is most likely due to its differing microstructure from the other rubbers tested.

Table 7.7. Modulus and loss factor data for Vinyl 70A rubber.

Frequency	Storage Modulus [MPa]	Shear Modulus [MPa]	Loss Factor
1	10.144	3.450340136	0.0929
5	11.748	3.995918367	0.13798
10	11.957	4.067006803	0.1786
15	9.8326	3.344421769	0.2349
28.19	19.134	6.508163265	0.5441

The storage modulus of the vinyl 70A rubber is much higher than the SBR 70A, having the same durometer, at all test frequency. The loss factors are much higher, often doubling those of SBR 70A. This suggests that the higher stiffness and higher loss factors are attributed to the bond structure and bond type between atoms and polymer

chains within a rubber. Thus, the ability of a material to damp out vibrations and dissipate energy is highly dependent on the microstructure and type of the material.

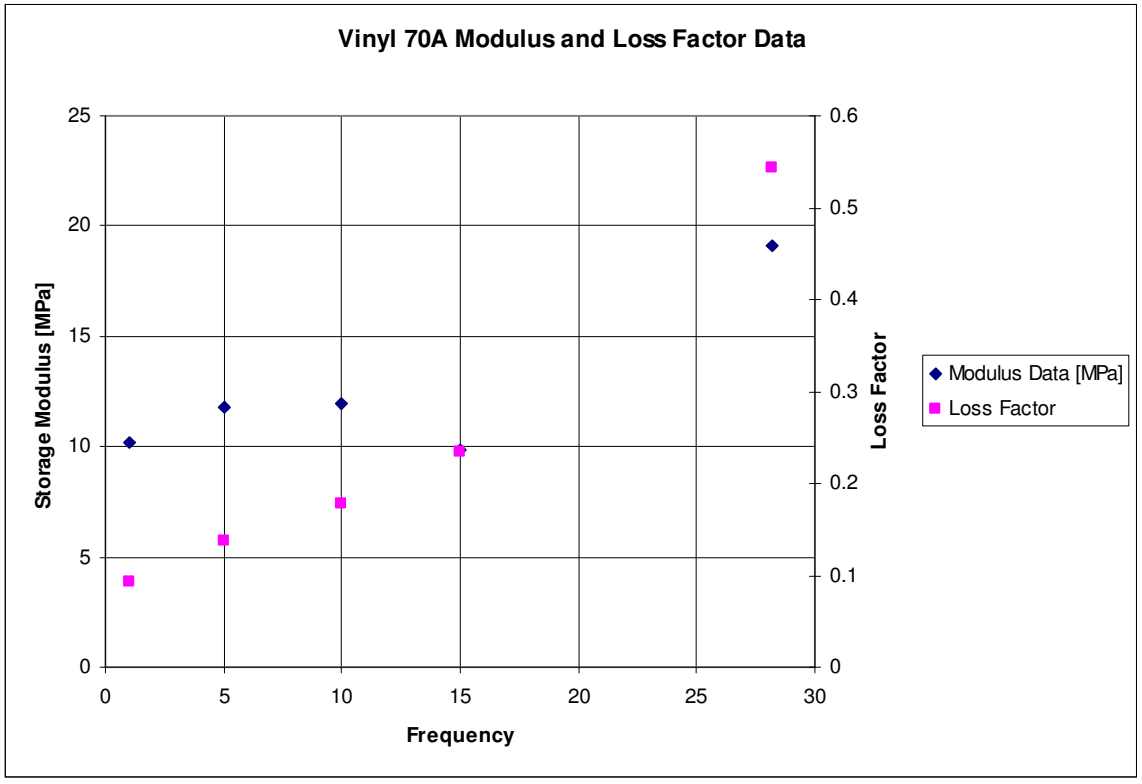

Figure 7.17. Storage modulus and loss factor data for vinyl 70A rubber.

From Figure 7.17 and Table 7.7, the storage modulus increases from 9.8 to 12 MPa from 1 to 15 Hz. But at 28.19 Hz the storage modulus jumps significantly by over 7 MPa. The loss factor, however, shows a fairly linear trend with frequency. Because the vinyl rubber is very stiff, but has only moderately high loss factors, the ratio of loss factor to shear modulus is still relatively low when compared to the other materials.

Vinyl 70A rubber has the fourth highest loss factor at 28.19 Hz and is bettered only by silicone 30A, nitrile 40A, and nitrile 60A out of the seven materials tested on the ElectroPuls cyclic loading machine. However, it is also the stiffest material tested at

28.19 Hz, suggesting that it will not offer as much damping performance as polymers which have about the same loss factor, but much smaller shear modulus.

7.9 Soundcoat Dyad Material Data

All seven of the materials loaded in the ElectroPuls cyclic loading machine were common rubbers available at almost any polymer distributor. Soundcoat Company produces specialty products for acoustical and vibration damping applications. Soundcoat Dyad is a line of product having three different grades, namely Dyad 601, Dyad 606, and Dyad 609. Each grade is intended for different temperature ranges, with Dyad 601 for lower temperatures and Dyad 609 for the upper extreme temperatures. Typical applications of Soundcoat Dyad are marine applications with steel and aluminum vessels, electronic equipment like disk drives and mass storage systems, engines and transmissions, machine tools, and aerospace and aircraft applications.

Soundcoat Dyad offers some unique benefits which many other specialty materials do not. Dyad will damp any thickness of metal while achieving significantly high loss factors. It has excellent chemical and heat resistance. The three grades can also be combined (laminated) to broaden the effective damping temperature range. For instance, grades 601, 606, and 609 can be bonded back to back to achieve significant damping levels over a broader temperature range than any one material alone, effectively combining each materials operating temperature range with the other two materials. For instance, if all three materials were laminated and tested at a single frequency as the temperature was slowly increased, at least one laminate layer would always be in its transition region, offering maximum damping. The other two materials would be operating in either a glassy region, if the testing temperature was less than the minimum

operating range temperature, or in a rubbery region, if the testing temperature was greater than the maximum operating range temperature. This behavior is illustrated in Figure 7.18.

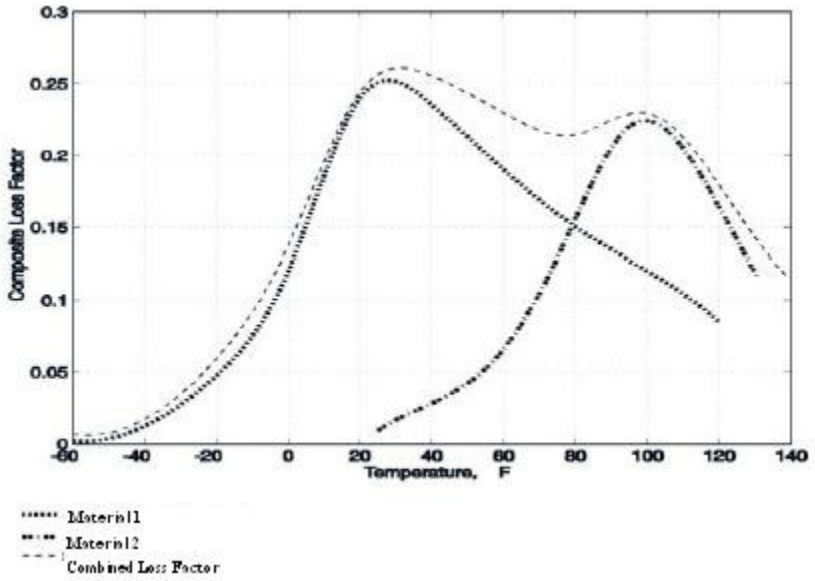

Figure 7.18. Combination of loss factor over broad temperature range by laminating damping materials (Soundcoat, Dyad Material Data Sheet, 2001).

Table 7.8 lists the three different types of Soundcoat Dyad as well as their temperature ranges and durometer values.

Table 7.8. Dyad material properties from Soundcoat (Soundcoat, Dyad Material Data Sheet, 2001).

	TYPE 601	TYPE 606	TYPE 609
Thickness, mm (in.):	All types available on 0.25 (.010)*, 0.50 (.020), 1.3 (.050) and 2.5 (.100)*		
Hardness, Durometer A:	44 +/- 3	67 +/- 3	98 +/- 3
Tensile Strength, N/mm^2 (PSI), per ASTM D-412:	6.7 (960)	17 (2400)	34 (4800)
Elongation, %; per ASTM D-412:	600	400	250
Brittle Point, °C (°F):	-30 (-22)	-29 (-20)	-30 (-22)
Effective Temperature Range, °C (°F):	-20 (-5) to 38 (100)	10 (50) to 66 (150)	49 (120) to 93 (200)

From Table 7.8, Dyad 601 offers a temperature range similar to that which would be seen by a landing gear system on an aircraft flying at relatively low altitude in multiple environments. It also has the lowest stiffness among the three Dyad grades, illustrated by its elongation percentage at break of 600, as well as the lowest durometer. Additionally, Figure 7.19 gives loss factor and shear modulus data at temperature versus frequency for Dyad 601, 606, and 609.

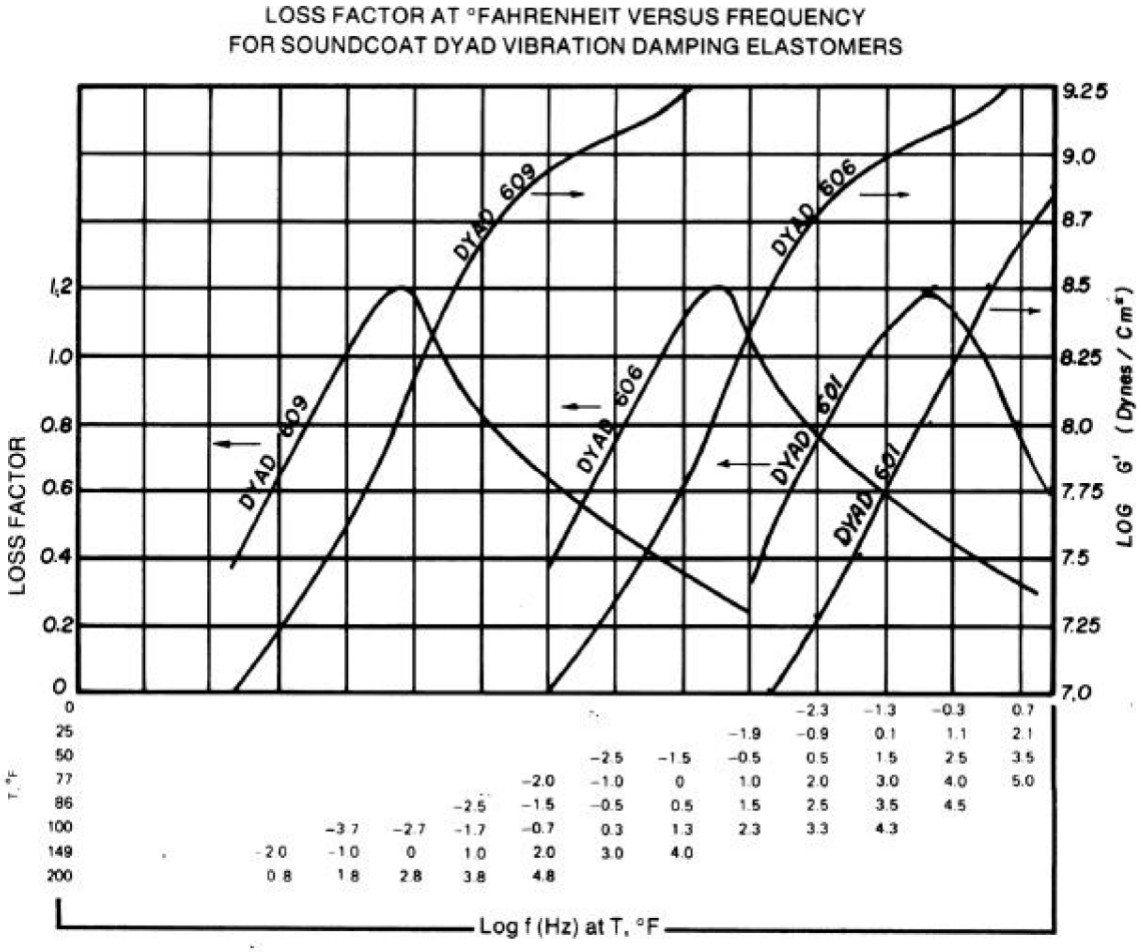

Figure 7.19. Dyad loss factor and shear modulus data at temperature for Dyad grades 601, 606, and 609 (Soundcoat, Dyad Material Data Sheet, 2001).

Figure 7.19 further illustrates that Dyad 601 has the highest loss factors of the Dyad products at the temperatures and frequencies the landing gear will experience. Figure

7.19 was generated by Soundcoat Company, so the testing of material samples in the ElectroPuls machine was not necessary.

When loaded at 28.19 Hz at 77 degrees Fahrenheit, Figure 7.19 shows that Dyad 601 has a loss factor of $\eta = .6$ and LOG G' = 7.1 $\frac{dynes}{cm^2}$ (1.259 MPa). Dyad 601 has a material loss factor closest to Buna-N/Nitrile 60A rubber, but a shear modulus closest to Buna-N/Nitrile 40A. This makes Dyad 601 the material with the third highest damping performance of all materials in this report. However, nitrile 40A rubber is still predicted to produce higher composite system loss factors because of its smaller shear modulus at 28.19 Hz.

7.10 Damping Material Conclusions

Per the cyclic loading tests using the ElectroPuls machine and the Dyad loss factor data courtesy of Soundcoat Co., the best viscoelastic damping materials were selected for testing using the cantilever beam system discussed in section 5.0. It was found that not only was the loss factor important in determining the damping performance of a material, but the storage and shear moduli were equally as important, as they help form the real part of a complex flexural rigidity formulated by the RKU equations. Thus, materials which have high loss factors and low shear modulus are desired for a landing gear application because the ratio of imaginary to real parts of the complex flexural rigidity will be maximized. The following section is dedicated to isolating the three best damping materials per the data collected via the cyclic loading tests and to compare the predictions of the RKU equations to an experimental cantilever beam test where actual materials are applied to a cantilever beam and tested.

Chapter 8

MATLAB Predictions and Trends

In this section, a simple MATLAB program utilizing the Ross, Kerwin, and Ungar equations for a damped cantilever beam is used to predict the loss factor using Soundcoat's Dyad 601, Buna-N/Nitrile 40A, and silicone 30A, the best damping materials found by cyclic loading tests. These materials were found to be the best materials to apply to a landing gear because they produce the highest composite system loss factors of all eight materials for a viscoelastic layer thickness between 1 and 3 millimeters. This fact is shown in Figure 8.1, where the composite system (host structure, damping material, and constraining layer) loss factor is plotted against viscoelastic layer thickness using RKU analysis and the MATLAB program found in Appendix A for reference.

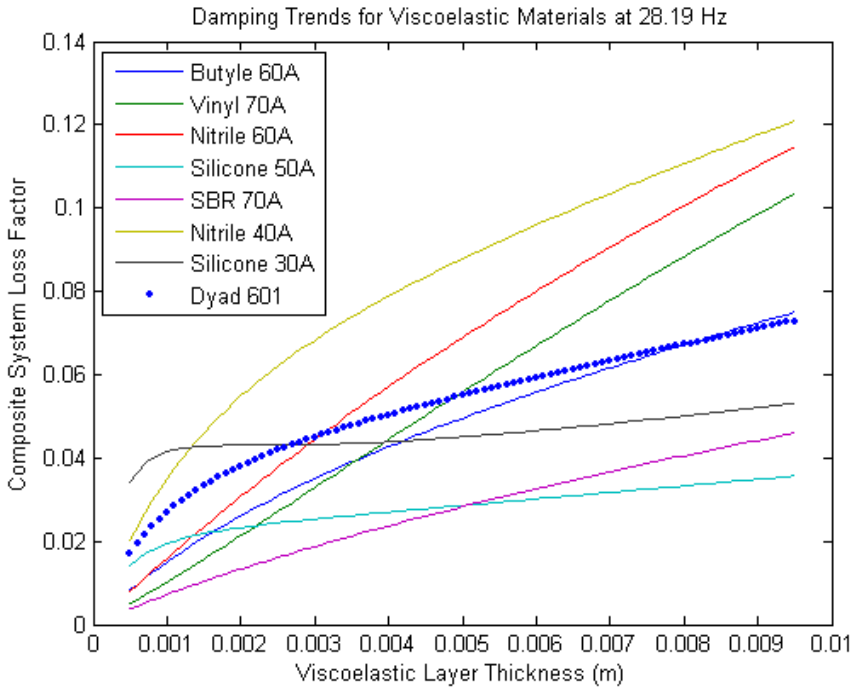

Figure 8.1. Cantilever Beam loss factor versus viscoelastic layer thickness for all damping materials

The MATLAB program takes inputs of shear modulus and elastic modulus in units of Pascals, thickness of the host structure, thickness of the constraining layer, and width of the constraining layer, in this case the same dimension as the thickness of the host beam. In Figure 8.1, the constraining layer is 1.31 mm and is the same for all materials.

The program generates a plot of damping factor of the composite system as a function of the thickness of the damping layer for the three best damping materials of sections 7.1 through 7.9, namely Dyad 601, Buna-N/Nitrile 40A, and Silicone 30A rubber. All plots and figures are for the first modal frequency of the cantilever beam. Furthermore, a short analysis of how the thickness and stiffness of the constraining layer affects composite loss factor will be given at the end of the MATLAB predictions for the damping materials. For sections 8.1 through 8.3, the host structure thickness is .375 inches (.0095 m), thickness of the constraining layer varies between .8 mm (.0008 m) and .96 mm (.00096 m), and the elastic moduli of the host structure and constraining layer are 209 GPa (4140 Steel) and 68 GPa (Aluminum T0), respectively. Furthermore, the damping treatment was only applied to one side of the cantilever beam prior to testing. If another constrained treatment were applied to the opposite side of the beam, resulting in a symmetric damping treatment, the damping would effectively double.

8.1 Using the RKU Equations to Predict Damping

Being able to predict effective damping of a structure pre-fabrication is a necessary process when dealing with structural damping. This section is dedicated to showing how the RKU equations can be used for a cantilever beam with a tip mass equal to the mass of the beam. By definition, the RKU equations, given in equation sets (3.1),

(3.2), and (3.3) and below for convenience, formulate a complex flexural rigidity of a damped constrained layer beam system

$$(EI)^* = \frac{E_s h_s^3}{12} + \frac{E_v^* h_v^3}{12} + \frac{E_c h_c^3}{12} - \frac{\frac{E_v h_c^2}{12}(d-D)}{(1+g_v^*)} + E_s h_s D^2$$
$$+ E_v^* h_v (h_{vs} - D)^2 + E_c h_c (d-D)^2$$
$$- \left[\frac{E_v^* h_v (h_{vs} - D)}{2} + E_c h_c (d-D) \right] \left[\frac{(d-D)}{(1+g_v^*)} \right]$$

$$D = \frac{E_v^* h_v (h_{vs} - \frac{d}{2}) + g_v^* (E_v^* h_v h_{vs} + E_c h_c d)}{E_s h_s + \frac{E_v^* h_v}{2} + g_v^* (E_s h_s + E_v^* h_s + E_c h_c)}$$

$$h_{vs} = \frac{h_s + h_v}{2}$$

$$d = h_v + \frac{h_s + h_c}{2}$$

$$g_v^* = \frac{G_v^*}{E_c h_c h_v p_1^2} = \frac{G_v^* L^2}{E_c h_v h_c \xi_n^2 \sqrt{C_n}}$$

$$\xi_n^4 = \frac{\rho_s b h_s \omega_n^2 L^4}{E_s I_s}$$

Additionally, η_r is the modal loss factor associated with G_v^*. The loss modulus is dependent on the mode because of frequency dependence on loss modulus. To find the loss factor of the composite system (host beam, damping layer, and constraining layer), one only need take the ratio of the imaginary to real parts of the complex flexural rigidity (Hao, 2005), namely

$$\eta_{composite} = \frac{\mathrm{Im}\, ag(EI^*)}{\mathrm{Re}\, al(EI^*)} \qquad (8.1)$$

This loss factor now incorporates the loss factor of the damping material into dynamics of the composite system, effectively giving an approximation of the rate of energy loss per cycle of the composite system. Thus, the complex moduli and loss factor data for the damping materials tested in this report can be used to find the loss factor of a cantilever beam system.

8.2 Dyad 601 Damping Prediction

The parameters taken from Figure 7.18 for Dyad 601 at 28.19 Hz and 77 degrees Fahrenheit where used as inputs into the RKU equations in the MATLAB program. These parameters are a loss factor of $\eta = .6$ and a shear modulus of LOG G' = 7.1 $\frac{dynes}{cm^2}$ (G'=1.259 MPa). Figure 8.2 shows the trend between damping layer thickness and composite loss factor for a steel cantilever beam with an aluminum constraining layer. The figure presented shows the predicted loss factor for the system used in the tests: a host beam of 3/8" (9.53 mm) square 4140 steel rod, and a .96 mm by 9.53 mm constraining layer.

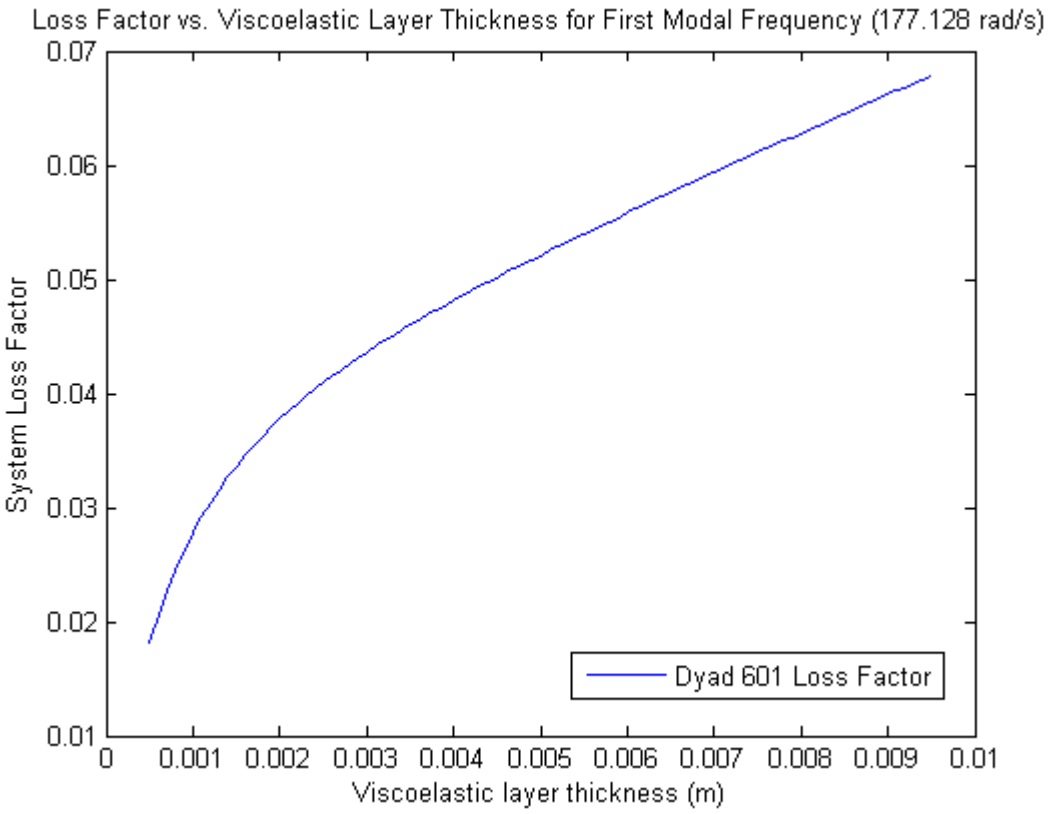

Figure 8.2. Cantilever beam loss factor as a function of Dyad 601 thickness.

This plot shows that for relatively small initial increases from .5 mm of the viscoelastic layer thickness, there are significant increases in damping up to about 2 mm. After the thickness of the damping layer passes 2 mm, the increases in damping begin to taper off slightly as the viscoelastic layer thickness is increased. This suggests that more significant damping increases can be gained without much weight addition to the landing gear for thin viscoelastic layers (~.5mm – 2mm).

8.3 Silicone 30A Damping Prediction

The material properties found in section 7.6 were used as inputs into the MATLAB prediction program. The results of the MATLAB prediction are shown in Figure 8.3. The RKU equations predict very sharp increases in loss factor for small increases in damping layer thickness for low thickness damping layers, about .5mm to

2mm. This rapid increase in loss factor at low viscoelastic layer thicknesses is much more pronounced than for Dyad 601. Thus, the most significant increases in damping will occur for low additions in weight caused by the damping layer to the cantilever beam.

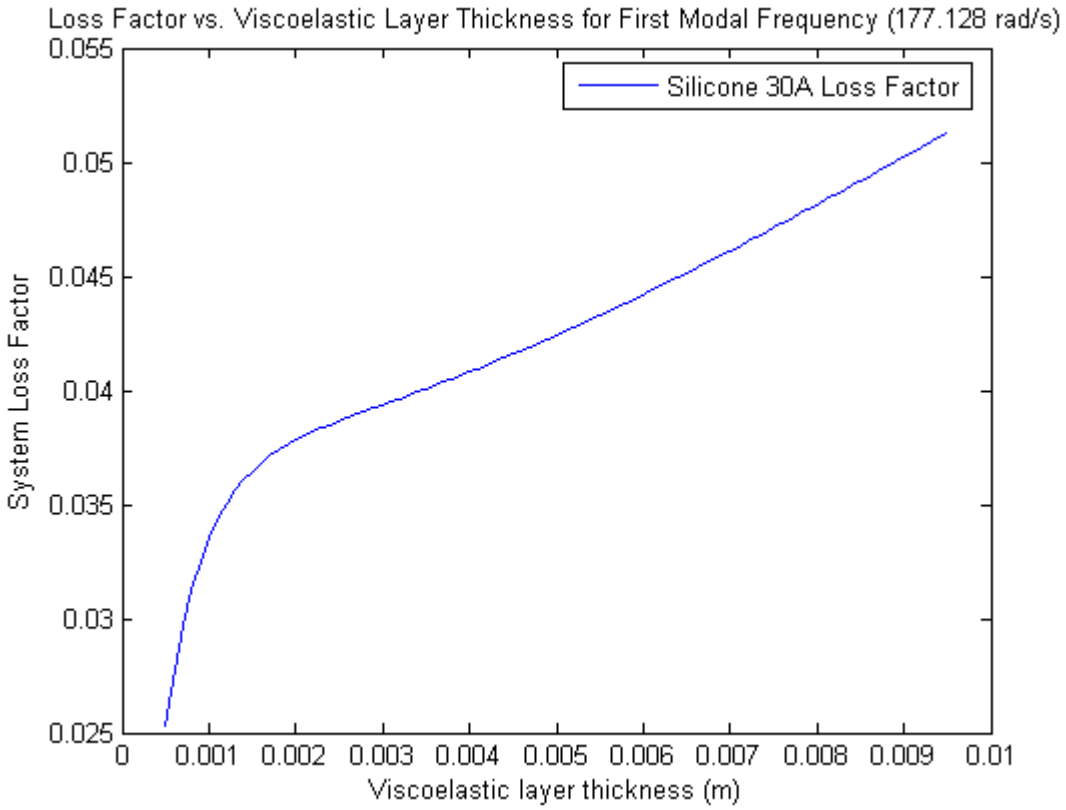

Figure 8.3. RKU Prediction of cantilever beam loss factor as a function of damping layer thickness for silicone 30A rubber.

To generate Figure 8.3, the constraining layer thickness was measured to be .8mm rather than .96mm as for Dyad 601. In the following chapter where cantilever beam tests are analyzed, the constraining layer thickness of the MATLAB prediction exactly matches that of the beam tests.

8.4 Buna-N/Nitrile 40A Damping Prediction

The material properties for Buna-N/Nitrile 40A found in section 7.4 at the first modal frequency of the cantilever beam were used as inputs to the RKU MATLAB program to generate a loss factor prediction as a function of viscoelastic layer thickness. Figure 8.4 shows the resulting trend. Unlike the silicone 30A prediction in the preceding section, there is no significant increase in loss factor for small increases in damping layer thickness, but instead a steady increasing trend of loss factor with increasing damping layer thickness.

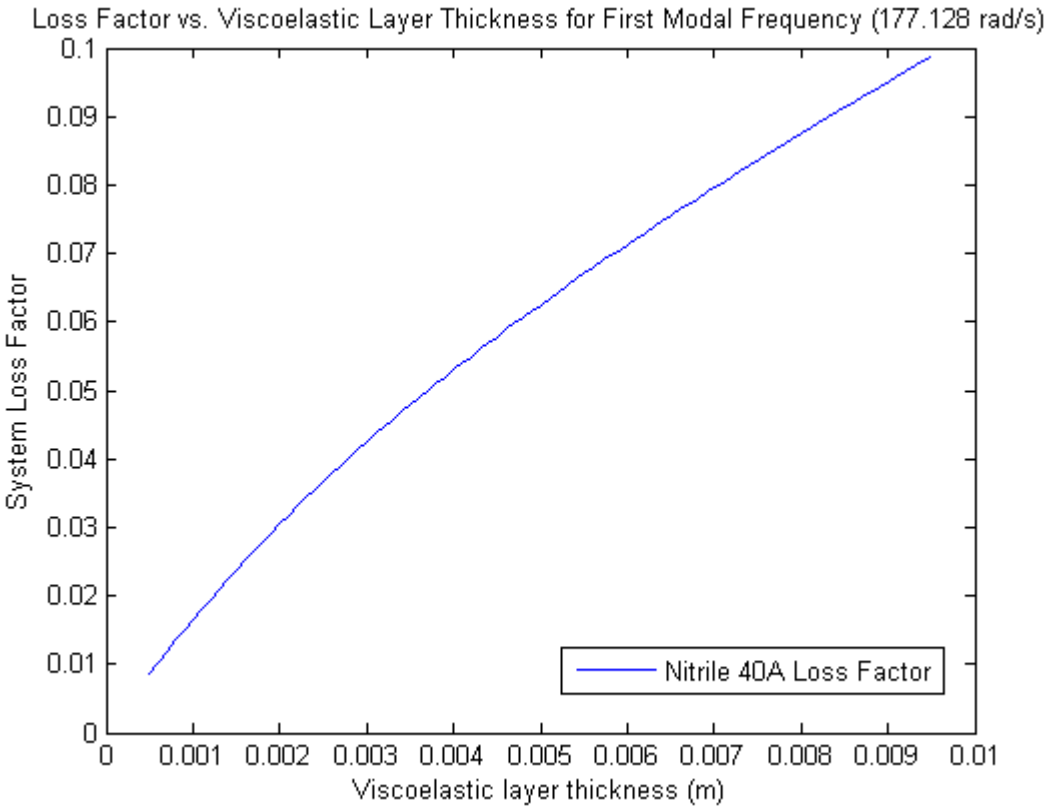

Figure 8.4. Loss factor trend for cantilever beam system as a function of viscoelastic layer thickness for Buna-N/Nitrile 40A rubber.

Like the silicone 30A prediction, a constraining layer thickness of .8 mm was used to generate Figure 8.4. It is evident from Figure 8.4 that nitrile 40A rubber produces the

lowest loss factors for low damping layer thickness and the highest loss factors for thicker damping layers. Thus, it is a better material to use for applications where a thicker damping layer is required. For a landing gear application however, nitrile 40A will be the least effective damping material between Dyad 601 and Silicone 30A because the damping layer should be kept as thin as possible while still achieving maximum damping for low increases in gear weight.

8.5 Constraining Layer Effects on Beam Loss Factors

This section analyzes how the constraining layer modulus of elasticity and thickness affect the composite system loss factor while keeping the material properties of the viscoelastic damping layer constant. Figure 8.5 shows the general trends of system loss factor as a function of variable constraining layer thickness and modulus of elasticity. For variable thickness, the plot was generated using silicone 30A complex modulus properties, a constraining layer elastic modulus of 68 GPa, and a frequency of 28.19 Hz. For variable constraining layer elastic modulus, the plot was generated using silicone 30A complex modulus properties, a constraining layer thickness of 1.31 mm, and a frequency of 28.19 Hz.

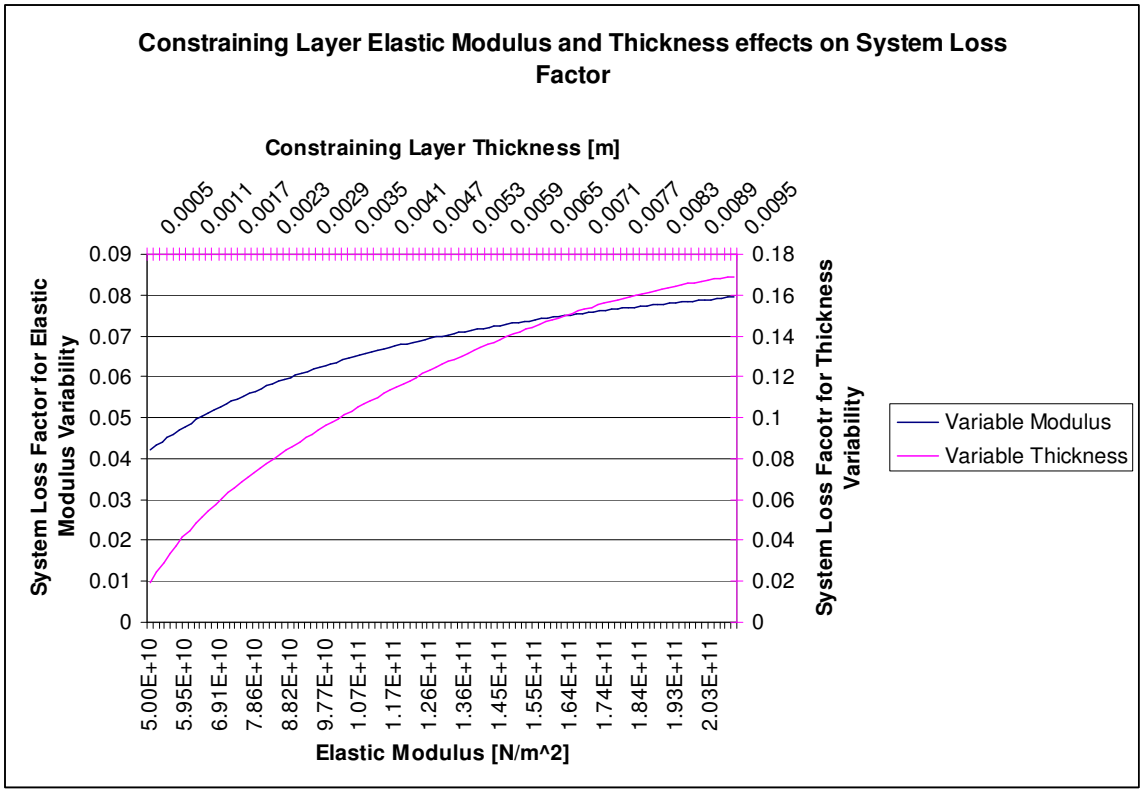

Figure 8.5. Effects of elastic modulus and thickness variability of constraining layer on system loss factor.

Figure 8.5 illustrates that both parameters significantly affect the loss factor of a beam system. However, the system loss factor produced by the RKU equations is much more sensitive to constraining layer thickness than a change in the elastic modulus. This was expected because of the higher order of the constraining layer thickness terms in the RKU equations. The thickness of the constraining layer appears as a cubic while the elastic modulus has a power of unity.

In regards to a landing gear application, by increasing the thickness of constraining layer, the weight of the gear will increase significantly. However, by changing the material to one with a larger elastic modulus, significant gains can still be seen without a significant increase in weight, depending on the material chosen. For instance, if the constraining layer material is changed from aluminum to steel, as in the

elastic modulus range in Figure 8.5, this results in a loss factor of about 2 times that of aluminum for constant thickness. Steel is about 3 times as dense as aluminum, meaning if aluminum was substituted for steel at the same thickness, essentially doubling the loss factor, the weight of the constraining layer would increase 3 fold. But if the aluminum constraining layer is increased to double its original thickness, effectively doubling the weight of the constraining layer, the loss factor can also be doubled. However, this is only true for relatively thin constraining layer thickness. So in order to see the same increases in loss factor either the constraining layer material is substituted for a much stiffer material, or the thickness of the layer can be increased. If the constraining layer material is changed from aluminum to a much lighter, much stiffer material like a carbon fiber or fiberglass, then thinner and lighter constraining layers can be used to achieve much higher loss factors than with heavier, softer metals. It is more advantageous, from a landing gear design perspective, to increase the modulus of elasticity of the constraining layer material so long as the density of the material is lower than the original material. By using lighter, stiffer materials, both the thickness and stiffness of the constraining layer will enhance the damping treatment while minimizing the addition of weight to the gear.

Chapter 9

Cantilever Beam Testing

Upon completion of the material property determination, selection of the three best damping materials per the cyclic loading tests, and MATLAB prediction using the RKU equations, cantilever beam tests were carried out using the cantilever beam system shown in Figure 9.1.

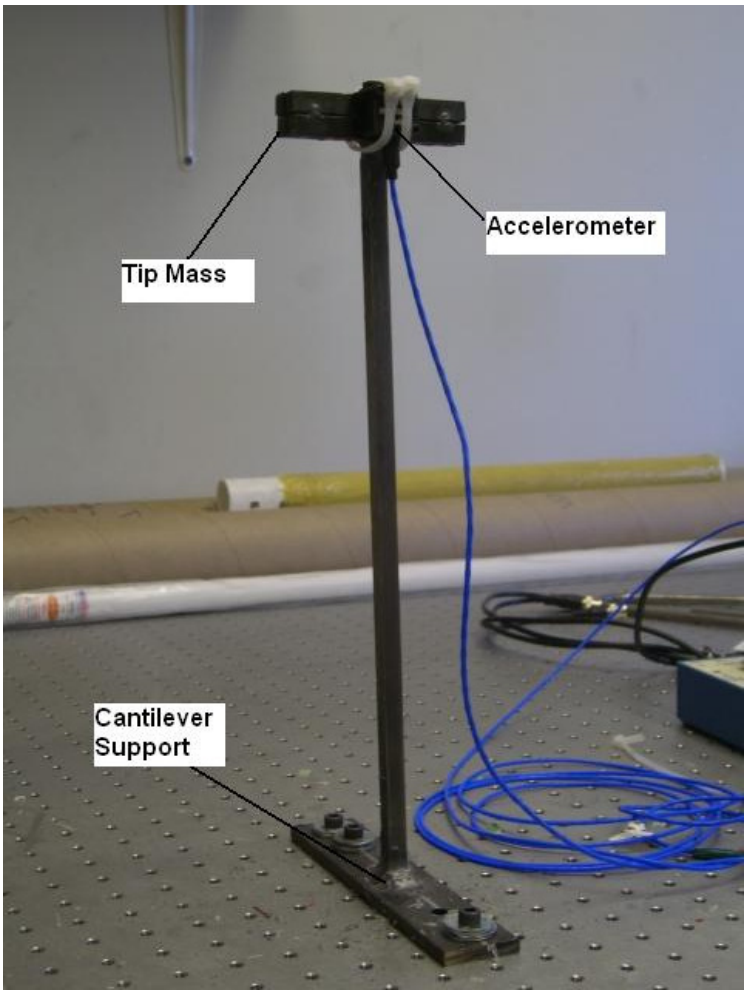

Figure 9.1. Cantilever beam system used for experimental loss factor determination.

The cantilever beam was 14 inches in length and constructed of 4140 "Chrome-Moly" steel. It had a tip mass equal to the mass of the 14 inch beam. This beam is the exact

beam analyzed using modal analysis in section 6.1.1, whose approximated modal frequencies are shown in Table 6.2. The accelerometer was glued to the cantilever beam tip mass and then tied to insure accurate data was recorded.

9.1 Loss Factor Measurement of Undamped Cantilever Beam

Before the addition of damping layers to the cantilever beam, the loss factor of the undamped beam was determined. The instrumentation outlined in section 5.0 was used to gather data for analysis using Microsoft Excel. Furthermore, once the data had been plotted for acceleration vs. time, the logarithmic decrement could be taken to determine damping factors (Meirovitch, 2001). These damping factors could then be used to find the loss factor. The logarithmic decrement is given by

$$\delta = \frac{1}{N} \ln\left(\frac{x_1}{x_2}\right) \qquad (9.1)$$

where N is the number of cycles between acceleration values x_1 and x_2. The acceleration values are shown in the sample acceleration versus time plot in Figure 9.2.

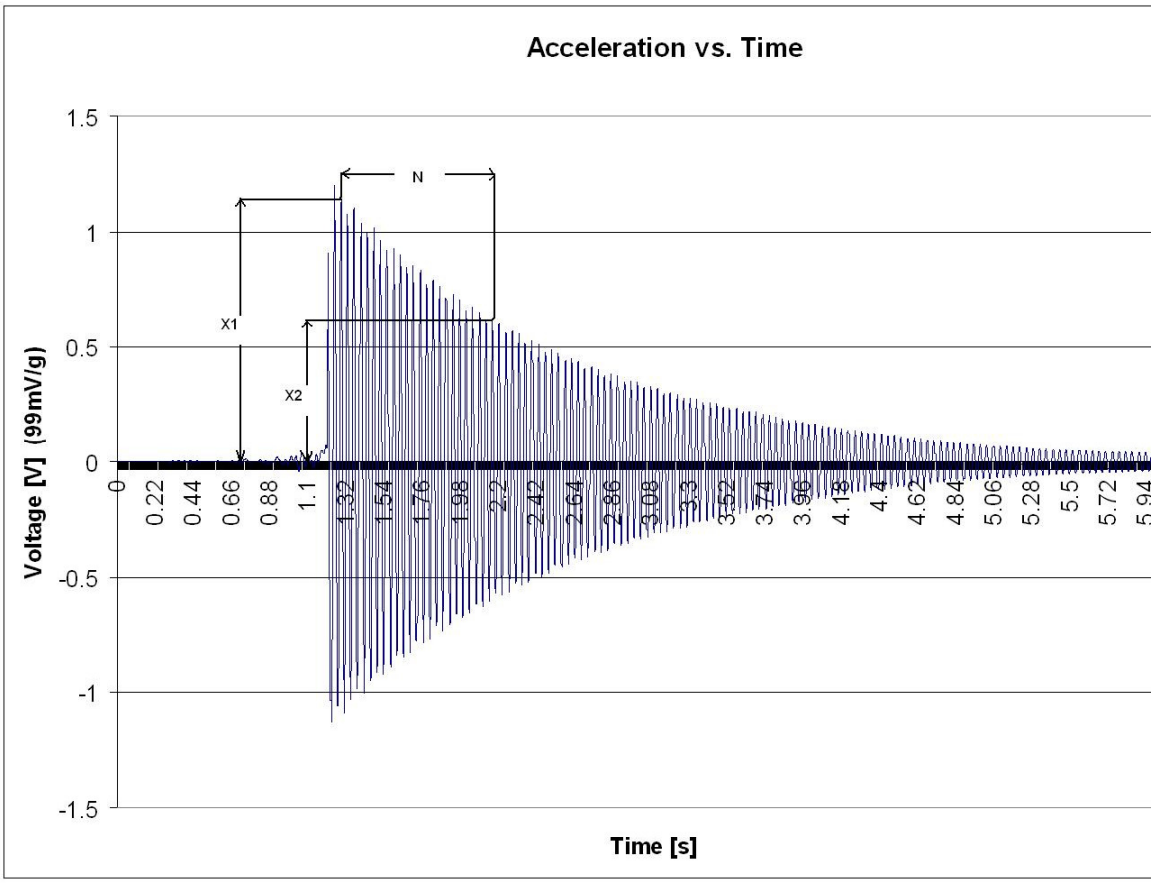

Figure 9.2. Example acceleration versus time plot and values needed to compute logarithmic decrement.

Once the logarithmic decrement was determined, the damping factor and loss factor were determined by

$$\zeta = \frac{\delta}{\sqrt{4\pi^2 + \delta^2}}$$
$$\eta = 2\zeta \tag{9.2}$$

This is a straight-forward and accurate method of determining the loss factor for the cantilever beam. It should be noted that the loss factor, η, is only two times the damping factor, ζ, at resonance frequencies. But it will be shown that the cantilever beam vibrates very close to its first modal frequency, making this relationship relatively accurate.

Three tests were conducted on the undamped beam and the frequency of oscillation and loss factors determined for each test. The results are concluded in Table 9.1.

Table 9.1. Experimental Frequency and Loss factor data for undamped cantilever beam in Figure 9.1.

Test Number	Accel Point 1 [V]	Accel Point 2 [V]	Time 1 [s]	Time 2 [s]	Frequency [Hz]	Log Decrement	Loss Factor
1	0.286215	0.199697	0.04774	1.18606	26.35	0.01199	0.0038
2	0.296216	0.203667	0.06634	1.20528	26.34	0.01249	0.00397
3	0.283473	0.198163	0.06944	1.20776	26.35	0.01196	0.00381

From Table 9.1, it is seen that the average experimental vibrating frequency is 26.35 Hz. The calculated first modal frequency of the beam in section 6.1.1 was 28.19 Hz. There is a difference of about 7.0% between the measured frequency and the first modal frequency of the beam. However, the beam, in actuality, does not vibrate at the first modal frequency, but rather, there are a combination of an infinite number of modes for a continuous system each having a different "weight" which, when combined using modal analysis, produce the actual frequency and dynamics of the beam. The largest contributor to the difference in calculated modal frequencies and the measured frequency of vibration of the beam was the neglect of rotary inertia in the modal analysis in section 6.1.1. What Table 9.1 does illustrate, in all certainty, is that the frequency of vibration of the beam is very close to the first modal frequency, meaning the first mode has a much larger "weight" in the combined dynamics of the beam than any other mode. Said differently, the first mode is the most prominent mode in the dynamics of the beam.

The loss factors of the undamped beam vary by 4.47% where the maximum loss factor is .00397. Because the beam does not yet have an applied damping treatment, the

loss factors are very low. Steel, as well as most other metals, have inherently low loss factors because of their high stiffness and high modulus of elasticity. Having a high stiffness makes them recover almost all of the loading energy after the load is removed. Thus, once a damping treatment is applied and analyzed in the following sections, it was expected that the damping and loss factors would greatly increase.

9.2 Dyad 601 Cantilever Beam Test Results

A strip of Dyad 601 was epoxied to the cantilever beam shown in Figure 9.1 and constrained by a .96 mm thick aluminum layer. The cantilever beam was excited by hand into transverse motion (pure pending) and allowed to vibrate freely for a period of 6 seconds. During this time, accelerometer data was being collected at 1600 Hz. A sample plot for the acceleration data for Dyad 601 is shown in Figure 9.3.

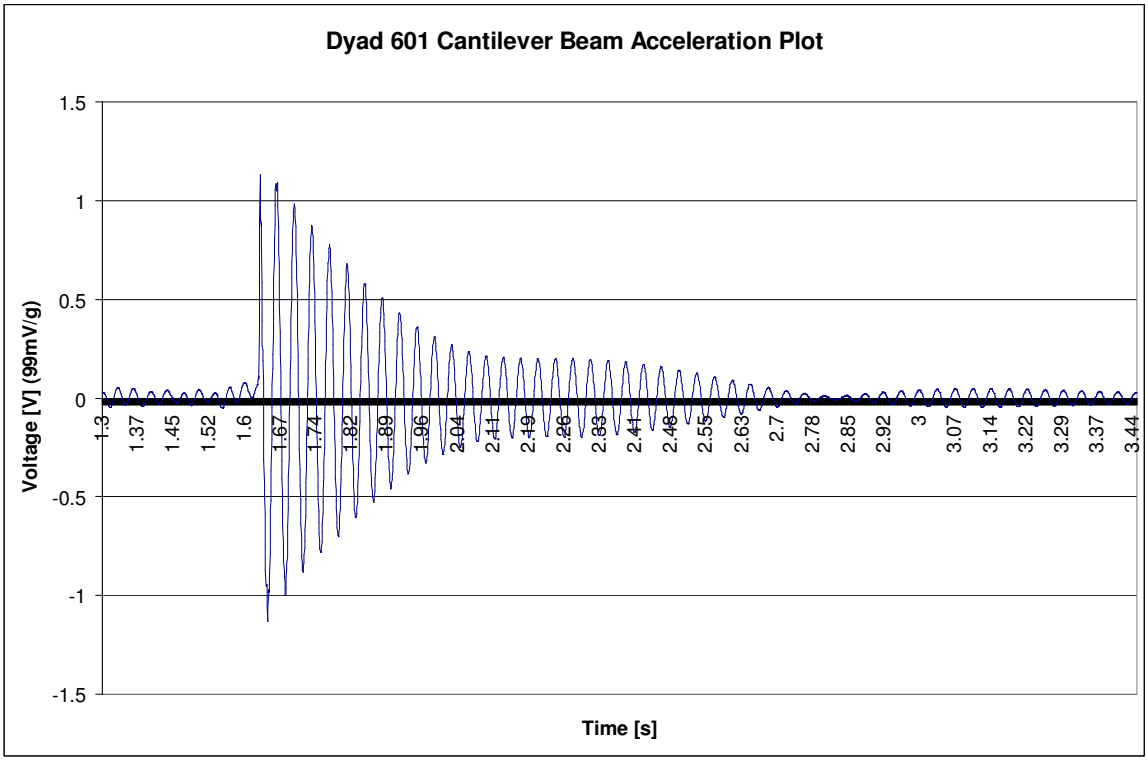

Figure 9.3. Acceleration data versus time for Dyad 610.

A total of three tests were carried out to insure accurate data was being recorded and to compare relative damping values from test to test. A summary of the results found from the Dyad 601 cantilever beam tests are shown in Table 9.2.

Table 9.2. Dyad 601 Cantilever beam test result summary.

Test Number	Accel Point 1 [V]	Accel Point 2 [V]	Time 1 [s]	Time 2 [s]	Frequency [Hz]	Log Decrement	Loss Factor
1	1.381299	0.066459	0.64356	1.5593	27.3	0.1214	0.03863
2	1.090353	0.099029	1.66346	2.57362	27.4677	0.09595	0.03054
3	1.086331	0.10941	1.98586	2.89602	27.4677	0.09182	0.02922

Test 1 shows a fairly large loss factor when compared to the other two tests, but will be shown to still correlate very well to a loss factor predicted by the RKU equations.

Figure 9.3 shows some very interesting behavior in that there is a reverberation of the initial vibration of the beam at about t = 2 seconds. This is caused by the cantilever beam having almost identical frequencies of vibration in the x and y-directions, perpendicular to the z-axis along the length of the beam. By adding a constraining layer and a damping layer, the stiffness of the beam perpendicular to the treatment face will increase slightly, causing the beam to vibrate in a "figure 8" or elliptical pattern rather than a linear back-and-forth motion. Each of the accelerometers had a slight sideways sensitivity, meaning that though they are single axis accelerometers, they will pick up slight movements in a perpendicular direction. This reverberation in Figure 9.3 is caused by the accelerometers outputting signals due to the sideways motion of the cantilever beam. Thus, the logarithmic decrements and loss factors listed in Table 9.2 are average values over the time interval of vibration. This is a reasonable approximation because the

viscoelastic layer will damp out vibration in any direction, albeit delayed in this case by the dynamics of the beam.

9.2.1 Dyad 601 Experimental and Theoretical Correlation

Per the composite loss factor for the cantilever beam given by the RKU prediction in section 8.2, Table 9.2 shows very close correlation between experimental and theoretical loss factor results. From Figure 8.2 given by the Dyad 601 RKU prediction, it was estimated that a 1.31 mm Dyad 601 layer (as measured from the experimental cantilever test) produced a composite loss factor of .0297 for a beam width of 9.53 mm and a constraining layer of .96 mm by 9.53 mm. The average loss factor produced by the cantilever tests was .0328, a value differing from the prediction by 9.47%. This average loss factor for Dyad 601 is about 9.5 times the loss factor of the beam with no treatment.

By a treatment weight addition of about 12 grams, the loss factor of the beam was increased almost 10 fold. Ultimately, the tested loss factor values prove that the RKU equations produce very accurate predictions. However, the RKU equations are meant to be an upper bound approximation, meaning they assume perfect energy conversion based on the properties of a given viscoelastic material. Why, then, is the average experimentally determined composite loss factor greater than the predicted value? The material used to bond the Dyad to the beam and the constraining layer is a specially formulated semi-flexible epoxy, which inherently carries small damping properties. In fact, this epoxy, called B-Flex, was specifically formulated for the bonding of Dyad materials to host structures to improve the damping of the Dyad polymer. Thus, there is often a slight increase in damping because of the addition of several semi-flexible bond layers which also promote damping.

In general, the bonding layer should be of comparable stiffness to the host structure, causing minimal slip between the host structure and damping material at the bond interface. B-Flex epoxy is still very rigid compared to the Dyad material, but because it was specifically formulated for Dyad materials, it was used in the beam tests. Nevertheless, the experimental and theoretical results correlate extremely well for Dyad 601 with only about a 9.47% difference between theoretically determined loss factors and those which were found experimentally.

9.3 Silicone 30A Cantilever Beam Test Results

A strip of silicone 30A rubber was sandwiched between the steel cantilever beam and the aluminum constraining layer and excited to vibrate. During vibration, accelerometer data was recorded and analyzed to find damping factors and loss factors of each test. A total of three tests were conducted on the cantilever beam using silicone 30A. A sample plot of one of the tests is shown in Figure 9.4 and a summary of the results from all three tests is provided in Table 9.3.

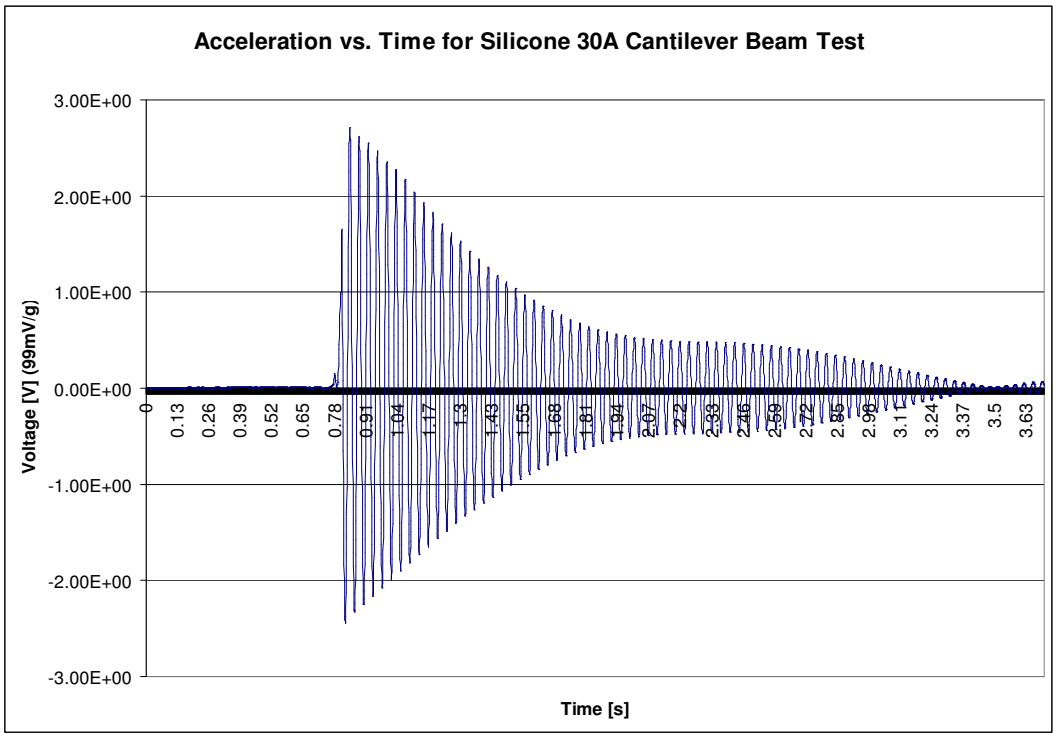

Figure 9.4. Acceleration vs. time plot for silicone 30A cantilever beam test.

From Figure 9.3, there is a slight reverberation of oscillation as discussed in section 9.2.

Table 9.3. Acceleration and loss factor data for cantilever beam tests for silicone 30A rubber.

Test Number	Accel Point 1 [V]	Accel Point 2 [V]	Time 1 [s]	Time 2 [s]	Frequency [Hz]	Log Decrement	Loss Factor
1	1.936445	0.47227	1.61758	2.56246	26.46	0.05644	0.01796
2	2.606792	0.624275	0.8773	1.82528	26.37	0.05717	0.0182
3	2.60566	0.592756	0.5156	1.46258	26.37	0.0592	0.01885

From the MATLAB prediction, a damping layer thickness of 1.51 mm and a constraining layer thickness of .8 mm should produce a composite system loss factor of .0361, about two times the loss factors seen in Table 9.3. However, this does not imply that the RKU equations or the material properties found from the cyclic loading tests are erroneous. The RKU equations, as well as many other analytical methods of damping prediction, assume there is a perfect shear transfer between the cantilever beam and

viscoelastic layer. This means that there is no slip at the bonding interfaces and that the viscoelastic layer is shearing according to the dynamics of the beam. Additionally, the bonding layer should be of comparable stiffness to the structural member to be damped, meaning the adhesive should be fairly rigid and stiff. However, it was found during the bonding of the silicone to the steel beam and aluminum constraining layer that silicone is very difficult to bond to metals with a bonding layer having comparable stiffness to the steel beam.

Several different grades of epoxy and cyanoacrylates were used and no sufficient bond was formed. One and two part silicone adhesives and RTV's were used with limited success. The best bond between the silicone rubber sheet and the metal components of the cantilever beam was made by using a general grade, clear RTV silicone adhesive sealant most commonly used for bonding weather stripping in automotive applications. However, this RTV adhesive, as well as almost all other RTV adhesives, formed a very rubber-like bond, causing much of the shear normally found in the viscoelastic layer to occur in the adhesive layer. Thus, the fundamental boundary conditions found in the RKU equations are no longer satisfied because there is an imitated slipping effect between the viscoelastic layer and the steel and aluminum faces it was bonded to.

Phrased differently, if the bonding layer is very stiff and thin, the magnitude of the vector from one point on the steel beam to its adjacent point on the viscoelastic layer at the steel-silicone interface should not change during vibration. If the bonding layer is very soft and rubbery, the magnitude of this vector will change. This concept is

illustrated in Figure 9.5 for visualization. The thickness of the bonding layer is exaggerated to illustrate the effect.

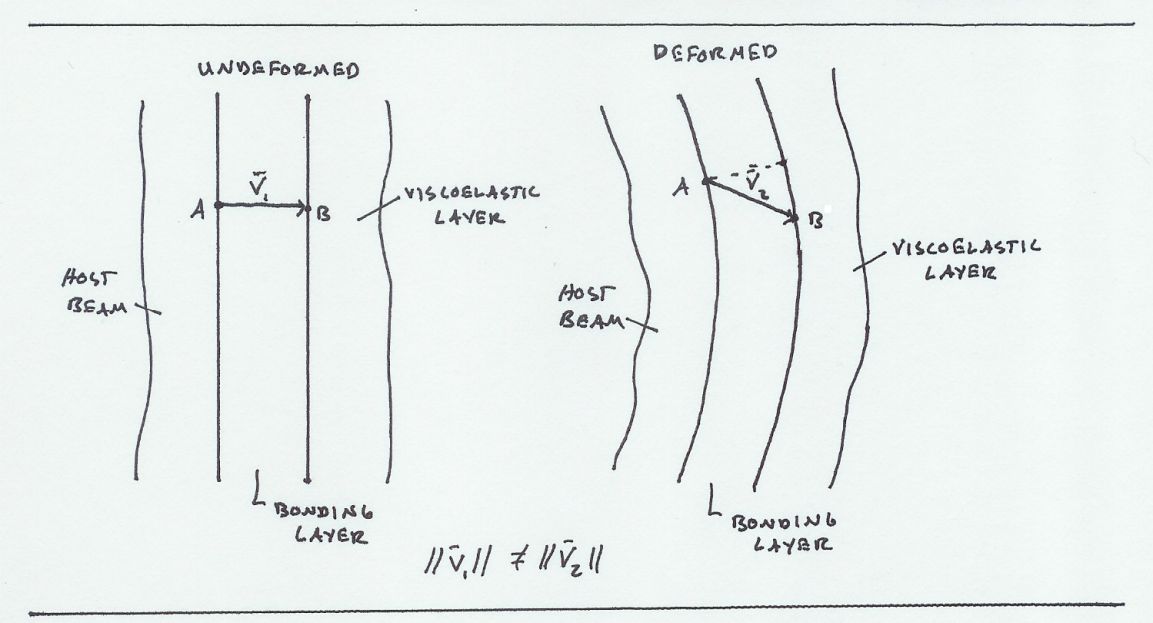

Figure 9.5. Deformation of rubbery bonding layer during bending.

With a rubbery bonding layer, the magnitude of this vector will change as the beam vibrates, essentially causing a slip condition at the steel-silicone or aluminum silicone interface. This rubbery bonding layer decreases the effectiveness of the silicone as a damping material and results in the relatively low loss factors seen in Table 9.3.

9.4 Buna-N/Nitrile 40A Cantilever Beam Test Results

Cantilever beam tests similar to those carried out for Dyad 601 and silicone 30A were also done using a nitrile 40A viscoelastic layer. The layer was measured to be 1.17 mm with a constraining layer thickness of .8 mm. The beam was excited to vibrate in bending with a sample acceleration versus time plot show in Figure 9.6. The logarithmic decrement was taken for each of three sets of acceleration data and the loss factor calculated from each. The results are summarized in Table 9.4.

From the RKU prediction, it was estimated that the cantilever beam loss factor would be .0181, about half that of either silicone 30A or Dyad 601. However, from Table 9.4, it is seen that the average loss factor of .0122 differs from the predicted value of .0181 by about 32.6%.

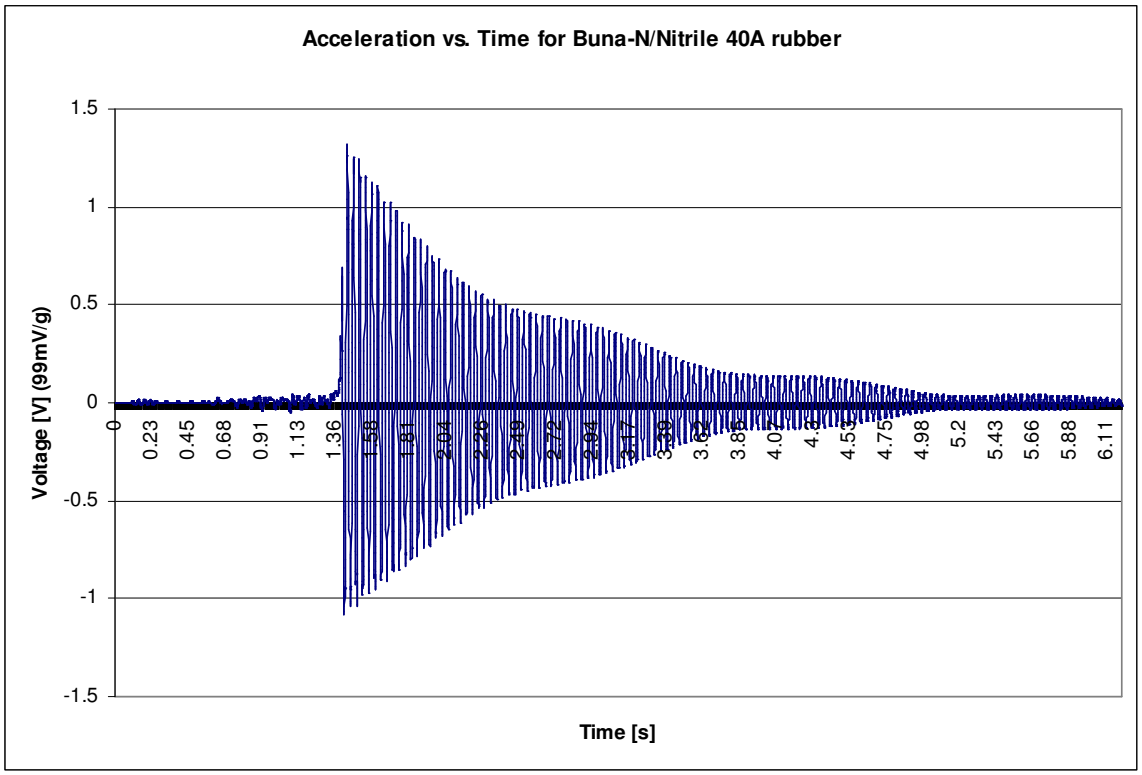

Figure 9.6. Sample acceleration vs. time plot for Buna-N/Nitrile 40A.

Like silicone 30A, achieving a strong, stiff bond between the nitrile rubber and the metal surfaces was impossible. Rather, the bonding layer was very rubbery, causing much of the shear to occur in the bonding layers rather than in the nitrile 40A layer.

Table 9.4. Acceleration and loss factor data for cantilever beam tests for Buna-N/Nitrile 40A.

Test Number	Accel Point 1 [V]	Accel Point 2 [V]	Time 1 [s]	Time 2 [s]	Frequency [Hz]	Log Decrement	Loss Factor
1	1.249442	0.44799	1.47064	2.59408	26.7	0.0342	0.01088
2	1.949579	0.61839	1.32246	2.45086	26.586	0.03827	0.0122
3	2.517485	0.704957	1.5872	2.7187	26.513	0.0424	0.0135

In order for accurate and representative loss factor values the nitrile rubber needed to be securely bonded to the metal surfaces of the beam and constraining layer. The bond inadequacies did not allow the nitrile 40A to damp out the vibration and oscillation of the beam to its full potential.

9.5 Cantilever Beam Test Conclusions

The three best materials found from the RKU predictions, with material properties found from cyclic loading tests, were bonded to a steel beam and constrained by a thin piece of aluminum along the length of the beam. It was found from these tests that the material properties of the damping layer were not always the most important factor in damping out vibrations. Though silicone 30A and nitrile 40A showed higher loss factor to shear modulus ratios than Dyad 601, they did not provide the expected damping per the RKU prediction. The bond between the viscoelastic material and the adjacent metal layers was determined to be the limiting factor in producing effective damping of the beam. Additionally, because approximate loss factor and storage modulus data was found per the cyclic loading tests, the discrepancy between the approximate complex modulus values for the silicone 30A and nitrile 40A also contribute to the error seen between RKU theoretical composite system loss factors and the system loss factors found from experimental cantilever beam results. These approximate complex modulus values vary from exact values by perhaps as much as 20% due to the assumptions made in section 7.1, namely that the stress is uniform across the entire cross sectional area of the test material and that the strain is uniform along the length of the test material.

Dyad 601, produced by Soundcoat Company, had a specially formulated epoxy to help bond it to metal surfaces. This bond was found to be both strong and stiff,

effectively eliminating any significant slip at the steel-Dyad and aluminum-Dyad interfaces. This allowed the Dyad to shear properly and resulted in both significant damping as well as the RKU prediction to be accurate. Both silicone and nitrile rubbers could not be bonded to the metal substrates by a stiff enough adhesive. The rubbery bonding layer of the silicone RTV did not allow the silicone or nitrile rubber to shear properly, voiding their effectiveness as damping materials. Thus, despite the better measured damping properties per the cyclic loading tests in section 7, Dyad 601 proved to be the best damping material when experimentally tested on the cantilever beam.

In regards to a landing gear, bonding between the gear structural materials, in this case 4140 steel, plays an even more significant role than bonding in the cantilever tests because of the amplitude of deflection of the gear. The gear of interest in this report was designed to deflect (change in height) several inches, much more than any tip deflection in the cantilever tests. With higher deflection and higher strain in the steel gear, the problem of delamination, or separation of the viscoelastic material from the gear structure, becomes a looming problem. If the bonding layer is too stiff, it is subject to crack and shear off of the gear material, which will render the damping layer useless. However, if the bonding layer is too flexible, it will not transfer shear forces effectively to the viscoelastic layer as seen with silicone 30A and nitrile 40A. Therefore, the B-flex epoxy, a semi-flexible yet strong adhesive layer, is the most promising bonding material for use in the gear. It showed excellent performance in the cantilever tests and is the bonding material of choice in the application of a damping layer to the landing gear.

Chapter 10

Landing Gear Geometry Considerations

Up until this point, only simple cantilever beam tests have been studied in reference to effective damping using viscoelastic materials. However, a simple cantilever design would be impractical for the particular aircraft application from which this research spawned. Figure 10.1 illustrates a landing geometry similar to that which will be used as the new gear design on the aircraft of interest, as well as high strain energy areas with intensity scale shown on the left hand side of the figure.

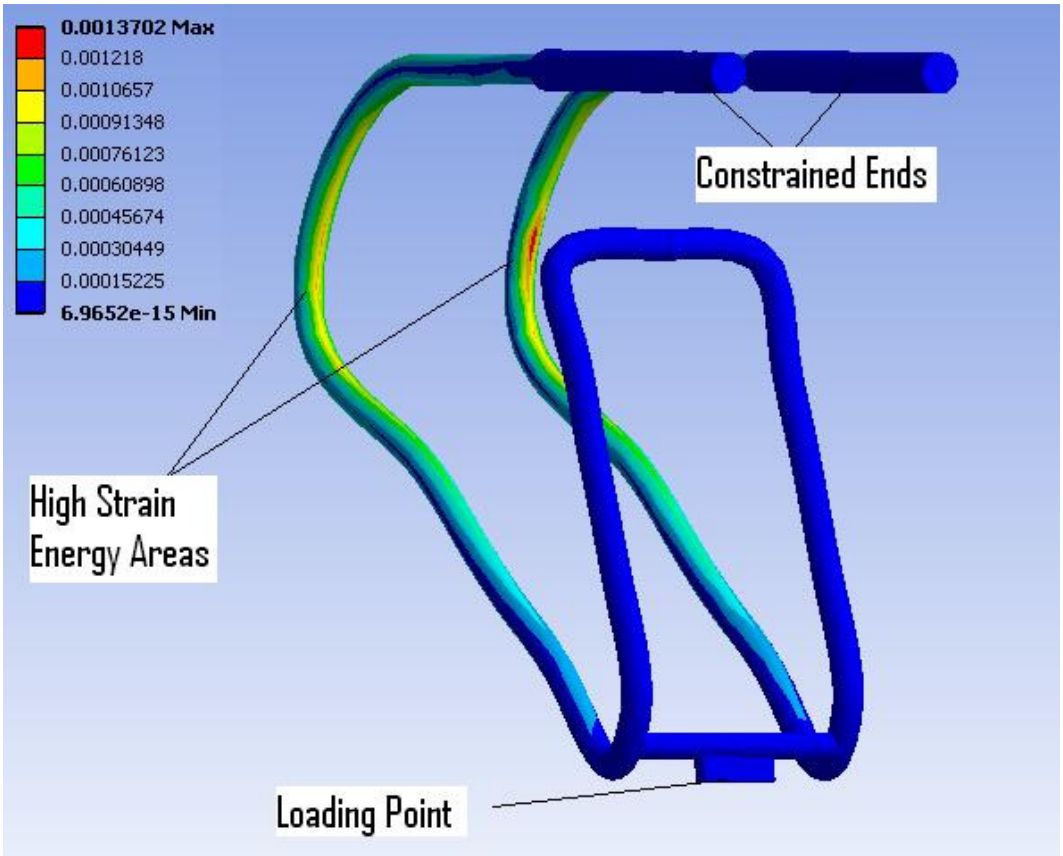

Figure 10.1. Basic landing gear geometry showing vertical loading point and high strain energy areas.

The geometry shown in Figure 10.1 is still a cantilever type system, but the geometry makes it much more difficult to effectively apply a damping layer because of curved

surfaces and bend radii. Viscoelastic materials like the rubbers and specialty dampers studied in this report are generally manufactured in the largest quantities as sheets. This makes them easy to apply to flat surfaces without much alteration in the geometry of the sheets. Additionally, constrained layer applications are even more difficult due to the necessary manipulation and rigid bonding of a stiff constraining layer to a viscoelastic material. Thus, a solution to this problem is proposed, although this solution is much more difficult to accurately model for reasons which will be discussed.

Application of the relevant viscoelastic materials in section 8 providing maximally effective damping would be difficult to apply if the material was kept in sheet-like form. However, if these sheets were cut into long, narrow strips they could be applied as a wrap. The application of the treatment would be slightly more tedious, but the resultant damping very similar to a complete treatment. Also, if the constraining layer were made thin enough, though this is undesirable (see section 8.5), it could also be cut into thin strips and applied as a successful constraining layer, making the treatment more effective than a free layer treatment.

The difficulty in modeling comes from the bonding layer, something that up until this point is assumed very thin and flat. The bonding layer would cover the outer surface of the gear host structure, but would also have a helical component bonding each section of wrap to its adjacent sections. Additionally, this helical bonding layer inherently means there would be gaps between each wrap, effectively making the treatment a partial constrained layer treatment, something significantly more difficult to model than a simple layer attached to the free surface of a cantilever beam. The helical component of the bonding layer, however, is relatively negligible, but is nevertheless another component to

account for in an accurate damping prediction of the gear geometry. Recall that the purpose of this report is to study and determine the best common damping materials which could be used as a damping treatment for a small aircraft landing gear. The data taken from these materials can then be extrapolated to other cantilever type systems without the need to explicitly analyze the damping of the gear.

10.1 Round versus Square Material Geometry

The influence of a damping treatment applied to round versus square rod is two fold. The first issue is a matter of mass and weight. Weight on an aircraft should be kept to a minimum to maximize the flight time and aerodynamic efficiency of the aircraft. Secondly, because damping via viscoelastic materials is dependent on shear, the distance of a damping treatment to a neutral plane should be at a reasonable maximum, while keeping any increases in mass and drag within proper limits.

Round rods have lower cross sectional area than square rods of the same minimum cross section distance. Thus, round rods inherently have lower mass for the same length and material of rod. They are, therefore, a better choice for a landing gear material geometry than square rod. Additionally, from a design and manufacturing perspective, round rod is easier to shape and form than square rod, making it cheaper and faster to fabricate landing gear from round stock.

From a damping perspective, round rod does not offer the same amount of damping per volume of damping treatment as square rod. A damping treatment need only be applied to the flat faces of a square rod which are furthest away from the neutral plane of the structural material during loading to achieve good damping. However, damping material would need to be applied to the entire circumference of a round rod and

this does not even achieve the same level of damping as a square rod with less damping material. More damping can be achieved with square rod using less material because there is a larger surface area having larger bending strains than round rod. With round rod, it is seen from Figure 10.1 that there is a thin strip of area, highlighted in red, having large strains. This strip is the area of the rod furthest away and parallel to the neutral plane during loading of the gear structure. Because there is a low surface area having large strains, the viscoelastic treatment would have low *effective* area in which it could utilize the strain energy of the area to dissipate energy. With a square rod however, if bent and loaded in the same configuration, there is a much larger surface area having large strains. Therefore it is not only the shear within the viscoelastic material, but also the volume of material which has large shear within the damping layer. To increase the volume of material with large shear, the treatment surface area should be increased and applied to areas having the largest strain energies, promoting the largest possible shear per volume within the viscoelastic layer.

Though square rod is initially more massive than round rod, round rod is a less desirable material from a design perspective because of larger additions in weight from a damping treatment and constraining layer and because it achieves less damping per volume of material than square rod. The additions of weight by a damping material and constraining layer to a round rod often nullify whatever weight advantage round rod had over square rod. Additionally, more damping material is needlessly added to areas close to the neutral plane of round rod, resulting in wasted material because the shear deformation of the treatment layer becomes small closer to the neutral plane. As the shear deformation decreases with the distance to the neutral plane, the material is no

longer effective at damping vibrations of the host structure because shear deformation is the primary mechanism of damping in viscoelastic materials.

10.2 Landing Gear Design Conclusions

It has been shown that though round rod is initially less massive than square rod, the damping of a round rod is much less for the same volume of damping treatment than a square rod. The aircraft of interest in this report is approximately 400 lbs, so the gear material was initially chosen to be 3/8" diameter steel rod. From Figure 10.1, a small material diameter was chosen to minimize drag. The design process in determining deflections and loads of the gear was facilitated by ANSYS finite element software.

The transition to square rod ultimately affects the design and dimension of the gear as a whole. In bending, square rod has a larger flexural rigidity than round rod for the same material and minimum cross section distance. The deflection and damping of the gear were of primary concern, so to keep the deflection upon loading a constant, the dimension of the square rod can be reduced to match that of the initial design using round rod. Because the materials were kept the same, only the cross sectional area of the square rod needed to be altered in order to produce a flexural rigidity matching that of the initial design using round rod. Thus, a square rod having the same deflection of round rod can be used where a much more efficient, weight saving damping treatment can be applied in a much simpler fashion.

Chapter 11

Summary, Conclusions, and Recommendations

The purpose of this report was to provide a basic knowledge of constrained layer viscoelastic damping and to identify the best viscoelastic damping material to apply to a landing gear while considering customer requirements such as cost, weight, aerodynamics, environmental factors, and damping effectiveness. Eight viscoelastic materials were chosen because of their low cost and durability. They were tested in an ElectroPuls E1000 cyclic loading machine and an energy analysis was used to determine their approximate elastic moduli and loss factors. These material parameters were then used to formulate a damping prediction of a cantilever beam using the complex flexural rigidity from the Ross, Kerwin, and Ungar analysis. The three best materials per the RKU analysis were Silicone 30A, Buna-N/Nitrile 40A, and Dyad 601. These materials were laminated to a cantilever beam and tested to experimentally determine the loss factor of the beam and then compared to the RKU predictions. Dyad 601 showed the best damping performance and correlation of experimental and theoretical loss factor results. Silicone 30A and nitrile 40A rubbers showed sub-par performance due to the difficulty in bonding these rubbers to metal surfaces.

In the application of these damping materials to the landing gear, these materials are more efficiently bonded to flat surfaces. Thus, square rod is a choice material geometry because less damping material can be bonded to the surfaces furthest away from a neutral plane than for a round rod, where the damping material must be wrapped around the entire circumference of the rod. Additionally, should round rod be bent into a similar configuration as Figure 10.1, more damping material, and therefore more mass,

must be added to the gear to achieve the same level of damping as a thinner damping layer applied to the faces furthest from the neutral surface of a square rod.

The aerodynamic efficiency will decrease slightly in a transition from round rod to square rod due to gear faces perpendicular to the free stream during flight. However, during the cantilever tests, only one side of the cantilever beam was laminated with a damping layer prior to testing. If both front and rear faces of a gear bent with square rod are laminated with a treatment, a constraining layer having a cross section of a half circle can be laminated to the viscoelastic treatment. This will increase weight by a small margin, but will greatly reduce the drag of the gear and increase the loss factor due to a thicker constraining layer.

11.1 Future Work

The first step in applying the conclusions found in this report is to fabricate and test a landing gear with an applied damping treatment, preferably Dyad 601. The structural member, steel rod, of the gear is cheap and relatively simple to fabricate. Thus, several different gear structures can be made and a different damping treatment can be applied to each, perhaps with a stand-off layer (Yellin, 1998), or spacer layer between the metal and damping material to promote increased stresses within the layers, and therefore better energy dissipation, within the damping layer. Each gear can then be fitted to the aircraft and drop tested to isolate the best result.

The bonding of the silicone and nitrile rubbers was found to be the limiting factor of damping in the cantilever beam tests. However, both silicone and nitrile rubbers are easily molded or extruded around structural members. If a silicone or nitrile extrusion, or even a mold encapsulating the metal of the gear and then filled with a pressurized flow of

viscoelastic material, could be applied to the gear structure, much better damping may be achieved. This would effectively eliminate any rubbery bonding layers with silicone or nitrile rubbers and would also increase the interaction between the gear surfaces and the damping layers.

As an alternative solution to using metal as the structural component in the gear, fiber enhanced viscoelastic polymers could also be used (Alberts, 1995). A fiber enhanced viscoelastic polymer is a series of thin, structural fibers like carbon or fiberglass, encapsulated by a viscoelastic material. A series of strands having a configuration similar to that of a frayed cable could be used as the basic structural member of the gear. These strands could then be placed in a pressurized mold, having the geometry of the gear in Figure 10.1, where a liquid viscoelastic material could then be injected around the structural fibers encapsulating them in a viscoelastic matrix. This would increase the contact surface area between the structural fibers and the damping material as well as significantly reduce weight. Any loss in aerodynamic efficiency would also be eliminated as the gear could take on the shape of the bare metal structure of Figure 10.1.

Possible problems may arise in that the structural fibers would not be able to accommodate loads on the extreme end of the landing gear design envelope. Additionally, the damping material may need to be stiffer to help handle a small portion of landing loads to assist the steel or composite fibers woven throughout the gear geometry. Though the cost of fabricating this gear may be slightly higher than for a metal gear, it is a viable solution for producing a gear with high damping, providing an

effective, lower weight and more aerodynamic efficient material substitute for traditional shock absorbers.

References

1) Alberts, T. E. and H. Xia. 1995. Design and Analysis of Fiber Enhanced Viscoelastic Damping Polymers. *Journal of Vibration and Acoustics.* 117: 4:398-404.

2) Bagley, R. L. and P. J. Torvik. 1985. Fractional Calculus in the Transient Analysis of Viscoelastically Damped Structures. *AIAA Journal.* 23: 6:918-925.

3) Birman, V. and L. W. Byrd. 2002. Analytical Evaluation of Damping in Composite and Sandwich Structures. *AIAA Journal.* 40: 8: 1638-1643.

4) Buhariwala, K. J. and J. S. Hansen. 1988. Dynamics of Viscoelastic Structures. *AIAA Journal.* 26: 2:220-227.

5) DiTaranto, R.A. 1965. Theory of vibratory bending for elastic and viscoelastic layered finite length beams. *Transactions of the ASME, Journal of Applied Mechanics, 87,* 881-886.

6) Hao, M. and M. D. Rao. 2005. Vibration and Damping Analysis of a Sandwich Beam Containing a Viscoelastic Constraining Layer. *Journal of Composite Materials.* 39: 18:1621-1643.

7) Jones, D. I. G. 2001. *Handbook of Viscoelastic Vibration Damping.* West Sussex, England: John Wiley and Sons, LTD.

8) Kalyanasundaram, S., D.H. Allen, and R.A. Shapery. 1987. Dynamic Response of a Timoshenko Beam. *AIAA Journal.* 559-567.

9) Kerwin, E.M. 1959. Damping of flexural waves by a constrained viscoelastic layer. *Journal of the Acoustical Society of America, 31*(7), 952-962.

10) Lemerle, P. 2002. Measurement of the Viscoelastic Properties of Damping Materials: Adaptation of the Wave Propagation Method to Tests Samples of Short Length. *Journal of Sound and Vibration.* 250: 2:181-196.

11) Markley, D. W. and N. H. Madsen. 1988. Development of a Model for Interfacial Damping. *AIAA Journal.* 1726-1732.

12) Mead, D.J., and Markus, S. 1969. The forced vibration of a three-layer, damped sandwich beam with arbitrary boundary conditions. *Journal of Sound and Vibration. 10*(2), 163-175.

13) Meirovitch, L. 2001. *Fundamentals of Vibrations.* New York, NY: McGraw Hill.

14) Moreira, R.A.S. and J.D. Rodrigues. 2006. Partial Constrained Viscoelastic Damping Treatment of Structures: A Modal Strain Energy Approach. *International Journal of Structural Stability and Dynamics.* 6: 3:397-411.

15) Nashif, A. D., Jones, D. I. G., and J. P. Henderson. 1985. *Vibration Damping.* Canada: John Wiley and Sons, Inc.

16) Rao, Y., V.K. Sadasiva, and Nakra, B.C. 1974. Vibrations of unsymmetrical sandwich beams and plates with viscoelastic plates. *Journal of Sound and Vibration, 34*(3), 309-326.

17) Ross, D., Ungar, E.E., Kerwin, E.M. Jr. 1959. Damping of plate flexural vibrations by means of viscoelastic laminate. In ASME (Ed.). *Structural Damping* (pp. 49-88). New York: ASME.

18) Saravanos, D.A. 1991. The Effects of Interply Damping Layers on the Dynamic Response of Composite Structures. *Proceedings, 32nd Structures, Structural Dynamics, and Materials Conference,* 2363-2370. Baltimore, MD: AIAA/ASME/ASCE/AHS/ASC.

19) Soundcoat Company. 2001. Soundcoat Dyad Material Data Sheet. www.soundcoat.com.

20) Sun, C. T. and Y. P. Lu. 1995. *Vibration Damping of Structural Elements.* Englewood Cliffs, NJ: Prentice Hall.

21) Torvik, P. J. 1996. Complex Rayleigh's Quotient – A Means of Estimating Loss Factors for Damped Systems. *Proceedings, 37th Structures, Structural Dynamics, and Materials Conference and Exhibit,* 1054-1063. Salt Lake City, UT:AIAA/ASME/ASCE/AHS/ASC.

22) Yan, M.J., and Dowell, E.H. 1972. Governing equations for vibrating constrained-layer damping of sandwich beams and plates. *Transactions of the ASME, Journal of Applied Mechanics, 94,* 1041-1047.

23) Yellin, J. M. and I. Y. Shen. 1998. Analytical Model for a Passive Stand-Off Layer Damping Treatment Applied to an Euler-Bernoulli Beam. *Proceedings, Smart Structures and Materials 1998: Passive Damping and Isolation.* 349-357. San Diego, CA: Society of Photographic Instrumentation Engineers.

Appendix A: MATLAB Programs

Damping Predictions

```
function LF = RKU_Loss1(E_v, G_v, H_s, H_c, T_c)

%This function uses the RKU equations with inputs of elastic and shear
%modulus of the viscoelastic material, thickness of the structural member,
%thickness of the constraining layer, and width of the constraining layer
%and outputs composite system loss factor as a function of varying
%viscoelastic layer thickness.


L = .3557; %meters
E_s = 205E9; %Pascals
E_c = 68E9; %Pascals

omega_1 = 177.128; %rad/s
rho_s = 7800; %kg/m^3

i = 1;
k = 1;

LF = [];

for H_v = .0005:.0001:.009527
   I_s = H_s^4/12; I_c = T_c*H_c^3/12;
   zeta = sqrt(rho_s*H_s^2*omega_1^2*L^4/(E_s*I_s));
   H31 = H_v + .5*(H_s+H_c);
   H21 = .5*(H_s+H_v);

   g = G_v*L^2/(E_c*H_v*H_c*zeta*sqrt(.9));

   D = (E_v*H_v*(H21 - .5*H31) + g*(E_v*H_v*H21 + E_c*H_c*H31))/((E_s*H_s +
.5*E_v*H_v + g*(E_s*H_s + E_v*H_v + E_c*H_c)));

   EI = E_s*H_s^3/12 + E_v*H_v^3/12 + E_c*H_c^3/12 - E_v*H_v^2/12*((H31 -
D)/(1+g))...
       +E_s*H_s*D^2 + E_v*H_v*(H21-D)^2 + E_c*H_c*(H31 - D)^2 -
(.5*E_v*H_v*(H21 - D) + E_c*H_c*(H31 - D))*((H31 - D)/(1+g));
   LF(i) = imag(EI)/real(EI);

   i = i+1;
end
```

```
H_v = [.0005:.0001:.009527];

plot(H_v, LF), xlabel('Viscoelastic layer thickness (m)'), ylabel('System Loss Factor')
title('Loss Factor vs. Viscoelastic Layer Thickness for First Modal Frequency (177.128
rad/s)')
```

Constrained Layer Effects

```
function LF = RKU_Loss_CL1(E_v, G_v, H_s, H_v, H_c, T_c)

%This function uses the RKU equations to predict changes in the loss factor
%of a composite beam system for varying constraining layer elastic modulus
%and thickness.  Each section of code holds one variable (modulus or
%thickness) constant and varies the other.

L = .3557; %meters
E_s = 205E9; %Pascals


omega_1 = 177.128; %rad/s
rho_s = 7800; %kg/m^3

i = 1;
k = 1;

LF = [];

for E_c = 50000000000:1590000000:209000000000
   I_s = H_s^4/12; I_c = T_c*H_c^3/12;
   zeta = sqrt(rho_s*H_s^2*omega_1^2*L^4/(E_s*I_s));
   H31 = H_v + .5*(H_s+H_c);
   H21 = .5*(H_s+H_v);

   g = G_v*L^2/(E_c*H_v*H_c*zeta*sqrt(.9));

   D = (E_v*H_v*(H21 - .5*H31) + g*(E_v*H_v*H21 + E_c*H_c*H31))/((E_s*H_s +
.5*E_v*H_v + g*(E_s*H_s + E_v*H_v + E_c*H_c)));

   EI = E_s*H_s^3/12 + E_v*H_v^3/12 + E_c*H_c^3/12 - E_v*H_v^2/12*((H31 -
D)/(1+g))...
       +E_s*H_s*D^2 + E_v*H_v*(H21-D)^2 + E_c*H_c*(H31 - D)^2 -
(.5*E_v*H_v*(H21 - D) + E_c*H_c*(H31 - D))*((H31 - D)/(1+g));
   LF1(i) = imag(EI)/real(EI);

   i = i+1;
```

```
end

E_c1 = [50000000000:1590000000:209000000000];


i = 1;
k = 1;

LF = [];
E_c = 68E9;

for H_c = .0005:.0001:.009527
   I_s = H_s^4/12; I_c = T_c*H_c^3/12;
   zeta = sqrt(rho_s*H_s^2*omega_1^2*L^4/(E_s*I_s));
   H31 = H_v + .5*(H_s+H_c);
   H21 = .5*(H_s+H_v);

   g = G_v*L^2/(E_c*H_v*H_c*zeta*sqrt(.9));

   D = (E_v*H_v*(H21 - .5*H31) + g*(E_v*H_v*H21 + E_c*H_c*H31))/((E_s*H_s +
.5*E_v*H_v + g*(E_s*H_s + E_v*H_v + E_c*H_c)));

   EI = E_s*H_s^3/12 + E_v*H_v^3/12 + E_c*H_c^3/12 - E_v*H_v^2/12*((H31 -
D)/(1+g))...
      +E_s*H_s*D^2 + E_v*H_v*(H21-D)^2 + E_c*H_c*(H31 - D)^2 -
(.5*E_v*H_v*(H21 - D) + E_c*H_c*(H31 - D))*((H31 - D)/(1+g));
   LF(i) = imag(EI)/real(EI);

   i = i+1;
end

H_c = [.0005:.0001:.009527];

LF1;
E_c1;


plot(H_c, LF, E_c1, LF1), xlabel('Constraining Layer Thickness (m)'), ylabel('System
Loss Factor')
title('Loss Factor vs. Constraining Layer Thickness for 1mm Damping Layer at 28.19
Hz')
```